Superstructure assembly 2D

by oriented attachment of PbX nanocrystals

Superstructuurconstructie 2D

door gerichte aanhechting van PbX nanokristallen

(met een samenvatting in het Nederlands)

Proefschrift

ter verkrijging van de graad van doctor aan de Universiteit Utrecht
op gezag van de rector magnificus, prof.dr. G.J. van der Zwaan,
ingevolge het besluit van het college voor promoties
in het openbaar te verdedigen op woensdag 7 maart 2018 des middags te 2.30 uur
door Carlo van Overbeek geboren op 20 februari 1989 te Utrecht

Promotor: Prof.dr. D.A.M. Vanmaekelbergh

Copromotor: Dr.ir. M.A. van Huis

Colofon

Geprint door: ProefschriftMaken || www.proefschriftmaken.nl
ISBN: 978-94-6295-850-0

Deze thesis is volledig geprint op gerecycled papier.

Het wetenschappelijke werk in deze thesis dat is verricht door de auteur werd gefinancierd door de Nederlandse Organisatie voor Wetenschappelijk Onderzoek (NWO) via de ECHO Project Grant 'Nanoperiodic semiconductors from colloids that react as atoms' (projectnummer 712.013.001).

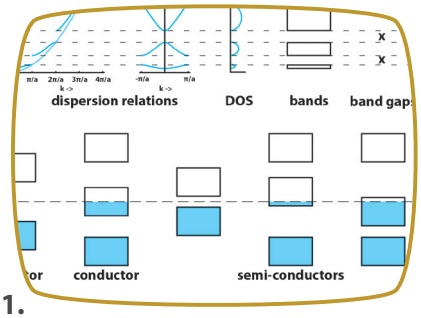
dispersion relations
DOS
bands
band gap
conductor
semi-conductors

1.

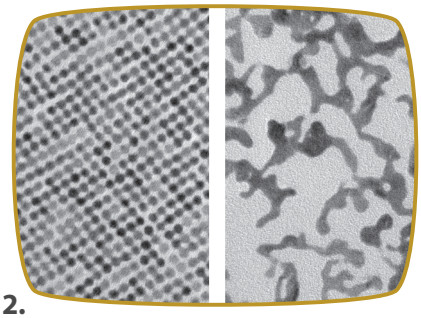

2.

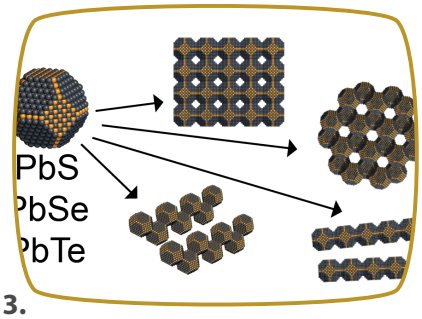
PbS
PbSe
PbTe

3.

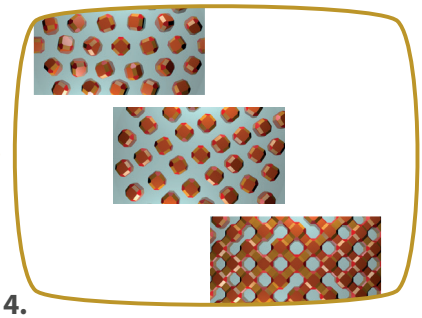

4.

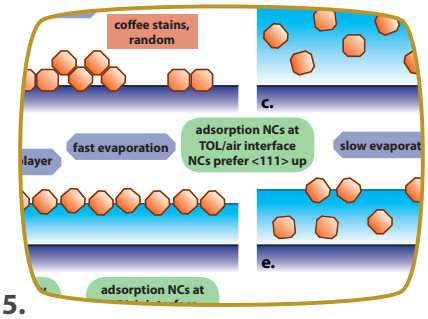
coffee stains, random
c.
fast evaporation
adsorption NCs at TOL/air interface NCs prefer <111> up
slow evaporat
e.
adsorption NCs at

5.

Table of contents

Foreword / Voorwoord **6 / 10**

1. Theoretical introduction:
the many facets of nanocrystal science **14**

2. Methodology:
synthesis of two-dimensional superstructures with square or honeycomb nanoperiodicity by interfacial self-assembly & oriented attachment of PbSe nanocrystals **50**

3. Interfacial self-assembly and oriented attachment in the family of PbX (X = S, Se, Te) nanocrystals **66**

4. In-situ study of the formation mechanism of two-dimensional superstructures from PbSe nanocrystals **92**

5. Towards a full description of PbSe nanocrystal self-assembly behavior at liquid interfaces **114**

Appendices **144**
List of publications *145*
Summary / Samenvatting *146 / 150*
Dankwoord - Acknowledgements *154*
About the author *160*

1.F

Foreword

Fusing objects is a general process known by everyone. Through gluing, soldering and welding, countless products are being manufactured every day. It should then not be surprising that fusing is also ubiquitous in nature and life. For example, wounds heal by growing together the wound edges, rain droplets form by merging of smaller water droplets in the air, and asteroids grow by crashing into each other.

In the 1990's, scientists discovered a new way by which crystallites can fuse together in a spontaneous way. They found evidence that some types of crystals had formed by fusing of microscopic crystallites. Before this discovery, it was thought that crystal growth exclusively happens through a process comparable to the formation of ice crystals or snowflakes, which happens roughly atom-by-atom. The newly discovered fusion process occurs when two microscopic crystallites are perfectly oriented with respect to each other. Notably, it happens without any binding substance such as glue, solder or other filler. The atoms of the original crystals themselves are used to form a crystalline neck between the two original building blocks. Furthermore, it was found that some bacteria facilitate this process in their metabolism. The new fusing process was named 'oriented attachment'.

Scaling down assembly to microscopic objects

The process of connecting and fusing objects together into a working product is called assembly. Assembling microscopic objects is a pivotal process in life. With reliable processes that facilitate hair growth, starch synthesis and DNA replication, life can be considered a true master of assembling microscopic objects. Modern technology is also rapidly picking up on the assembly of microscopic objects. This happens mainly in the field of information and computer science. This has led to the development of applications such as LCD computer screens, microscopic transistors and computer hard drives.

A rather obvious problem in assembling microscopic objects is that they cannot be assembled by humans directly. Because of their small size, human eyes cannot directly observe them nor can human hands individually manipulate them. There is, of course, machinery available to overcome this problem, but every available apparatus has its limitations.

Another route towards assembling microscopic objects is by making them to assemble themselves: this is called self-assembly. Self-assembly might sound like something too good to be true, but it is a very real phenomenon. In fact, nearly all assembling processes

in life are self-assembly processes. To make self-assembly sound more like a reasonable process, it might be instructive to compare it with a marble track. The marble is not moved from the top to the bottom by direct manipulation. Rather, it follows a path that was planned for it to follow. The path in self-assembly, however, does not consist of physical bends and pit falls, but subtle pushes and forces from other microscopic objects. These mold an object into the desired assembled product.

Self-assembly processes are not possible for macroscopic objects, such as tables, toilets and tree houses, because those are big enough to be appreciably affected by forces from gravity and friction. These two forces do not give enough room for creatively balancing an object through a predefined path of subtle pushes and forces.

Making microscopic objects assemble themselves by the pushes and forces from other microscopic objects, however, brings a new problem to the drawing table. Before a path can be created towards a certain product, the exact ways in which the microscopic objects push and force each other must be understood. This is no easy task. To put it into perspective, try to predict exactly where the next drop will land during rain. There are just too many seemingly random fluctuations in forces that affect a rain droplet to make this possible. Those seemingly random fluctuating forces only become more important upon scaling down to microscopic objects.

However, immense technological progress could be achieved with control over microscopic self-assembly. Better displays, personalized medicines and faster computers are a few envisioned examples. Gaining control over microscopic self-assembly is not just a nice scientific fantasy, as life is the living proof this can be done successfully. These two considerations have fueled decades of dedicated scientific research in microscopic self-assembly. Many more years of research will follow until science exactly understands and eventually masters those microscopic pushes and forces.

Contents of this thesis

In this thesis, the self-assembly and oriented attachment of microscopic crystallites forming flat materials with a square and honeycomb geometry has been studied. These materials are of interest for the computer industry, because they are supposed to conduct electricity controllably and extremely fast. Whether these theoretical predictions can be observed and whether these materials can indeed lead to faster computers are topics beyond the scope of this thesis. Before such follow-up research can be done, it must be known how to create these materials with the best possible crystallographic quality. To this end, the work described in this thesis will focus on exactly how, in other words, through which pushes and forces, the microscopically small crystallites form these materials.

A brief outline of this thesis is given below to facilitate its further reading.

In chapter 1, a brief scientific introduction to oriented attachment and self-assembly of microscopic crystals is given.

In chapter 2, the experimental methods and equipment that were used to perform the work in this thesis are described.

In chapter 3, assembly and oriented attachment is investigated of microscopic crystallites within the lead chalcogenide family of materials, namely lead sulfide, lead selenide and lead telluride. All three of these compounds can form the same four types of 'low-dimensional' materials: 1D lines and zigzags and 2D materials with a square and honeycomb 'nanogeometry'.

In chapter 4, the self-assembly of 2D materials with a square nanogeometry starting from microscopic lead selenide crystallites is studied (partly 'in-situ') by advanced microscopy techniques, namely electron microscopy, electron diffraction, X-ray scattering and X-ray diffraction. The observed behavior of the crystallites was successfully rationalized with a computer model.

In chapter 5, the behavior of microscopic lead selenide crystallites at liquid/air interfaces is studied with the techniques mentioned for chapter 5. Also, a hypothesis on the formation of the 2D honeycomb materials is presented. This hypothesis is based on trends in the synthesis conditions and findings described in recent scientific literature.

Non-exact scientific readers may want to skip chapters until the summary. The summary is written such that no prior knowledge of exact science is necessary. But all readers are of course warmly invited to boldly take the full scientific route!


1.F

1.0

Voorwoord

Binden van verschillende objecten is een algemeen proces dat bij iedereen bekend is. Door middel van lijmen, solderen en lassen worden dagelijks ontelbaar veel producten geproduceerd. Het is dan ook niet vreemd dat binden een alom vertegenwoordigd proces is in de natuur en het leven. Wonden dichten door het binden van de randen, regendruppels vormen door het condenseren van water en meteoren groeien door in elkaar te rammen.

Wetenschappers ontdekten in de jaren negentig een nieuwe manier waarop objecten in de natuur met elkaar kunnen binden. Ze vonden bewijs dat sommige kristallen waarschijnlijk zouden zijn gevormd door het versmelten van microscopische kristalletjes. Voor deze ontdekking werd gedacht dat kristalgroei enkel gebeurde op een manier die te vergelijken is met het bevriezen van water. Het nieuw ontdekte bindproces vindt plaats wanneer twee microscopisch kleine kristallen zich perfect naar elkaar uitlijnen. (Zoals wel vaker werd dit tien jaren later geobserveerd, nadat het voor het eerst was gespeculeerd.) Merkwaardig genoeg blijven er in de nieuw gevormde kristallen na dit proces weinig tot geen resten achter van waar ooit de randen van de versmolten kristalletjes waren. Daarnaast heeft het proces ook geen bindmiddel nodig zoals lijm, soldeer of slak. Verder ontdekte men dat sommige bacteriën dit bindproces faciliteren in hun metabolisme. Het nieuwe bindproces werd gerichte aanhechting genoemd.

Constructie met microscopische objecten

De meeste processen gaan soms goed en soms fout. Het verbinden van twee auto's in een auto-ongeluk wordt meestal als een fout gezien. Als bindingen echter goed en gericht worden aangebracht, dan hebben we het meestal over constructie. Constructie van microscopische objecten is een essentieel proces in levende wezens. Het leven op zich is een meester in het construeren van microscopische objecten. Dit valt af te leiden uit hoe goed de natuur de volgende processen bijvoorbeeld laat verlopen: het groeien van haar, de productie van zetmeel of het kopiëren van genetisch materiaal. Moderne menselijke technologie wordt ook steeds beter in het construeren van microscopische objecten. Dit is vooral duidelijk in het veld van computer- en informatietechnologie. Daarin zijn de laatste decennia bijvoorbeeld lcd-computerschermen, microscopische transistoren en harde schijfgeheugens ontwikkeld met behulp van microscopische constructie.

Een voor de hand liggend probleem bij het construeren van microscopische objecten is echter dat mensen dit niet direct kunnen doen. Juist door de kleine grootte van de objecten kunnen menselijke ogen ze niet zien, noch kunnen menselijke handen de

objecten individueel schikken. Er zijn natuurlijk veel apparaten beschikbaar om dit mee te kunnen doen, maar ook die hebben allemaal zo hun beperkingen.

Een andere manier om microscopische objecten te construeren is door ze dit zelf te laten doen. Dit heet zelf-constructie. Zelf-constructie klinkt misschien als iets dat te mooi is om waar te zijn. Het is echter een fenomeen dat in de natuur heel normaal is. Sterker nog, bijna alle constructieprocessen binnen het leven zijn zelf-constructieprocessen! Om het wat aannemelijker te laten klinken, is het inzichtelijk zelf-constructie te vergelijken met een knikkerbaan. De knikker beweegt niet over de baan omdat iets hem duwt. In plaats daarvan volgt de knikker een vooraf vastgelegd pad. Het pad van microscopische zelf-constructie bestaat echter niet uit bochten en gaten in de weg, maar uit subtiele duwtjes en trekjes van andere microscopische objecten. Deze 'kneden' het object in de goede vorm en fungeren tevens als een soort mal. Als deze microscopische duwtjes en trekjes binnen zelf-constructie beschouwd kunnen worden als een knikkerbaan en atomen als knikkers, dan zou het leven gezien kunnen worden als de meest gecompliceerde knikkerbaan ooit.

Zelf-constructieprocessen bestaan niet voor macroscopische objecten, zoals tafels, toiletten en boomhutten, omdat die alleen merkbaar door de zwaartekracht en frictie worden beïnvloed. Deze twee krachten bieden niet genoeg opties om een object op een creatieve manier door een complex voorbestemd pad heen te loodsen. Of om het wat beeldender te zeggen: mensen zullen altijd hun eigen meubels van de IKEA in elkaar moeten 'construeren'.

Microscopische objecten zichzelf laten construeren brengt wel een nieuw probleem op de tekentafel. Voordat er een pad uitgestippeld kan worden naar een bepaald product moeten alle mogelijke microscopische duwtjes en trekjes daarop in kaart gebracht worden. Om in perspectief te plaatsen hoe ontzettend moeilijk dit is, beschouw dan het volgende voorbeeld: probeer tijdens een regenbui te voorspellen waar exact de eerstvolgende druppel zal vallen. Er zijn gewoon teveel schijnbaar willekeurige fluctuaties in de krachten die werken op een regendruppel om dit mogelijk te maken. Dit wordt alleen maar moeilijker, als je gaat kijken naar nog kleine dingen dan regendruppels.

Er zou echter enorme technologische vooruitgang geboekt kunnen worden, als mensen volledige controle krijgen over zelf-constructie van microscopische objecten. Betere tv-schermen, gepersonaliseerde medicijnen en snellere computers zijn een paar voorbeelden daarvan. Daarnaast bewijst het leven ons dagelijks dat gecontroleerde zelf-constructie mogelijk is. Die twee argumenten hebben wetenschappers ertoe aangezet om jaren van onderzoek te wijden aan microscopische zelf-constructie. En er zullen nog vele jaren onderzoek volgen, totdat menselijke technologie alle microscopische duwtjes en trekjes onder de knie heeft.

Inhoud van dit proefschrift

In dit proefschrift worden gerichte aanhechting en zelf-constructie gebruikt om van microscopische kristalletjes platte materialen te maken die er van bovenaf uitzien als een honingraad. Deze materialen kunnen een belangrijke rol gaan spelen in de computerindustrie. Er is namelijk berekend dat deze materialen gecontroleerd en ontzettend snel elektriciteit kunnen geleiden. Of deze wiskundige voorspellingen kloppen en of deze materialen dan echt kunnen worden toegepast in computers zijn onderwerpen die buiten de reikwijdte van deze thesis vallen. Voordat zulk vervolgonderzoek kan worden gedaan moeten deze materialen eerst met de grootst mogelijke kwaliteit gemaakt kunnen worden. Daarom wordt er in deze thesis gefocust op hoe, in andere woorden: onder invloed van welke duwtjes en trekjes, de microscopische kristalletjes deze materialen vormen.

Hieronder staat per hoofdstuk een korte toelichting om potentiële lezers erin wegwijs te maken.

In hoofdstuk 2 worden de theoretische concepten gerichte aanhechting en zelf-constructie wetenschappelijk uitgediept. Wetenschappelijk begrip van deze onderwerpen is een vereiste om het werk in dit proefschrift goed te kunnen begrijpen.

In hoofdstuk 3 worden de methodes en spullen beschreven die zijn gebruikt bij de experimenten in dit proefschrift. Dit om auto-ongelukken op een laboratoriumschaal te voorkomen.

In hoofdstuk 4 wordt de reikwijdte van de in hoofdstuk 3 beschreven methoden getest binnen de lood chalcogenide familie van chemicaliën. Alle drie de lood chalcogenides, namelijk lood sulfide, lood selenide en lood telluride, blijken dezelfde vier platte materialen te kunnen maken. Deze vier materialen kenmerken zich door een vierkante, lineaire, honingraadachtige of zigzaggende geometrie.

In hoofdstuk 5 wordt het proces geobserveerd hoe uit microscopische lood selenide kristalletjes platte materialen met een vierkante geometrie vormen door middel van zelf-constructie en gerichte aanhechting. Dit gebeurt met geavanceerde microscopische technieken, namelijk elektronenmicroscopie, elektronendiffractie, Röntgendiffractie en Röntgenverstrooiing. Het geobserveerde gedrag van de kristalletjes valt te rationaliseren met behulp van berekeningen op een computer.

In hoofdstuk 6 wordt een hypothese uiteengezet hoe microscopische kristalletjes platte materialen met een honingraadachtige geometrie kunnen vormen. De hypothese is gebaseerd op trends die in verschillende experimenten zijn waargenomen en bevindingen die worden beschreven in de publicaties van andere wetenschappers.

Niet-bètawetenschappers zullen misschien het liefst door willen bladeren naar de samenvatting, hoofdstuk 7. Deze is zo geschreven dat er geen wetenschappelijke voorkennis nodig is om hem te begrijpen. Overigens wordt deze afsnijroute niet nemen uiteraard alleen maar aangemoedigd!

Level up!

Chapter 1

Theoretical introduction: the many facets of nanocrystal science

Abstract **17**

1.1. Introducing: crystals **17**
1.1.1. Towards defining crystals as an ordered array of atoms *17*
1.1.2. Crystals: the best solid-state model system *19*

1.2. Crystal growth processes and theories **23**
1.2.1. Thermodynamic warm-up *23*
1.2.2. Nucleation *25*
1.2.3. Growth *26*
1.2.4. Crystal facets *28*
1.2.5. Attaching crystallites *29*

1.3. Crystal growth methods in nanoscience **31**
1.3.1. The hot injection method *31*
1.3.2. Post-synthetic treatments *33*

1.4. Colloidal crystals **34**
1.4.1. Colloids *34*
1.4.2. Self-assembly in theory *35*
1.4.3. Self-assembling colloidal nanocrystals in practice *38*
1.4.4. Other fields in self-assembly *40*

1.5. Measuring & modelling **41**
1.5.1. Microscopy *41*
1.5.2. Scattering & diffraction *42*
1.5.3. Spectroscopy *43*
1.5.4. Computer modelling *43*

References **44**

1.1

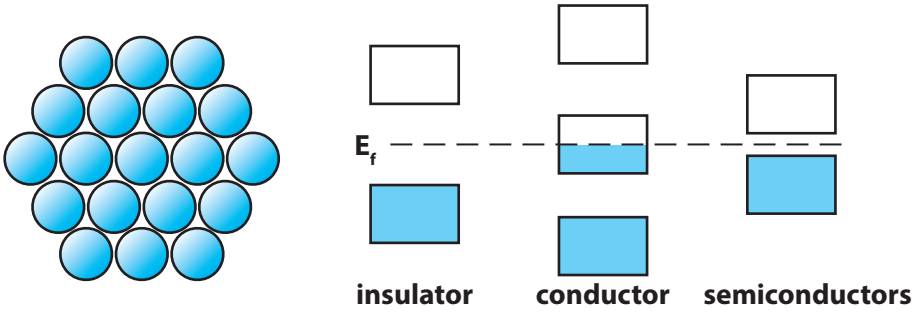

Crystals are ordered arrays of atoms. The specific kind of atoms and ordering in a crystal gives rise to distinct optoelectronic properties of a material. Materials can roughly be divided in three classes of electrical conductivity: insulator, conductor or semiconductor.

Abstract

The research and discussions presented in this thesis mainly link to three areas of current scientific interest, namely: nanocrystals, colloidal nanocrystal self-assembly, and oriented attachment. In this chapter, I will present a brief introduction to these topics. As crystallization and creating hierarchical structures is the recurrent theme in my work, the topics will be discussed with emphasis on crystallography. Finally, I will briefly outline the methods that have been used to study the crystallizing nanocolloids: electron microscopy, X-ray scattering, X-ray diffraction and computer simulations.

1.1. Introducing: crystals

Crystals are probably the most ordered thing in nature and they have attracted the interest of mankind, scientists in particular, even before their structure was known (1, 2). Precious crystals like amethyst, sapphire and diamond have been collected throughout the entire history of humankind for their beauty. Early human civilizations already recognized the potential of crystals as high purity materials. Therefore, they used crystallization techniques to obtain high-grade sugar and salt. Metal refinery and pottery can also be seen as crude crystallization techniques. Figure 1.1a and 1.1b display images of crystals known and used since ancient history.

Crystals underlie several foundations of our modern society (3). Examples can be found in computers and communication, radars and night vision, solar energy conversion and large-scale lighting (4, 5). The recent introduction of semiconductor nanocrystals, quantum dots, as a luminescent material in the display industry is a specific example directly related to the colloidal nanocrystals studied in this thesis (6). Crystallization is also still being used today as a method of purification in preparing consumer products such as sugar, salt, soda and medicines (7). Science and technology also employ crystallization techniques, for obtaining for example pure silicon for semiconductors (8) or protein crystals for their structure determination (9). Figure 1.1c and 1.1d display images of crystals used in modern times.

1.1.1. Towards defining crystals as an ordered array of atoms

The first scientific foundation towards describing the nature of crystals was laid in the 17th century. Nicolas Steno then discovered that crystal facets have fixed angles with respect to each other. This has become known as the first law of crystallography (2, 13). He discovered this for quartz, but Arnould Carrangeot later found that his law holds for many other minerals too. Steno also proposed that crystals grow by deposition of new

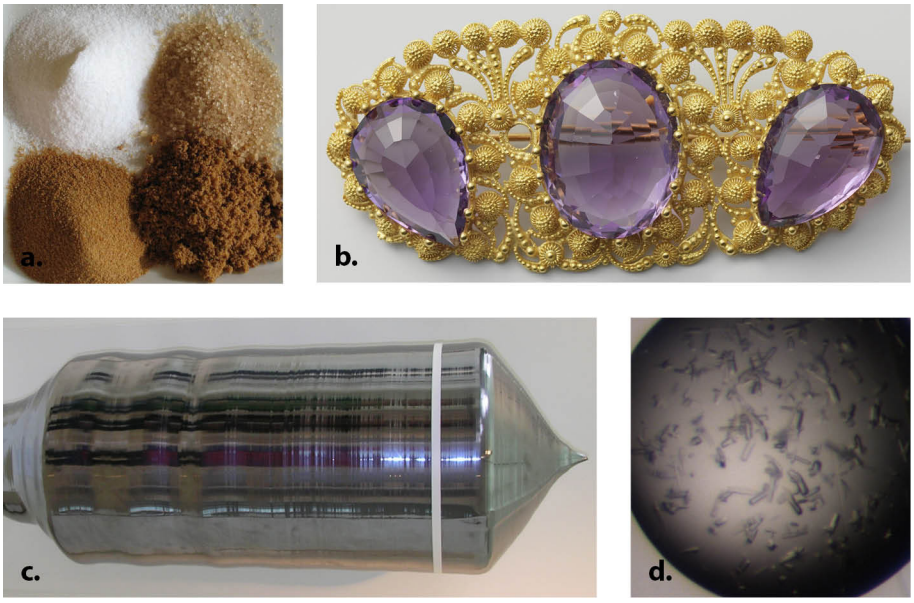

Figure 1.1. Examples of crystals used in historic (a/b) and modern (c/d) times.
(a) sugar in four refined states towards crystal sugar; image taken from ref. (10). Crystallization was and is a pivotal process in sugar refinery and in producing other consumables, such as table salt and medicines. (b) jewel amethysts, as shown in the picture, and other crystal gem stones have been used for their beauty throughout all human history; image taken from ref. (11). (c) a single-crystalline silicon ingot; image taken from ref. (12). Ultrapure silicon is the fundamental building block of modern transistors and solar cells. (d) crystallized ectodomain of mouse PirB protein; image courtesy Hedwich Vlieg. Proteins are crystallized to determine their structure through diffraction.

material on the crystal's surface and that crystal growth and dissolution are each other's exact reciprocals. Especially Steno's latter observation might seem trivial to us now, but back then it was believed that crystals grow from the inside out.

Around the time that Arnould Carrangout was diligently measuring angles between crystal facets, René-Just Haüy was smashing crystals to pieces with a hammer. He observed that the broken pieces have a very similar morphology to the original piece (14). Combining this observation with the first law of crystallography, he deduced that a crystal is a regular array of chemically identical species. See Figure 1.2a for the illustration of his original idea. Building further on this theory, he rationalized that all crystal facets and the angles between them can be described by planes of regularly packed building blocks. This way of describing crystal facets was mathematically formalized by William Miller who stated that each crystal plane can be described by an orthogonal vector defined with integer divisions on the vertices of a polyhedron, usually simply a cube (15).

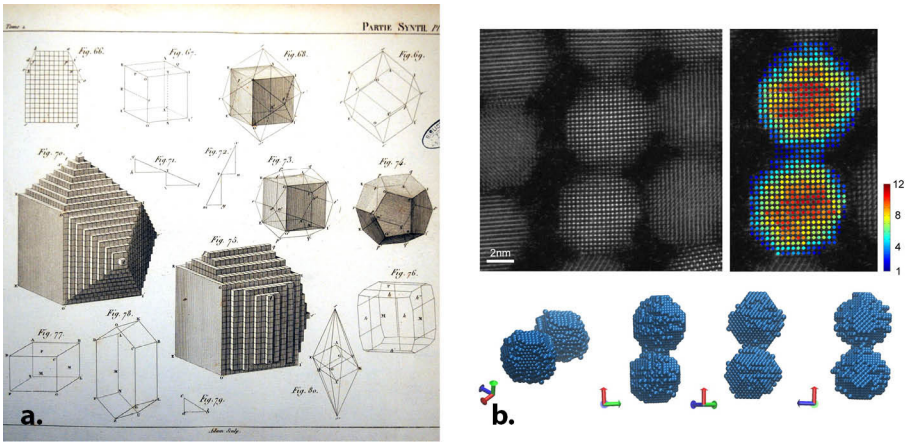

Figure 1.2. A comparison between crystal models from the Enlightenment and modern times.
Evidence for crystal systems was then still inconclusive, but some models come stunningly close to today's standards. (a) sketches of how René-Just Haüy explained the morphology of pyrite crystals with repeating arrays of (chemically identical) cubic building blocks before atomic theory or the nature of crystals were known; image taken from ref. (16). Pyrite indeed has a cubic crystal structure. (b) the structure of crystallites, such as these PbSe nanocrystals, can be directly observed with state-of-the-art electron microscopy techniques, such as HAADF-STEM combined with tomography (17) or atom counting (18); image courtesy Bart Goris and Sara Bals.

In a timeline parallel to the story above, philosophers and scientists were debating whether matter is continuous or atomic in nature. When this debate was combined with the study of crystals and the packing of cannonballs, another discussion sprang of: in how many unique ways can one regularly order points in space? Auguste Bravais proved mathematically that there are 14 unique ways of regularly ordering points in three-dimensional space (19). These are the so-called Bravais lattices, constituted to form the basis of the modern atomic description of crystals.

When atomic theory was accepted in the early years of the 20th century, it could finally be stated that crystals are a regularly ordered array of atoms. Figure 1.2b shows that state-of-the-art microscopy techniques, such as electron microscopy, can now directly observe the regular atomic nature of crystals.

1.1.2. Crystals: the best solid-state model system

Understanding the atomic ordering of crystals has not meant their end as objects of scientific interest, in fact quite the contrary. No less than 29 Nobel prizes have been awarded to studies related to crystallography (20), which is roughly 5% of all Nobel prizes ever awarded!

The main attraction of crystals for science and technology comes from the atomic order. It makes them both a reproducible material to work with and a rational model system. At the forefront of scientific discovery, however, the synthesis of nanocrystals and their assembly into larger atomically coherent superstructures can be far more fickle, as will be become clear from the results presented in this thesis.

Electronic dispersion relations and band diagrams

1.1

The research in this thesis aims to describe a reproducible synthesis and a formation mechanism of materials that are interesting because of their optoelectronic properties (21–24). Therefore, we will show a simple example of how crystals can be used as a theoretical model system that predicts a material's electronic properties.

The simplest way of describing electricity is as the motion of electrons. In vacuum, electrons generally behave according to regular, Newtonian, laws of motion (25, 26). Then, there is a continuous quadratic relation between the kinetic energy and velocity of the electron:

Eq.1.1 $$E_{kin} = {}^1\!/_2\, m_e v^2$$

in which m_e is the (rest) mass of an electron. This law as such does not hold in crystals, because some crystals do and some do not conduct electricity. Therefore, the relation between kinetic energy and velocity for electrons cannot span a continuum in crystals. A more sophisticated way of describing electrons in crystals has to be established.

Another way to look at this problem is by stating, like Louis de Broglie, that an electron can also be described as a wave (27, 28). A particle's wavelength then depends on its momentum, which in turn has a linear relation with its velocity. Electrons conducting electricity are in motion, so it makes more sense to describe their kinetic energy by their wavevector instead of simply their wavelength. The kinetic energy of an electron is then given by the relation:

Eq.1.2 $${}^1\!/_2\, m_e v^2 = \frac{p^2}{2m_e} = \frac{h^2}{2m_e\lambda^2} = \frac{\hbar^2 k^2}{2m_e} = E_{kin}$$

in which k stands here for the magnitude of the electron's wavevector.

Electrons in crystals experience a periodic potential due to the regular array of atomic nuclei (29, 30). Felix Bloch realized that the electrons cannot simply be described as purely plane waves due to this potential landscape. He could prove that the wavefunctions obtained the following form:

Eq.1.3 $$\psi_k(r) = u_k(r)e^{ikr}$$

in which ψ is an electron's wavefunction and u the periodic potential it experiences. Describing travelling waves in a medium, in this case electrons in crystals, is called a dispersion relation.

Working out a solution of the Schrödinger equation for such a system is quite tedious and not really relevant in the context of this thesis. Instead, a qualitative discussion of the interactions of electron waves and the crystal lattice will be given below.

The motion of electrons in a crystal depends strongly on their momentum and related de Broglie wavelength with respect to the atomic periodicity. Electrons that propagate with a wavelength very different from the crystal's periodic lattice will not significantly interact with the periodic potential. Therefore, they will still have a regular quadratic relation between their kinetic energy and wavevector. However, when the wavelength of the electrons becomes similar to the lattice period, strong wave interference occurs, this will significantly change their energy and thereby also the relation between their energy and momentum.

Strong interference of the electron plane waves opens energy gaps at wavevectors equal to the inverse of crystal lattice's periodicity. This can be rationalized by considering that electrons propagating with a similar wavelength to the crystal's periodicity, but in or out of phase with the crystal's potential landscape, will have a lower or higher potential energy, respectively. In the extreme case, i.e. at the edges of the allowed energy bands, electrons are represented as standing waves, that cannot propagate through the crystal. These gaps are usually referred to as band gaps. See Figure 1.3a for a simple electronic dispersion relation that displays such energy bands.

These gaps represent energy regions in which there are no electron energy levels available. This means that in a material in which the energy levels of a band are completely occupied up to the band edge, electrons cannot be accelerated in an electric field, i.e. they cannot conduct electricity. There are simply no suitable eigenstates available for such electronic charge transport. Such materials are therefore electrical insulators.

The density of energy levels as a function of the total (kinetic + potential) energy is called the density of states. This density rapidly increases at the edges of energy bands and stays rather constant in the center, so they are often simplified to block models, see Figure 1.3b. The energy up to which a material is filled with electrons is called the Fermi energy. Normally, the Fermi energy is simply determined by the amount of electrons donated to the crystal by its constituent atoms and the amount of electrons that can have a particular wavevector-energy combination, i.e. the density of states.

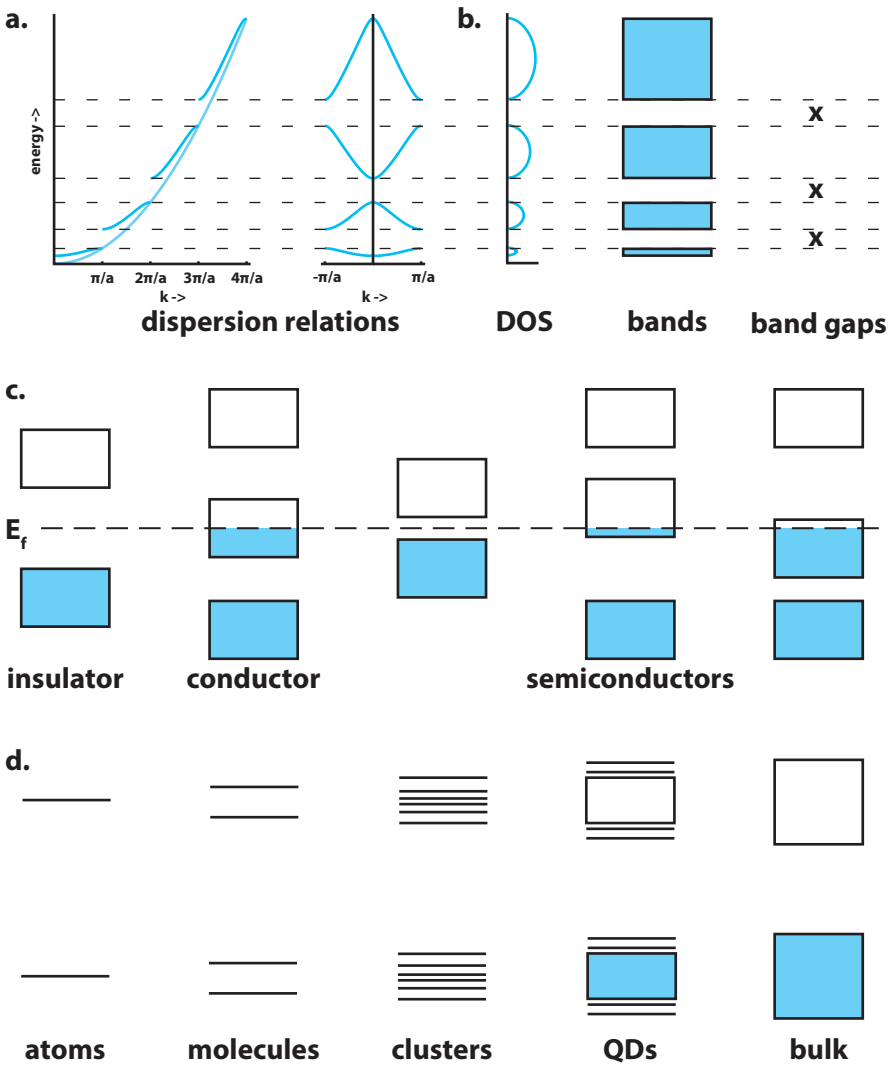

Figure 1.3. Models towards explaining the electronic behavior of bulk crystals.
(a) a Kronig-Penney dispersion relation (31) for a 1D crystal in k-space and its reduction to the first Brillouin zone. (b) a typical density of states (DOS) diagram for the allowed energy-k combinations and its simplification to a band diagram. (c) the allowed bands are filled up with electrons to the Fermi energy (E_f). This determines the electronic nature of a material. (d) energy band diagrams can also be obtained through linear combination of atomic orbital (LCOA) theory. This method works particularly well for qualitatively explaining the optoelectronic behavior of small atomic ensembles.

• • • •

Logically, filling up a band only partly with electrons will result in an electrical conductor. Boundary cases also exist in which bands are almost filled up or almost empty. Those materials are called semiconductors. Materials with a filled band and an empty

band separated by a small band gap are also semiconductors. All crystalline materials of interest to this thesis are semiconductors of the latter category. See Figure 1.3c for a schematic band diagram representation of insulators, conductors and semiconductors.

Small and moderate band gap semiconductors, such as Si, are of great importance to the computer industry. By chemical doping and applying an external electrical potential, the occupation of the bands, and thus the number of electrons available for conduction can be manipulated in a fabulous way, forming the basis of the electronic transistor.

The bottom-up method towards band diagrams

Another way to arrive at a band structure (energy-wavevector) diagram that can be used to understand the optoelectronic behavior of a material is with the so-called 'bottom-up' method. In the bottom-up method, single atoms form the starting point, as opposed to a whole crystal in the Bloch wave method. An atom has discrete electronic orbitals. When atoms in close encounter start to interact, the electrons start to become delocalized over several atoms. This coupling is described by the construction of molecular orbitals built up from a linear combination of atomic orbitals (LCAO method). A number N of atomic orbitals result in N molecular orbitals with discrete energies below (bonding) and above (anti-bonding) the energy of the atomic orbitals (28, 32, 33).

If the electronic coupling occurs over many atoms in three dimensions, the system reminisces a bulk solid close enough. The molecular orbitals are then organized in quasi-continuous bands, separated by forbidden band gaps. See Figure 1.3d for a visualization of how to arrive at a band structure diagram via the bottom-up method. Such intuitive reasoning works surprisingly well for a qualitatively explanation of the optoelectronic properties of semiconductor materials and nanocrystalline semiconductors (quantum dots). For a more quantitative energy spectrum, energy-minimizing methods for the expectation values of each crystal orbital constructed by LCAO must be used.

1.2. Crystal growth processes and theories

Now that the technological and scientific relevance of crystals has been discussed, the readers may wish to know how crystals can be grown. It is instructional to first discuss the general principles behind crystal growth, before we summarize the crystallization methods that are currently used at the forefront of nanoscience.

The theory below is called the classic nucleation model. Interestingly, this model was developed when atomic theory and statistical thermodynamics were not yet widely accepted. It is mainly based on what was known at that time about bulk thermodynamics of phase equilibria, capillarity and diffusion. No atomistic monomer dynamics are considered. Nonetheless, the model provides a qualitative understanding of the energetics of crystal nucleation and growth.

Intermezzo: quantum dots

It´s impossible to get away with not having a few words dedicated to quantum dots when doing research on semiconductor nanocrystals, even though this thesis focuses on self-assembly, and not on the optoelectronic properties, hence this intermezzo.

1.2

Quantum dots are nanoscale crystals made from semiconductor materials. Nanocrystalline materials alike to quantum dots have already been used throughout history as chromophores: as hair-dyes in ancient Egypt (34) and vibrant colorants in stained-glass (35). (Colors of metallic nanocrystals in stained-glass originate from collective electronic motions, called surface plasmon resonances (36).)

The scientific interest in quantum dots has tremendously increased over the past three decades. In earlier times, solid-state semiconductor QDs could only be synthesized in glasses or by vapor deposition (3). The invention of a colloidal synthesis of nanocrystalline quantum dots in organic non-polar suspensions (37), discussed in the main text under the hot injection method, provided suspended quantum dots with bright emission, which has recently led to the development of LCD's with quantum dot chromophores (6). The synthesis results in sterically stabilized nanocrystals in organic suspensions, which proved to be an appropriate starting point for the fabrication of new materials by nanocrystal self-assembly (38).

A quantum dot typically contains on the order of a thousand atoms, which is a lot, but not enough to be correctly described as a bulk material. This is where the bottom-up method described in the main text conveniently steps in. (In top-down methods, like the Bloch waves, the size tunable behavior is usually explained through quantum confinement of the excited electronic state.) Figure 1.3d shows where quantum dots roughly lie between single atoms and bulk materials in a bottom-up band diagram.

One of the striking optoelectronic properties of quantum dots are sharp emission and absorption peaks. This can be rationalized by the fact that the mixing of states through electronic coupling of atomic orbitals (LCAO) will quickly produce a lot of states in the middle of a band, but only few at its edges. The edge states slowly shift towards the energy band edges, as more atoms are added to the system. Quantum dots therefore have single discrete energy states at the edges of their bands and the exact position of these states is dictated by their size (39, 40). These properties give rise to sharp, size-tunable emission and absorption features. See Figure 1.4 for a beautiful example of the size-tunable optical properties of quantum dots.

Because this thesis focusses on self-assembly and crystallization rather than optoelectronics, the word "nanocrystal" will mostly be used instead of quantum dot throughout the rest of this work.

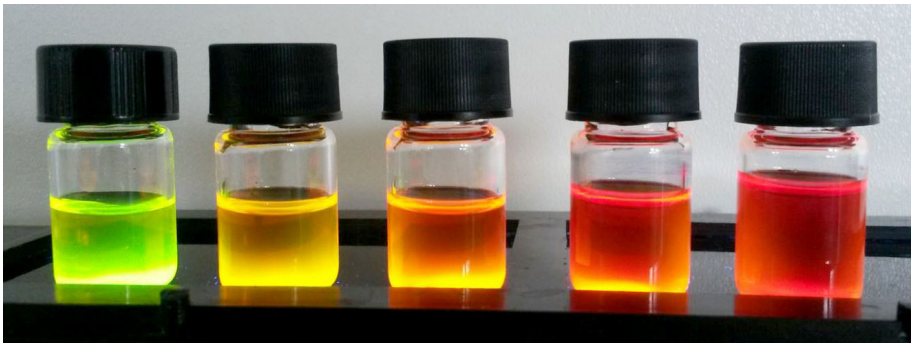

Figure 1.4. A 'rainbow' of InP nanocrystals that display size dependent optoelectronic properties: the wavelength of the emitted light decreases with a decrease in nanocrystal size, this effect is called quantum confinement; image courtesy Elleke van Harten.

1.2.1. Thermodynamic warm-up

A very basic starting point in thermodynamics is the internal energy of a system given by the formula:

Eq.1.4 $$U = TS + pV + \sum_{i=1}^{n} \mu_i N_i + \cdots$$

which is basically an endless summation over all conjugate intensive and extensive variables (28).

For bulk systems the only relevant variables are the first four: temperature, entropy, pressure and volume. Willard Gibbs recognized that from such a system the maximum amount of energy that can be extracted and converted (at constant volume) to work is:

Eq.1.5 $$dG = Vdp - SdT$$

which is the change in the so-called Gibbs free energy (41). An important property of the change in Gibbs free energy is that its sign predicts whether a process is spontaneous or not. A negative Gibbs free energy change means a process will spontaneously happen, a positive one means it won't.

1.2.2. Nucleation

Naturally, growing crystals has to start with something. This first clump of material that finally grows into a crystal is called a nucleus and forming one is the starting point for making crystals. Whether this process of nucleus formation, nucleation, is likely to

happen can be described by the associated change in Gibbs free energy:

Eq.1.6 $$\Delta G_{nucleation} = G_{crystal} - G_{liquid}$$

Usually the atomic or molecular precursors that will form a crystal are in the gas phase or dissolved in a liquid. The latter will be the case in the present thesis.

1.2

Crystallization can be rationalized by the fact that monomers can maximize their favorable interactions in a solid material with neighboring monomers. However, this holds only for the bulk part of the crystal and not at its surface. Still, both the monomers on the surface and in the bulk lose their freedom of motion, i.e. their translational entropy. This trade-off in energies, i.e. $\Delta G_{nucleation}$, is therefore usually expressed a bulk term promoting and a surface term inhibiting crystallization, respectively.

The relevant thermodynamic variables for creating a new (solid) phase and a surface are the chemical potential and the surface tension (1, 42, 43). A chemical potential describes how comfortable a chemical species is in a given state, in this case either the crystal or the liquid state. A surface tension defines the energy penalty per formed surface. The Gibbs free energy for nucleation then becomes, assuming a spherical nucleus:

Eq.1.7 $$\Delta G_{nucleation} = \frac{4}{3}\pi r^3 \rho \Delta\mu + 4\pi r^2 \gamma$$

in which γ is the surface tension, ϱ the density and $\Delta\mu$ the difference in chemical potential for the chemicals in the crystal and the liquid state.

The first term in the equation scales with r^3 and the second one with r^2. Thus, if $\Delta\mu$ is negative, then making a big crystal will always be favorable. However, the surface tension γ is always positive. Therefore, making a small crystal might not be favorable at all. The break-even point can be found by differentiation of $\Delta G_{nucleation}$ with respect to r which results in:

Eq.1.8 $$r_c = \frac{2\gamma}{\rho|\Delta\mu|}$$

which is called the critical radius of nucleation. Controlling this barrier is essential in the hot injection method discussed below.

In conclusion, randomly formed nuclei with a radius smaller than this value will redissolve into the so-called 'mother liquid', while bigger nuclei can grow further. This is graphically depicted in Figure 1.5a.

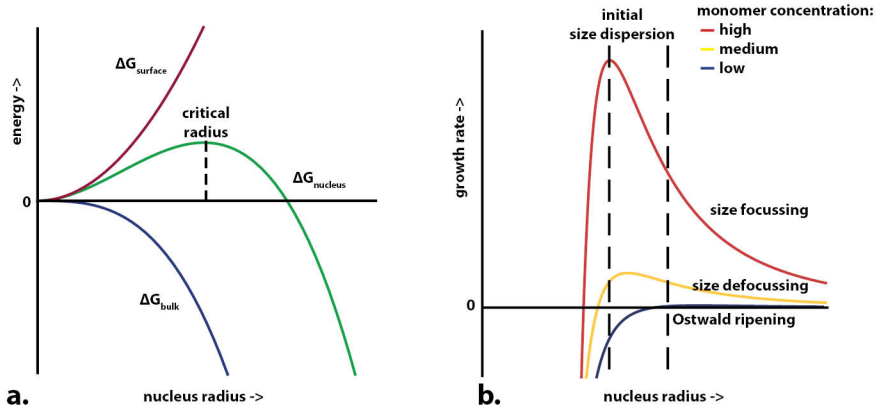

Figure 1.5. Graphs of thermodynamic formulae from classic nucleation theory for describing crystal nucleation and growth.
(a) the Gibbs free energy change for creating a crystal nucleus can be divided in two dominant contributions: 1) the energy penalty for creating a surface, which is dominant in small crystallites, 2) the energy release for creating a solid phase, which is dominant in big crystallites. This balance causes only crystallites with a radius bigger than the critical radius to grow. Smaller ones redissolve. (b) by expressing the Gibbs-Thompson relation in terms of the critical radius and combining it with Fick's law of diffusion, the growth rate of crystallites can be predicted as a function of their radius and the monomer activity. The plots show that a high monomer activity generally favors further growth towards a monodisperse ensemble of particles and vice versa.

1.2.3. Growth

Now that it should be clear why and how crystal nuclei form, crystal growth can be discussed. By simple extrapolation of the formula above it can be seen that adding more material, i.e. monomers, to a crystal is a spontaneous process.

Intuitively, the classic nucleation theory can be expanded by considering that small, but stable, nuclei are more reactive than very stable big nuclei. The former will therefore grow faster by quickly taking up monomers, as long as those are available in its surrounding liquid. A more accurate formula on crystal growth that takes these considerations into account can be derived by inserting the critical nucleation radius into the Gibbs-Thompson relation and combining it with Fick's law of diffusion:

Eq.1.9
$$\frac{dr}{dt} = \frac{\gamma D a_0}{\rho^2 k_b T}\left(\frac{1}{r_c r} - \frac{1}{r^2}\right)$$

in which D is the diffusion constant and a_0 the equilibrium monomer activity between a crystal and a liquid phase (43, 44). The monomer activity is used here instead of simply the monomer concentration, because the former more realistically takes into

account that monomers do not go to the crystal phase by definition. Some might want to linger in the liquid phase for entropic reasons. For practical purposes though, the monomer activity can be read as the concentration in all further considerations.

Figure 1.5b shows three plots of this function with a high, medium and low monomer concentration, respectively. It can easily be seen that the function correctly predicts that small crystals grow faster at a high monomer activity. This counteracts a size dispersion in crystallites and vice versa. Also, it still correctly shows that crystals with a radius smaller than the critical one have a negative growth rate, i.e. they will redissolve.

Ostwald ripening

Also, as crystal growth proceeds, the concentration and thereby the activity of the monomers decreases. At some point this is likely to cause a lot of small crystallites to go into the negative growth regime. This is depicted in Figure 1.5b. The big crystallites, however, stay in the positive growth regime. The end of the story is then logically that only a few big crystallites remain or at least the size dispersion in crystallites notably increases. This somewhat capitalist process in crystallization is called Ostwald ripening (28, 45).

1.2.4. Crystal facets

Classic nucleation theory predicts that crystals should be spherical in shape to minimize their surface energy penalty. This is in striking discrepancy with reality as macroscopic crystals show clear facets. It is caused by the ignorance of the classic nucleation theory that a crystal is an ordered structure of discrete building blocks.

Wulff construction

Because a crystal is a regular array of monomers, not any shape is possible. The edge of a crystallite also has to be built up from an integer amount of monomers in a regular array, i.e. a crystal facet. Naturally, not every facet is energetically just as favorable. The equilibrium shape of a crystal can be predicted by determining the surface tension of possible facets and minimizing the total energy penalty of the complete surface. This method for predicting a crystal's shape is called the Wulff construction (1, 46).

Heterogenous nucleation

The growth of a new layer of material on a perfect facet has to start with an atomic nucleus on top of that facet. Thus, we encounter here a problem similar to the original crystal nucleation. It can be stated that the nucleation of new crystal facets is held back by a line energy penalty, i.e. the energy necessary for creating the perimeter around a new layer of monomers. This facet nucleation is called heterogenous nucleation.

Some crystal facets have their monomers arranged in such a way that nucleating a new layer of monomers on top can be done with a moderate energy penalty. Crystals

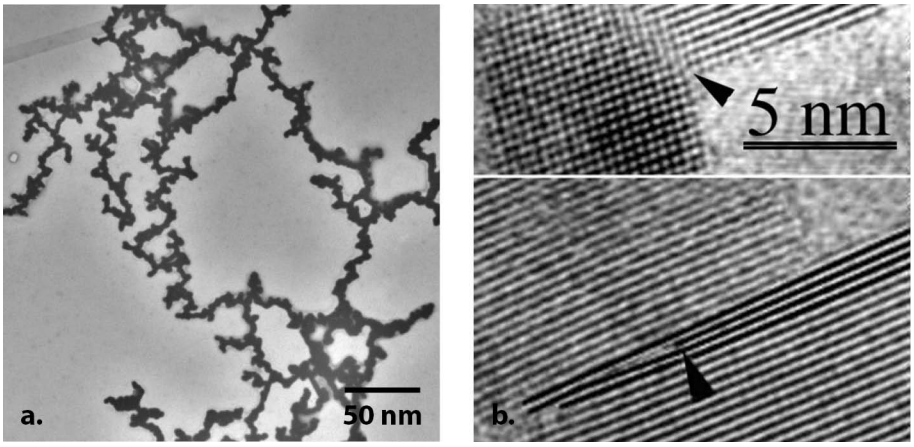

Figure 1.6. TEM images of attached nanocrystals.
(a) randomly attached PbSe nanocrystals that formed fractal-like agglomerates without any crystalline order. (b) TiO2 crystallites that performed oriented attachment; image taken from ref. (49). Oriented attachment can produce perfectly crystalline structures, but can also form slightly misaligned structures such as twin boundaries and edge dislocations as shown in these images.

• • • •

will grow faster in the direction of those facets and vice versa. Also, some facets might simply be sterically hindered to grow any further.

Still, creating new facets usually costs more than the available thermal energy. The temperature at which spontaneous new layers of monomers can form on a facet is called the roughening temperature. Below this temperature crystals might still be able to grow, but then this usually happens at (reactive) dislocation sites (1, 47).

1.2.5. Attaching crystallites

For simplicity, it was assumed in the discussion above that particles do not directly interact with each other during crystallization. This has worked fairly well in describing crystal growth theory so far. There are however no practical constrictions for two particles bumping into each other. In fact, both particles could immediately lower their surface energy by clicking together.

Agglomeration

Formation of fractal networks from attaching particles has numerously been reported throughout the past century (48). However, these fractal structures are not crystalline on any length scale (beyond the particle size) and the process is therefore not considered as a crystallization process. The disorder can be explained by considering that the surfaces of these particles can lower their energy with such a great amount by attaching, that it happens in very little time. The reaction then happens irreversibly and the thermodynamic minimum, i.e. atomic periodicity, is highly unlikely to be reached.

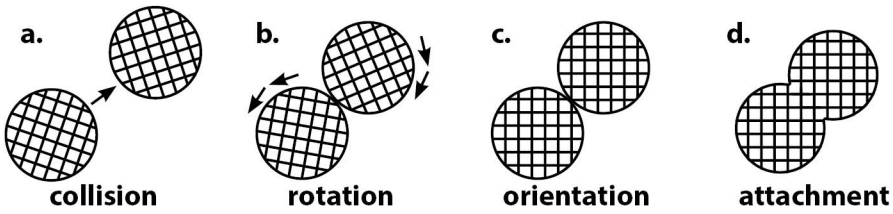

Figure 1.7. Schematic images of the oriented attachment process.
(a) crystallites randomly collide. The attraction between the atoms in the particle are strong enough to make the particles stick upon collision, but not strong enough to make them fuse instantaneously. (b) rotational Brownian motion causes the particles to probe each other's surface in many configurations. (c) interaction between the particles becomes much greater, if the particles randomly come into crystallographic alignment before they detach. (d) the particles fuse with atomic motion much faster than the Brownian motion of the individual crystals.

1.2

The system is stuck in a local thermodynamic minimum of suboptimally interacting and unordered atoms. See Figure 1.6a for an example of particles agglomerated by unorderly attaching.

Oriented attachment

Late in the past century, however, reproducible complex structures were also observed in crystallization studies. This hinted at the possibility that particles might not always attach randomly in solution. In 1992 this was tentatively described with "Not only the kinetics, but also the colloidal interactions must be understood to control the formation of unusual particle morphologies" (50). Also in mineralogy (51) and microbiology (52, 53) observations were made of crystal structures which were likely formed by epitaxial attachment of smaller crystals, also called oriented attachment.

Oriented attachment truly took off when it was used to explain the many defects that occur in natural crystals (49). Crystals formed by this "imperfect oriented attachment" were observed to possess screw dislocations, twinning and edge dislocations, shown in Figure 1.6b. This was an important discovery, because macroscopic crystals show such irregularities far more often than can be expected from very reversible processes like classic crystal nucleation and monomer-by-monomer growth.

Oriented attachment was later hypothesized to happen with weakly interacting colloidal crystallites (54, 55). This hypothesis was confirmed only several years later by direct observation with time-resolved high-resolution electron microscopy (56). The crystallites exhibit Brownian motion and can thereby probe each other's surfaces until the most favorable spot for attaching is found, the latter contrary to random agglomeration. This process is schematically depicted in Figure 1.7.

Of course, the particles do not necessarily attach in the thermodynamic minimum of perfectly ordered structures. They simply attach when the interactions of their constituent

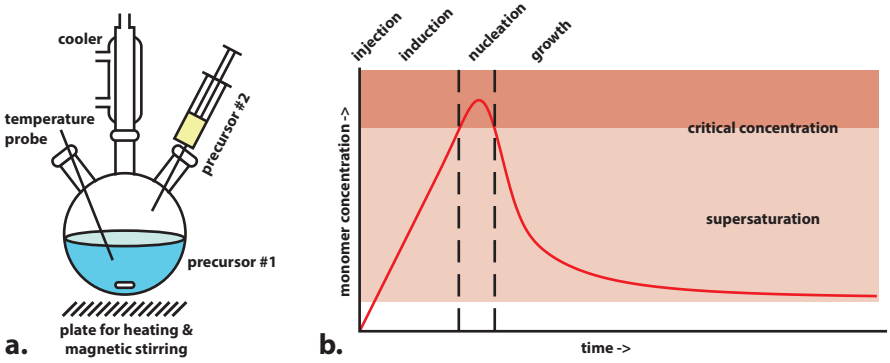

Figure 1.8. Schematic illustrations of equipment and theory for making monodisperse nanocrystals.
(a) laboratory set-up for the hot injection method. (b) LaMer diagram of the monomer concentration and resulting crystallization phases after injection in the hot injection method.

monomers become greater than the energy penalty of desorbing ligands or species from the surrounding liquid from their crystal facets. This is what causes the enhanced occurrence of defects when comparing structures formed by oriented attachment and monomer-by-monomer addition. Sometimes such imperfect crystals formed by oriented attachment 'repair' defects or protrusions by solution and reintegration of some of their monomers. This results in a more stable final structure, making such a self-repairing process somewhat reminiscent to Ostwald ripening (57).

Considering that oriented attachment can produce both very well-ordered structures, but not per se perfectly crystalline structures, it remains to be seen if oriented attachment will be considered simply as upgraded agglomeration or a true crystallization process in the future (58).

1.3. Crystal growth methods in nanoscience

A basic understanding of what makes crystals grow and what inhibits crystal formation has been established above. Now, we will describe the synthesis of colloidal nanocrystals used in the self-assembly studies in this thesis.

1.3.1. The hot injection method

The formation of superstructures by nanocrystal assembly necessitates a large ensemble of particles with a small size dispersion. The usual way to achieve this is via the hot injection method (37), which is an adaptation of the procedure from Viktor LaMer and Robert Dinegar for making monodisperse sulfur colloids (59).

In the hot injection method, one precursor liquid is heated to a few hundred degrees Celsius and then another precursor liquid at room temperature is rapidly injected. To prevent oriented attachment and particle flocculating during the synthesis, at least one of the precursors should be bound to a ligand species, usually a long carbohydrate chain. (Although for some nanocrystals oriented attachment might actually be part of the formation mechanism (60, 61).) Figure 1.8a presents a schematic drawing of a set-up for this procedure.

1.3

The rapid addition of the two precursors, in this thesis mainly Pb and Se, at high temperature causes a steep increase in the molecular, PbSe, monomer concentration. This is called the induction phase. See Figure 1.8b for a graph depicting the phases that the system goes through after injection. The chance of that PbSe monomers come together to form a (PbSe)n nucleus with radius above the critical radius increases markedly with an increasing monomer concentration.

Another way to describe the ensuing process is with the chemical potential. This depends on the concentration of a chemical species. The chemical potential of PbSe monomers is strongly enhanced during the induction phase. This potential and the Gibbs energy of the system can then be lowered by formation of stable crystal nuclei, see Equation 1.7. The concentration at which this happens is called the critical concentration. This phase of the hot injection process is called the nucleation phase.

Logically, the nucleation and growth of nanocrystals consumes monomers. By carefully tuning the concentration of the used precursors there will only be a very short time window during which nucleation is likely to happen. After that time, only already formed particles can grow further. This final phase is called the growth phase.

Note that nucleation and growth of particles are separated in the above process. As all particles were created at approximately the same time and grew in the same environment, the resulting particles should have a minimal size dispersion. Separation of nucleation and growth is an important concept for the formation of dispersions with nanocrystals with a low dispersity in their size (≤10 %).

Quenching of the growth for a small size dispersion

The particles can be left to grow until the monomer concentration has returned to the liquid's solubility limit again. This is material efficient, but usually a bad idea in terms of resulting sample quality. In most procedures, the monomer activity, i.e. reactivity, drops when the monomer concentration drops as well. As Figure 1.5b shows, this causes smaller particles to grow slower and bigger ones to grow faster. Eventually the particles might even start to perform Ostwald ripening.

Both these processes cause the size dispersion of the crystallites to increase (62). Therefore, the growth is usually quenched after a few minutes by injecting a cold liquid

into the reaction vessel. This 'freezes' the monomers in the nanocrystals, they do not have the energy anymore to go out of the crystal and redissolve into the liquid. Also, the temperature drops below the roughening temperature, i.e. no more heterogenous nucleation of new layers on existing crystallites can happen.

Ligands and anisotropy

Another important variable in the NC synthesis is the kind of ligands and other coordinating molecules that are present during the synthesis. The ligands might lower the surface energy of the nucleus, but also control the growth rate in a facet-specific fashion. Often, ligands bind only to a specific crystal facet inhibiting further growth in that direction. This can explain the formation of anisotropic particles such as two-dimensional nanoplatelets (63) or 'nanostars' (64).

1.3.2. Post-synthetic treatments

Although the nanocrystals made through the hot injection method are monodisperse and can already display interesting optoelectronic behavior, just making them is rarely the end point in any synthetic procedure in scientific literature. Some tweaks in their composition can greatly enhance their stability (65), processability (66) or luminescent properties (67). In fact, one of the strong features of nanocrystals is that they can usually be post-synthetically tailored to specific needs in relatively facile ways.

Ion exchange

A frequently used method in nanocrystal science is ion exchange (68, 69). In this procedure, the nanocrystals are dissolved in a liquid together with an ion bound to a coordinating molecule. The coordinating molecule should preferentially coordinate to one of the ions in the nanocrystal instead of the one it is coordinated to. Whether a molecule preferentially coordinates one or another ion is usually determined by hard-soft-acid-base theory. By exchanging ions on the nanocrystal surface and ion diffusion through the crystal, a nanocrystal can exchange one of its constituent ions. Ion exchange can also be employed to create core-shell nanocrystals and doped nanocrystals. A drawback of ion exchange is that it can usually only be performed for the smallest ion in the crystal, while the larger ion-type constitutes a stable structural frame. In the case of PbSe nanocrystals for instance, the Pb-ions can be exchanges for Cd-ions. Rock salt PbSe nanocrystals can be transformed in zinc blende CdSe nanocrystals in such a way.

Ion exchange is a valuable tool in nanoscience. First and foremost, this is because some interesting nanocrystal compositions, e.g. CuInS2 (70), are impossible to make by direct synthesis. Specifically, nanocrystals with more than two atomic building blocks are hard to make through direct synthesis, because balancing the chemistry of three or even more precursors in the hot injection method can be extremely hard. Second,

because nanocrystals are rather small and ion exchange is a diffusion process, it can be performed quite fast, at least compared to procedures for bulk materials.

SILAR

Another well-known post-synthetic treatment is successive ion layer adsorption and reaction, SILAR (71). With this procedure, extra layers of crystalline material are deposited on the nanocrystal. By alternatingly adding only one precursor and just enough for a single layer of material, nucleation of new nanocrystals is forestalled. SILAR is usually done with different materials than those that constitute the composition of the nanocrystal. This way, for example, the optoelectronic properties of the core crystal can be shielded from the surrounding medium, which can create nanocrystals with far more efficient luminescence.

Ligand exchange

Analogously to ion exchange, nanocrystals can be brought into contact with molecules that coordinate the nanocrystal better than its native ligands, upon which ligand exchange happens (72). This can be beneficial, because nanocrystals are usually made with large organic ligands on their surfaces to prevent oriented attachment and flocculation during synthesis. A logically limiting property is then that these nanocrystals cannot be processed in polar liquids (73). Also, envisioned devices for which nanocrystals have interesting optoelectronic properties, such as transistors and solar cells, necessitate that the nanocrystals are sufficiently electronically coupled (74). This is hardly the case when they are separated by their bulky non-conducting ligands. Also, the ligands of nanocrystals play an important role in their self-assembly (75).

1.4. Colloidal crystals

The theoretical thermodynamic framework discussed above was formulated very generally. It does not need to be applied solely to atomic crystallization. In fact, granular matter that is one or more orders of magnitude bigger, such as the nanocrystals discussed above, can form so-called colloidal crystals (76).

1.4.1. Colloids

The assumption underlying crystallization is that the monomer species can freely move around until they find a thermodynamic energy minimum so deep that they cannot get out. Atoms and molecules are not the only forms of matter that show such behavior. Robert Brown has been the first to observe and scientifically document such random motion for grain pollen suspended in water (77). This 'Brownian motion' has later been explained by the theoretical work from William Sutherland (78) and Albert Einstein (79) as thermal motion caused by collisions with atoms and molecules. The experiments from Jean Perrin (80) have established that this is indeed the case and matter is therefore granular, i.e. atomic, in nature.

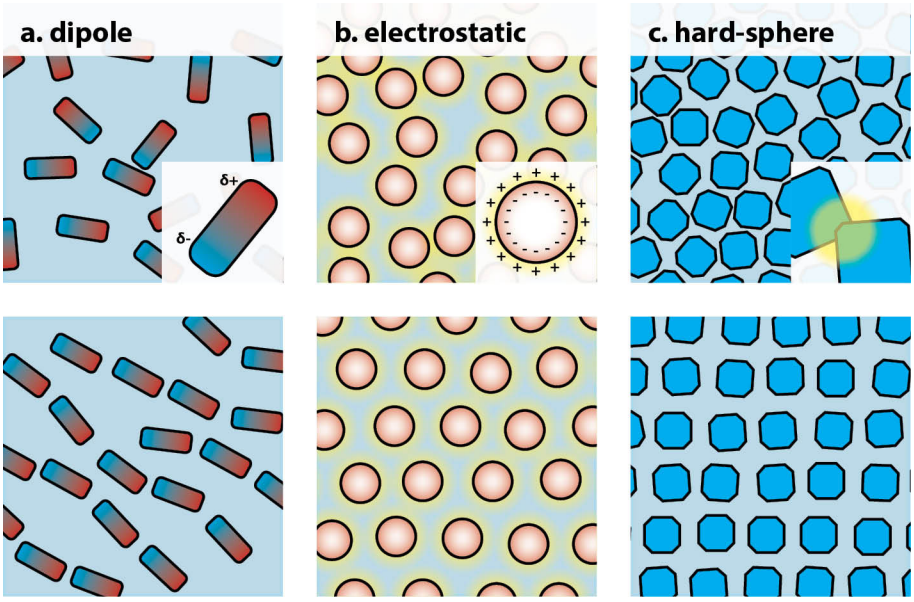

Figure 1.9. Schematic illustrations of direct particle-particle interactions that can occur between colloids in solution.
(a) dipoles in colloids can cause particle alignment and sometimes formation of linearly self-assembled structures. (b) electrostatic interactions can cause self-assembly based on attraction of opposite charges or repulsion of alike-charge. (c) even particles without any interaction but their 'hard-sphere' (Pauli exclusion) potential can self-assemble if this lowers the entropy of the system. (The hard-sphere potential is illustrated here with cubes to enhance the clarity of the figure.)

••••

Particles which show such behavior are called colloids. Usually colloidal behavior is observed for particles up to 1 μm in size, particles smaller than 1 nm are generally considered molecules or sometimes clusters. Colloidal behavior is immensely important for life on Earth. Proteins, DNA and lipid vesicles are all colloids. Human technology also broadly applies colloids, mainly in food processing, cosmetics and coatings. Deliberate human use of colloids can be dated back to ancient times, when inks were prepared by colloidally stabilizing soot particles in water with Arabic gum (81).

1.4.2. Self-assembly in theory

Like atoms and molecules, also colloids may find interacting with each other energetically more favorable than residing in a liquid phase. Equation 1.7 could in principle be reused to describe colloidal crystallization. However, colloidal interactions can be much more richly tuned than interactions between atoms and molecules. Also, the surface energies of making colloidal crystals are much smaller than those for atomic crystals. Therefore, instead of reusing Equation 1.7, the Gibbs free energy change for colloidal crystallization (at constant temperature) is usually described as:

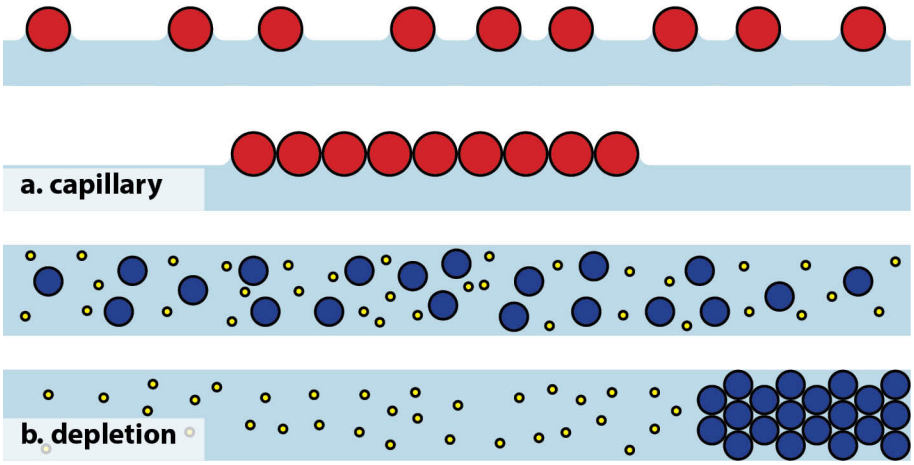

Figure 1.10. Schematic illustrations of indirect effects that can self-assemble colloids in solution.
(a) particles adsorbed at an interface have a preferred adsorption depth and wetting angle. This can cause an increase in the total surface area of the liquid, which costs energy. The liquid can reduce the extra amount of surface by pushing the particles together. (b) small particles contribute more to the entropy of a system than big particles. Big particles and the areas around them cannot be entered by the small particles. Forcing the big particles together reduces this 'excluded volume' for the small particles and so increases the total entropy of the system.

Eq1.10 $$dG = dH - TdS$$

in which H is the enthalpy of the system. Enthalpy can be seen as the heat that a system can release. In the case of colloidal crystallization heat is released when particles lower their energy with favorable interactions. This definition of the Gibbs free energy change can then be seen as a balance between the interaction potential of the colloids and the entropy of the system.

Colloids can be made to directly interact through Van der Waals or Coulombic forces by tuning their dipole moments or electrostatic charges (82). See Figure 1.9a and 9b for an illustration of such interactions. Colloids can also indirectly interact with each other through the medium in which they are dispersed. This can be done through depletion interaction (83): molecules also dispersed in the medium can increase their entropy by forcing the colloids to self-assemble. Also, a bulk liquid can decrease its total surface area by self-assembling particles at its interface, this happens through capillary interactions (84). See Figure 1.10a and 10b for a simple example illustration of such interactions.

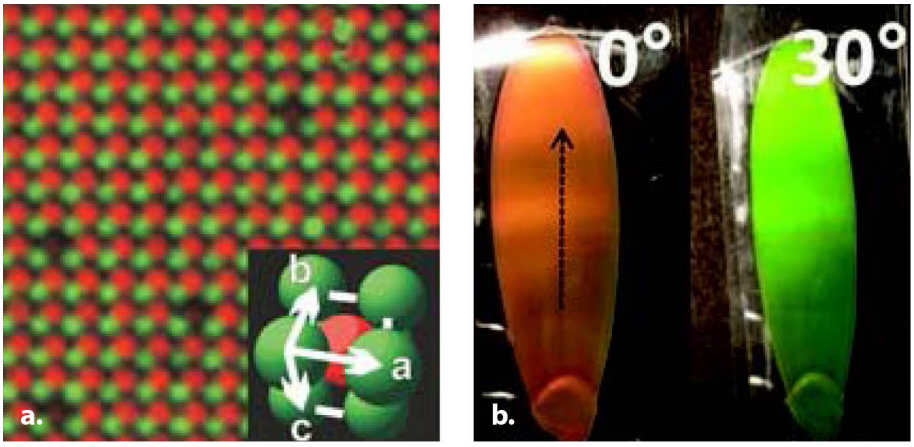

Figure 1.11. Examples of colloids used by science and technology.
(a) microscopy image of oppositely charged 1 μm PMMA colloids in an assembly resembling an ionic crystal lattice; image taken from ref. (86). Forming crystals with colloids allows for direct microscopic observation of a crystallization process, which is not (yet?) possible with atomic crystals. (b) a film of highly ordered polystyrene colloids with sizes close to the wavelength of light; image taken from ref. (93). Scattering in the material causes each wavelength of visible light to exit the material at a different angle, i.e. the material's color changes depending on the direction it is looked at.

Even without long-range interactions or medium effects colloids can show self-assembly. Colloids that have no interactions with each other, except for their excluded volume, are usually described as hard spheres. As the change in enthalpy for these systems is always zero, only their entropy dictates their behavior. Intuitively, one might think that such systems then always reside in a liquid-like state, or a glassy state when strongly confined. Contrary to these notions, it was later experimentally proven that even hard sphere systems can form colloidal crystals through self-assembly (76). Notably, this is the first scientific case in which computer simulated predictions were one step ahead of experiments and scientific consensus (85).

This peculiar crystallization without long-range interactions can be rationalized with the following consideration. The ensemble of colloids has more total entropy when each colloid has an average amount of freedom in movement instead of a few colloids having all freedom for moving around. See Figure 1.9c for an illustration of this effect. For dispersions of hard spheres, it is shown that the particle volume concentration can be increased to 49 %. Above this, crystallization sets on.

Applications

Colloids can function as model system to better understand 'regular' crystallization with the added benefit that colloids can be directly observed under a microscope. Figure

1.11a shows a beautiful example of oppositely charged colloids mimicking an ionic crystal (86). Colloidal self-assembly can also be used as a model system for biological processes, such as virus capsid assembly (87).

Besides as model systems, colloidal self-assembly is also used in industry. The use of colloids in the food industry, paints and thin-film passivation technology is well known, and will not be discussed further. In optoelectronics, strongly interacting cylindrical shaped colloids are used in liquid crystal displays or simply LCDs; the colloidal rod orientations are controlled by an external field and determine the brightness of pixels (88). Recently, E ink displays (89) were brought to the market. This technology uses colloids as colorants, allowing for non-light emitting screens, which is more energy efficient and more relaxing to look at.

In the case of colloidal crystals and superlattices, the energy vs. wavevector dispersion relation is a good way to describe the photonic or electronic band structure, as was discussed above for atomic crystals. The main difference compared to atomic lattices is the length scale of the periodic lattice. As colloids are much larger than atoms they interfere with light waves which are much larger (90). Natural opals (91) and some exotic beetles (92) display bright and speckled colors upon illumination because of interferences of light in the colloidal lattice. This effect has been copied by technology to create brightly colored opalescent materials that exhibit changing colors by varying the angle at which they are viewed (93). See Figure 1.11b for an example of such a material. Materials that controllably disperse light are also used as photonic waveguides with which perhaps all-optical computers might someday be realized.

1.4.3. Self-assembling colloidal nanocrystals in practice

The nanocrystals that were discussed above are usually around 5 nm in size. Of course, these particles behave as colloids in good solvents, usually apolar solvents like toluene, and can then be used in self-assembly procedures.

In solution, the particles have a lot of freedom of motion and are therefore high in entropy. According to Equation 1.10, either the colloids' enthalpy has to decrease through interactions or their entropy has to increase when forming crystals. Procedures for both approaches are found in scientific literature. The first and simplest one is by slowly evaporating the solvent of the particles (94). This decreases their freedom of motion in the solution and will eventually make particle self-assembly into an ordered state entropically positive, analogous to the hard-sphere crystallization. Another way is by adding a so-called anti-solvent to the solution, usually polar solvents like methanol (95). Anti-solvents unfavorably interact with the particles and thereby makes particle-particle interactions more favorable, resulting in a strong decrease of the enthalpy upon crystallization.

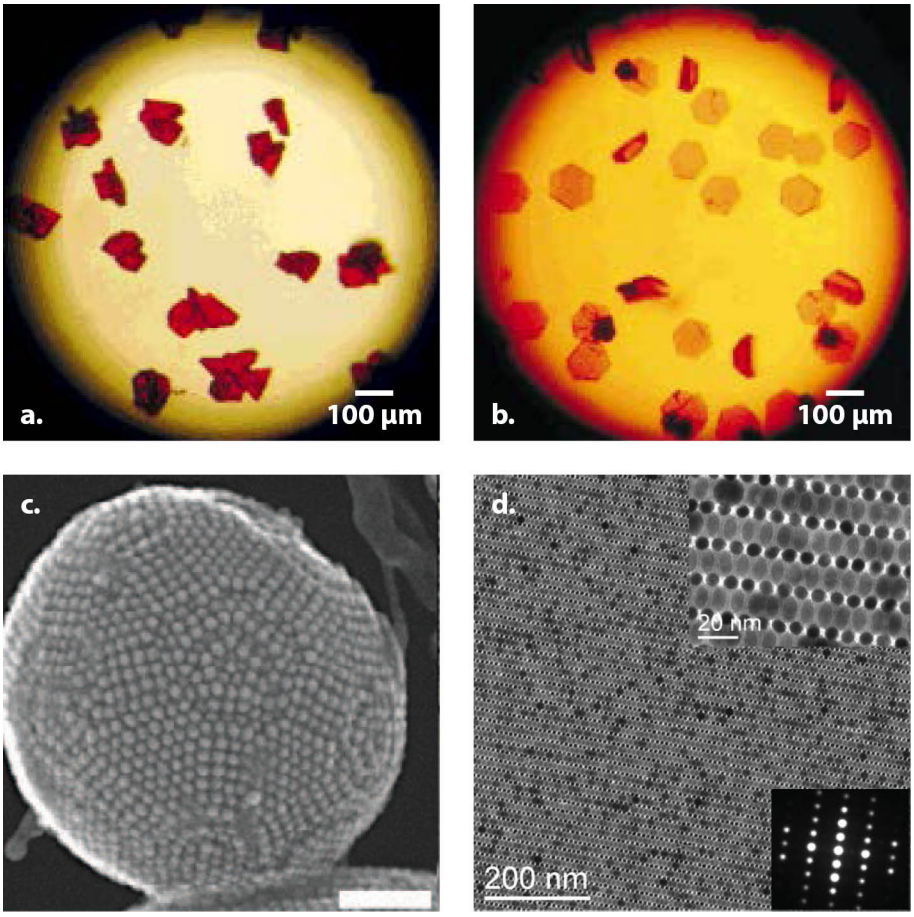

Figure 1.12. Example images of nanocrystal self-assembly.
(a) CdSe nanocrystals that have formed irregular assemblies by direct addition of a non-solvent. (b) CdSe nanocrystals that have formed highly-ordered hexagonal platelets by addition of the non-solvent through a buffer layer. The buffer layer slows down the addition of the non-solvent and thereby gives the particles more time to self-assemble. Images (a/b) taken from ref. (96). (c) 6 nm iron cobalt oxide nanocrystals self-assembled in icosahedrally packed spherical superlattices through spherical confinement of the self-assembly in emulsified droplets; image taken from ref. (97). (d) 15 nm iron oxide and 6 nm iron platinum nanocrystals self-assembled in a binary superlattice of only two unit cells thick through two dimensional confinement of the self-assembly in a thin liquid layer on an immiscible liquid substrate; image taken from ref. (98).

••••

Glasses

An important factor to consider in these procedures is time. If interaction potentials are increased at a too rapid pace the particles will stick at every collision. Then, they will not form an ordered crystal, but a glassy state analogous to the agglomeration of crystallites in solution. The trick in all crystallization procedures is to make it happen so slow and reversible that particles will only want to condense in the thermodynamic

minimum, i.e. a perfect crystal, and not in any other local minimum. The influence of time on self-assembly of nanocrystals is well exemplified by the images shown in Figure 1.12a and 12b (96).

Self-assembly in confinement

Particles that self-assemble in the bulk of the dispersion usually form large three-dimensional colloidal crystals. For some scientific studies, like in this thesis, it is however desired that the particles form anisotropic assemblies, e.g. two-dimensional structures that are one monolayer thick. This can be done by confining the volume in which the colloids are allowed to self-assemble. Two confinement regimes have been described in scientific literature so far.

First is the spherical confinement regime, which is created by emulsifying droplets of good solvent containing nanocrystals into a continuous phase of anti-solvent. The good solvent can gradually dissolve into the anti-solvent which usually has a higher boiling point than the good solvent. By heating the emulsion, the good solvent will then completely dissipate and spherical self-assemblies of nanocrystals are formed (97), as shown in Figure 1.12c.

The second confinement regime is two-dimensional. This is the confinement regime in which particles will be assembled throughout this thesis. Two-dimensional confinement is usually induced by drop casting a dilute nanocrystal dispersion in apolar solvent onto a polar liquid, acting as an immiscible liquid substrate. The good solvent with nanocrystals spreads over the surface of the substrate. After a while the good solvent will have evaporated to a degree that the colloids in suspension will start to self-assemble in the remaining liquid, producing assemblies as depicted in Figure 1.12d (98).

1.4.4. Other fields in self-assembly

Some other sub-fields of self-assembly will shortly be discussed to clarify the scope of this research.

Patchy particles

Scientific research has dedicated decades of research on describing the behavior of isotropic colloids, as this is the easiest starting point in understanding colloidal behavior. Also, other shapes like rods and platelets have been thoroughly investigated, but also these usually have an isotropic character as their surfaces are the same everywhere. Colloidal proteins in nature can have very anisotropic interaction potentials on their surfaces, which is most prominently exemplified by catalytic proteins. A lot of recent scientific studies are aimed at more biomimetic and so-called patchy colloids (99).

The nanocrystals in this study exhibit clear crystal facets on their surfaces. These surfaces all have different compositions and behavior, most clearly exemplified by

oriented attachment. Still, nanocrystals are usually not considered to be patchy particles, as their facets are intrinsic nanocrystal properties and not deliberately synthesized to be there. Though the fact that different crystal facets each have their own specific chemistry is important to remember throughout this thesis.

Self-assembly in external fields

So far only particle-medium and particle-particle interactions have been discussed. Particles can also interact with potentials resulting from external fields. The most common one is of course gravity, but also electric or magnetic potentials can be used to assemble colloids (100). These fields of science are only relevant to the work in this thesis through colloidal purification by centrifugal sedimentation.

Out of equilibrium self-assembly

The discussions on (colloidal) crystallization above are mostly concerned with spontaneous processes with a decrease of the free energy of the system until equilibrium, i.e. a thermodynamic minimum, is reached. The resulting structures are static and solid-like, except for thermal vibrations and rotations of their building blocks. Self-assembly that results in such structures is therefore called static self-assembly.

A whole other field of science is dynamic self-assembly, which concerns systems which require constant input of energy to preserve their state (101). For example, living cells need a perpetual influx of high-energy molecules to maintain their state. Dynamic self-assembly is thought to be far more complex than static self-assembly and research into this field is just starting up. Still, some examples of progress can be given, like self-assembly of colloids under shear (102) and colloidal microswimmers (103).

1.5. Measuring & modelling

Logic is of primary importance to modern science. Philosophers in ancient times even put so much trust in their collective capacities of deduction that they found it superior to any other form of finding truth. Founding fathers of modern science, such as Galileo Galilei, changed this paradigm: theory is great, but only if it can be backed up with experimental observation.

1.5.1. Microscopy

The primary system of interest in this thesis, nanocrystals, cannot be directly observed by the human eye, because they are too small. Like Galileo had a telescope to observe the heavenly objects, modern science uses microscopes to observe the microscopic world. Still, nanocrystals are much smaller than the wavelength of visible light and can therefore not be individually observed in ensembles by regular light microscopy.

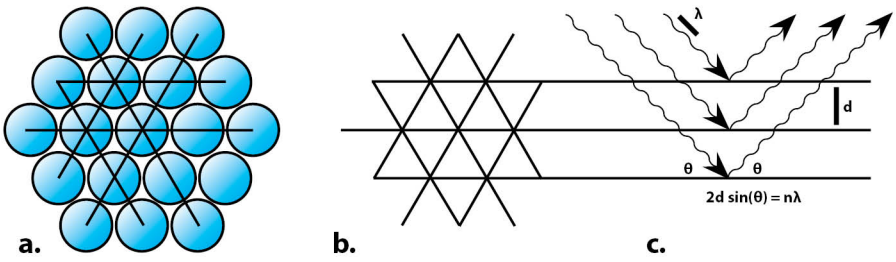

1.5

Figure 1.13. Schematic illustration of the Bragg model of diffraction.
(a) schematic illustration of a crystal lattice. (b) the layers of monomers in a crystal lattice can be simplified as stacks of planes. (c) the regular periodic nature of the crystal causes waves reflecting on these planes to interfere such that the waves can only exit the crystal at fixed angles depending on their wavelength.

• • • •

Electrons accelerated over potentials of multiple kV to high velocities can reach much shorter wavelengths, as is shown by Equation 1.2. This way, scattering interactions of such an electron beam with a sample can be localized to much smaller domains, sometimes even showing atomic contrast. Methods of imaging that harness this principle are together called electron microscopy (104).

In this thesis, transmission electron microscopy (TEM) will used as a standard technique to investigate nanocrystals and the structures they form by self-assembly and oriented attachment. With TEM, electrons impinging on the sample at high speeds. When they collide with sample material, some of them are scattered. By collecting only the light that was not scattered, a 'shadow image' of the sample can be obtained. Technically harder to achieve, but possible, is collecting only the scattered electrons from a focused spot on the sample. The latter technique is referred to as high-angle annular dark-field scanning TEM (HAADF-STEM). For samples composed of somewhat heavier chemical elements, which is the case in this thesis, it has a superior image contrast over TEM, but also a longer image recording time. Both techniques rely on electron transmission and therefore can only be used on thin samples. This is no problem in this thesis, as here only two-dimensional structures are of interest.

1.5.2. Scattering & diffraction

When waves interact with matter without exchange of energy, it is called elastic scattering. In this thesis, only elastic scattering experiments are used. Furthermore, the interaction between the waves and samples in this thesis is rather weak. It can then be assumed that each wave has only one scattering interaction in the sample. This is called the single scattering regime.

Intermezzo: nomenclature

In this thesis, colloidal crystals are studied; they consist of regular arrays of colloidal nanocrystals; each nanocrystal building block on itself being a regular array of atoms. Also, diffraction at the atomic lattice should be clearly distinguished from diffraction from the ordered array of nanocrystals in the colloidal crystal. For these reasons, it might be useful to define the use of ambiguous words at least for the rest of use of this thesis.

The word "crystals" will be used here in the classical meaning: a regular array of atoms "Superlattices" will indicate regular arrays with colloids as their principal building blocks. "Superstructures" will be considered superlattices in which the colloids are nanocrystals and have performed oriented attachment. "Supercrystals" will be used for superstructures in which the particles have performed oriented attachment with such perfect precision that there is a long-range atomic coherency over multiple nanocrystal building blocks. "Agglomerates" will be considered structures that show no larger-scale order than that of the atoms in their constituent building blocks.

"Scattering" will be used here for the interaction of light with the nanocrystal superlattice planes in a superstructure. It is harder make such an exact definition for "diffraction" as it used on both nanocrystal superlattice and atomic planes. Still, it will mostly be used here for the interaction of light with the atomic lattice planes.

Interactions between waves is called interference. The extreme cases of interference are 1) constructive interference in which waves with a similar wavelength and phase amplify each other, and 2) destructive interference in which waves with a similar wavelength but half a period difference in phase damp each other.

When periodic materials are shone upon with light (or electron-waves), the regular ordering of the constituent particles causes regular phase changes between the scattered waves. Therefore, when these materials are illuminated by a monochromatic and unidirectional light beam, the light can only exit them at specific angles upon scattering and interference. This effect is called diffraction and is schematically depicted in Figure 1.13. Rationalizing this process in reverse order: by measuring diffracted beams from a sample, its internal periodic structure can be determined. The logic connecting diffraction to order in a material is the definite prove that crystals are indeed a periodic array of chemical species (105).

Scattering and diffraction are pivotal techniques in this thesis. The subject has, however, not been given the space in this theoretical introduction it perhaps deserves, as reference can be made to a recently published fantastic overview of the deeper theory behind these techniques (106).

1.5.3. Spectroscopy

As discussed in the intermezzo on quantum dots, semiconductor nanocrystals have size-dependent light absorption and emission behavior. Spectroscopy of quantum dots is a field of science on its own, but in this thesis it will only be employed to measure the monodispersity and average ensemble size of lead chalcogenide nanocrystals (107).

1.5.4. Computer modelling

1.5

By observing a sample, its behavior can be determined. It is a whole lot harder to actually understand a sample's behavior. Until relatively recently, theory and experiment were the only tools for scientific work. The development of automated calculations on computers has created a third option: modelling. The true power of modelling is that some theories cannot be solved analytically or simply take very long for humans to solve manually, increasing the chance of errors.

Simulations

Systems that involve many particles can only be described correctly by a manually unsolvable amount of equations. Computers can solve many equations numerically with such speed that at least statistical predictions of such systems can be done. This way, predictions for new systems can be made based on existing theories or theories about experimentally new systems can be validated. The latter is employed in this thesis (108).

Calculating optoelectronic properties

Another field of computer modelling is solving tediously large equations. Correctly calculating the values in quantum mechanical states of dopant ions in a crystal lattice or the gravitational fields of a spaceship flying to the Moon would take humans far longer than a computer and they would probably make lots of errors in the process.

In fact, the work in this thesis is motivated by atomistic calculations predicting surprising and highly interesting electronic band structures of 2D supercrystals formed by oriented attachment of nanocrystals (21–24).

References

1. Hurle, D. T. J. Handbook of Crystal Growth. (1993).

2. Molčanov, K. & Stilinović, V. Chemical Crystallography before X-ray Diffraction. Angew. Chemie Int. Ed. 53, 638–652 (2014).

3. Springer Handbook of Crystal Growth. (Springer Berlin Heidelberg, 2010). doi:10.1007/978-3-540-74761-1

4. Meijerink, A., Wegh, R., Vergeer, P. & Vlugt, T. Photon management with lanthanides. Opt. Mater. (Amst). 28, 575–581 (2006).

5. MAIMAN, T. H. Stimulated Optical Radiation in Ruby. Nature 187, 493–494 (1960).

6. Nanocrystals in their prime. Nat. Nanotechnol. 9, 325–325 (2014).

7. Rohani, S., Horne, S. & Murthy, K. Control of Product Quality in Batch Crystallization of Pharmaceuticals and Fine Chemicals. Part 1: Design of the Crystallization Process and the Effect of Solvent. Org. Process Res. Dev. 9, 858–872 (2005).

8. Eranna, G. Crystal Growth and Evaluation of Silicon for VLSI and ULSI. (CRC Press, 2016).

9. Wlodawer, A., Minor, W., Dauter, Z. & Jaskolski, M. Protein crystallography for aspiring crystallographers or how to avoid pitfalls and traps in macromolecular structure determination. FEBS J. 280, 5705–5736 (2013).

10. Behar, R. Sucre blanc cassonade complet rapadura. Wikimedia commons (2006). Available at: https://commons.wikimedia.org/w/index.php?title=File:Sucre_blanc_cassonade_complet_rapadura.jpg&oldid=195651564. (Accessed: 3rd October 2017)

11. Bonnard, J. B. Broche van goud en amethist. Rijksmuseum (1824).

12. Lincetto, M. No Title. Wikimedia commons (2008). Available at: https://commons.wikimedia.org/w/index.php?title=File:Silicon_single_crystal.jpg&oldid=154705756.

13. Steno, N. De solido intra solidum naturaliter contento Dissertationis Prodromus, sub signo Stellae. (1669).

14. Hauy, R.-J. Essai d'une theorie sur la structure des crystaux. (Gogue & Ne de La Rochelle, 1784).

15. Miller, W. H. A treatise on crystallography. (J. & J. J. Deighton, 1839).

16. Haüy, R. J. Traité de minéralogie. (Chez Louis, 1801).

17. Boneschanscher, M. P. et al. Long-range orientation and atomic attachment of nanocrystals in 2D honeycomb superlattices. Science (80-.). 344, 1377–1380 (2014).

18. Peters, J. L. et al. Ligand-Induced Shape Transformation of PbSe Nanocrystals. Chem. Mater. 29, 4122–4128 (2017).

19. Bravais, A. Etudes Crystallographiques. (Gauthier-Villars, 1866).

20. Of, I. U. & CRYSTALLOGRAPHY. Nobel Prize winners associated with crystallography. Available at: https://www.iucr.org/people/nobel-prize. (Accessed: 3rd October 2017)

21. Kalesaki, E. et al. Dirac Cones, Topological Edge States, and Nontrivial Flat Bands in Two-Dimensional Semiconductors with a Honeycomb Nanogeometry. Phys. Rev. X 4, 11010 (2014).

22. Delerue, C. & Vanmaekelbergh, D. Electronic band structure of zinc blende CdSe and rock salt PbSe semiconductors with silicene-type honeycomb geometry. 2D Mater. 2, 34008 (2015).

23. Beugeling, W. et al. Topological states in multi-orbital HgTe honeycomb lattices. Nat. Commun. 6, 1–7 (2015).

24. Delerue, C. From semiconductor nanocrystals to artificial solids with dimensionality below two. Phys. Chem. Chem. Phys. 16, 25734–25740 (2014).

25. Newton, I. Philosophiæ Naturalis Principia Mathematica. (Edmund Halley, 1687).

26. Young, H. D. & Freedman, R. A. University Physics with Modern Physics. (Pearson, 2007).

27. Broglie, L.-V. de. RECHERCHES SUR LA THEORIE DES QUANTA. (1924).

28. Ball, D. W. Physical Chemistry. (Brooks/Cole - Thompson Learning, 2002).

29. Bloch, F. Uber die Quantenmechanik der Elektronen in Kristallgittern. Zeitschrift f r Phys. 52, 555–600 (1929).

30. Kittel, C. Introduction to Solid State Physics. (Wiley, 1996).

31. de L. Kronig, R. & Penney, W. G. Quantum Mechanics of Electrons in Crystal Lattices. Proc. R. Soc. A Math. Phys. Eng. Sci. 130, 499–513 (1931).

32. Jones, J. E. On the Determination of Molecular Fields. II. From the Equation of State of a Gas. Proc. R. Soc. A Math. Phys. Eng. Sci. 106, 463–477 (1924).

33. Hickel, E. Quantentheoretische Beitrage zum Benzolproblem. Zeitschrift fur Phys. 70, 204–286 (1931).

34. Walter, P. et al. Early Use of PbS Nanotechnology for an Ancient Hair Dyeing Formula. Nano Lett. 6, 2215–2219 (2006).

35. Freestone, I., Meeks, N., Sax, M. & Higgitt, C. The Lycurgus Cup — A Roman nanotechnology. Gold Bull. 40, 270–277 (2007).

36. Mulvaney, P. Not All That's Gold Does Glitter. MRS Bull. 26, 1009–1014 (2001).

37. Murray, C. B., Norris, D. J. & Bawendi, M. G. Synthesis and characterization of nearly monodisperse CdE (E = sulfur, selenium, tellurium) semiconductor nanocrystallites. J. Am. Chem. Soc. 115, 8706–8715 (1993).

38. Vanmaekelbergh, D. Self-assembly of colloidal nanocrystals as route to novel classes of nanostructured materials. Nano Today 6, 419–437 (2011).

39. Bawendi, M. The Quantum Mechanics Of Larger Semiconductor Clusters (. Annu. Rev. Phys. Chem. 41, 477–496 (1990).

40. Alivisatos, A. P. Perspectives on the Physical Chemistry of Semiconductor Nanocrystals. J. Phys. Chem. 100, 13226–13239 (1996).

41. Gibbs, J. W. A Method of Geometrical Representation of the Thermodynamic Properties of Substances by Means of Surfaces. Trans. Connect. Acad. Arts Sci. 2 382–404 (1873).

42. Thomson, W. 4. On the Equilibrium of Vapour at a Curved Surface of Liquid. Proc. R. Soc. Edinburgh 7, 63–68 (1872).

43. Putnis, A. Introduction to mineral sciences. (Cambridge University Press, 1992).

44. Fick, A. Ueber Diffusion. Ann. der Phys. und Chemie 170, 59–86 (1855).

45. Ostwald, W. Studien über die Bildung und Umwandlung fester Körper. Zeitschrift für Phys. Chemie 22U, (1897).

46. Wulff, G. Zur Frage der Geschwindigkeit des Wachstums und der Auflösung der Krystallflächen. Zeitschrift für Kryst. und Mineral. 449–530 (1901).

47. Burton, W. K., Cabrera, N. & Frank, F. C. The Growth of Crystals and the Equilibrium Structure of their Surfaces. Philos. Trans. R. Soc. A Math. Phys. Eng. Sci. 243, 299–358 (1951).

48. Lin, M. Y. et al. Universality in colloid aggregation. Nature 339, 360–362 (1989).

49. Penn, R. L. & Banfield, J. F. Imperfect Oriented Attachment: Dislocation Generation in Defect-Free Nanocrystals. Science (80-.). 281, 969–971 (1998).

50. Bailey, J. K., Brinker, C. J. & Mecartney, M. L. Growth Mechanisms of Iron Oxide Particles of Differing Morphologies from the Forced Hydrolysis of Ferric Chloride Solutions. J. Colloid Interface Sci. 157, 1–13 (1993).

51. Penn, R. L. & Banfield, J. F. Oriented attachment and growth, twinning, polytypism, and formation of metastable phases; insights from nanocrystalline TiO 2. Am. Mineral. 83, 1077–1082 (1998).

52. Onuma, K. & Ito, A. Cluster Growth Model for Hydroxyapatite. Chem. Mater. 10, 3346–3351 (1998).

53. Banfield, J. F., Welch, S. A., Zhang, H., Ebert, T. T. & Penn, R. L. Aggregation-Based Crystal Growth and Microstructure Development in Natural Iron Oxyhydroxide Biomineralization Products. Science (80-.). 289, 751–754 (2000).

54. Niederberger, M. & Cölfen, H. Oriented attachment and mesocrystals: non-classical crystallization mechanisms based on nanoparticle assembly. Phys. Chem. Chem. Phys. 8, 3271–87 (2006).

55. Dalmaschio, C. J., Ribeiro, C. & Leite, E. R. Impact of the colloidal state on the oriented attachment growth mechanism. Nanoscale 2, 2336 (2010).

56. Li, D. et al. Direction-specific interactions control crystal growth by oriented attachment. Science 336, 1014–8 (2012).

57. Zhang, J., Huang, F. & Lin, Z. Progress of nanocrystalline growth kinetics based on oriented attachment. Nanoscale 2, 18–34 (2010).

58. De Yoreo, J. J. et al. Crystallization by particle attachment in synthetic, biogenic, and geologic environments. Science (80-.). 349, aaa6760-aaa6760 (2015).

59. LaMer, V. K. & Dinegar, R. H. Theory, Production and Mechanism of Formation of Monodispersed Hydrosols. J. Am. Chem. Soc. 72, 4847–4854 (1950).

60. Liao, H.-G., Cui, L., Whitelam, S. & Zheng, H. Real-time imaging of Pt3Fe nanorod growth in solution. Science 336, 1011–4 (2012).

61. Schliehe, C. et al. Ultrathin PbS sheets by two-dimensional oriented attachment. Science 329, 550–3 (2010).

62. Abé, S., Karel, R., Geyter, B. De & Hens, Z. Tuning the Post-Focused Size of Colloidal Nanocrystals by the Reaction Rate : from theory to application. 1–11

63. Ithurria, S. & Dubertret, B. Quasi 2D Colloidal CdSe Platelets with Thicknesses Controlled at the Atomic Level. 16504–16505 (2008).

64. Houtepen, A. J., Koole, R., Vanmaekelbergh, D., Meeldijk, J. & Hickey, S. G. The hidden role of acetate in the PbSe nanocrystal synthesis. J. Am. Chem. Soc. 128, 6792–3 (2006).

65. Woo, J. Y. et al. Ultrastable PbSe Nanocrystal Quantum Dots via in Situ Formation of Atomically Thin Halide Adlayers on PbSe(100). J. Am. Chem. Soc. 136, 8883–8886 (2014).

66. Yang, Y. et al. Entropic Ligands for Nanocrystals: From Unexpected Solution Properties to Outstanding Processability. 6–11 (2016). doi:10.1021/acs.nanolett.6b00730

67. Hines, M. A. & Guyot-Sionnest, P. Synthesis and Characterization of Strongly Luminescing ZnS-Capped CdSe Nanocrystals. J. Phys. Chem. 100, 468–471 (1996).

68. Rivest, J. B. & Jain, P. K. Cation exchange on the nanoscale: an emerging technique for new material synthesis, device fabrication, and chemical sensing. Chem. Soc. Rev. 42, 89–96 (2013).

69. Beberwyck, B. J., Surendranath, Y. & Alivisatos, A. P. Cation Exchange : A Versatile Tool for Nanomaterials Synthesis. (2013).

70. van der Stam, W. et al. Luminescent CuInS 2 Quantum Dots by Partial Cation Exchange in Cu 2– x S Nanocrystals. Chem. Mater. 27, 621–628 (2015).

71. Li, J. J. et al. Large-Scale Synthesis of Nearly Monodisperse CdSe / CdS Core / Shell Nanocrystals Using Air-Stable Reagents via Successive Ion Layer Adsorption and Reaction. 933–937 (2003).

72. Anderson, N. C., Hendricks, M. P., Choi, J. J. & Owen, J. S. Ligand Exchange and the Stoichiometry of Metal Chalcogenide Nanocrystals: Spectroscopic Observation of Facile Metal-Carboxylate Displacement and Binding. (2013).

73. Kovalenko, M. V., Scheele, M. & Talapin, D. V. Colloidal Nanocrystals with Molecular Metal Chalcogenide Surface Ligands. Science (80-.). 324, 1417–1420 (2009).

74. Talapin, D. V, Lee, J., Kovalenko, M. V & Shevchenko, E. V. Prospects of Colloidal Nanocrystals for Electronic and Optoelectronic Applications. 389–458 (2010).

75. Boles, M. a & Talapin, D. V. Many-body effects in nanocrystal superlattices: departure from sphere packing explains stability of binary phases. J. Am. Chem. Soc. 137, 4494–502 (2015).

76. Pusey, P. N. & van Megen, W. Phase behaviour of concentrated suspensions of nearly hard colloidal spheres. Nature 320, 340–342 (1986).

77. Brown, R. XXVII. A brief account of microscopical observations made in the months of June, July and August 1827, on the particles contained in the pollen of plants; and on the general existence of active molecules in organic and inorganic bodies. Philos. Mag. Ser. 2 4, 161–173 (1828).

78. Sutherland, W. LXXV. A dynamical theory of diffusion for non-electrolytes and the molecular mass of albumin. Philos. Mag. Ser. 6 9, 781–785 (1905).

79. Einstein, A. Über die von der molekularkinetischen Theorie der Wärme geforderte Bewegung von in ruhenden Flüssigkeiten suspendierten Teilchen. Ann. Phys. 322, 549–560 (1905).

80. Perrin, J. Mouvement Brownien et réalité moléculaire. Ann. Chim. Phys. (1909).

81. Jones, R. A. L. Soft Machines. (Oxford University Press, 2008).

82. Israelachvili, J. N. Van der Waals Forces. in Intermolecular and Surface Forces 107–132 (Elsevier, 2011). doi:10.1016/B978-0-12-375182-9.10006-5

83. Mao, Y., Cates, M. E. & Lekkerkerker, H. N. W. Depletion force in colloidal systems. Phys. A Stat. Mech. its Appl. 222, 10–24 (1995).

84. Chan, D. Y. ., Henry, J. . & White, L. . The interaction of colloidal particles collected at fluid interfaces. J. Colloid Interface Sci. 79, 410–418 (1981).

85. Alder, B. J. & Wainwright, T. E. Phase Transition for a Hard Sphere System. J. Chem. Phys. 27, 1208–1209 (1957).

86. Leunissen, M. E. et al. Ionic colloidal crystals of oppositely charged particles. Nature 437, 235–240 (2005).

87. Evers, C. H. J., Luiken, J. A., Bolhuis, P. G. & Kegel, W. K. Self-assembly of Microcapsules via Colloidal Bond Hybridization and Anisotropy. Nature 534, 364–368 (2015).

88. Castellano, J. A. Liquid Gold: The Story of Liquid Crystal Displays and the Creation of an Industry. (World Scientific Publishing Company, 2005).

89. Jacobson, J., Comiskey, B., Albert, J. D. & Yoshizawa, H. An electrophoretic ink for all-printed reflective electronic displays. Nature 394, 253–255 (1998).

90. Hynninen, A.-P., Thijssen, J. H. J., Vermolen, E. C. M., Dijkstra, M. & van Blaaderen, A. Self-assembly route for photonic crystals with a bandgap in the visible region. Nat. Mater. 6, 202–205 (2007).

91. SANDERS, J. V. Colour of Precious Opal. Nature 204, 1151–1153 (1964).

92. Anderson, T. F. & Richards, A. G. An Electron Microscope Study of Some Structural Colors of Insects. J. Appl. Phys. 13, 748–758 (1942).

93. Finlayson, C. E. et al. 3D Bulk Ordering in Macroscopic Solid Opaline Films by Edge-Induced Rotational Shearing. Adv. Mater. 23, 1540–1544 (2011).

94. Murray, C. B., Kagan, C. R. & Bawendi, M. G. Self-Organization of CdSe Nanocrystallites into Three-Dimensional Quantum Dot Superlattices. Science (80-.). 270, 1335–1338 (1995).

95. Kiely, C. J., Fink, J., Brust, M., Bethell, D. & Schiffrin, D. J. Spontaneous ordering of bimodal ensembles of nanoscopic gold clusters. Nature 396, 444–446 (1998).

96. Talapin, D. V et al. A New Approach to Crystallization of CdSe Nanoparticles into Ordered Three-Dimensional Superlattices. Adv. Mater. 13, 1868 (2001).

97. de Nijs, B. et al. Entropy-driven formation of large icosahedral colloidal clusters by spherical confinement. Nat. Mater. 14, 56–60 (2014).

98. Dong, A., Chen, J., Vora, P. M., Kikkawa, J. M. & Murray, C. B. Binary nanocrystal superlattice membranes self-assembled at the liquid-air interface. Nature 466, 474–7 (2010).

99. Bianchi, E., Blaak, R. & Likos, C. N. Patchy colloids: state of the art and perspectives. Phys. Chem. Chem. Phys. 13, 6397 (2011).

100. Yethiraj, A., Thijssen, J. H. J., Wouterse, A. & van Blaaderen, A. Large-Area Electric-Field-Induced Colloidal Single Crystals for Photonic Applications. Adv. Mater. 16, 596–600 (2004).

101. Whitesides, G. M. Self-Assembly at All Scales. Science (80-.). 295, 2418–2421 (2002).

102. Vermant, J. & Solomon, M. J. Flow-induced structure in colloidal suspensions. J. Phys. Condens. Matter 17, R187–R216 (2005).

103. Paxton, W. F. et al. Catalytic Nanomotors: Autonomous Movement of Striped Nanorods. J. Am. Chem. Soc. 126, 13424–13431 (2004).

104. Erni, R. Aberration-corrected Imaging in Transmission Electron Microscopy: An Introduction. (Imperial College Press, 2010).

105. Bragg, W. H. & Bragg, W. L. The Reflection of X-rays by Crystals. Proc. R. Soc. A Math. Phys. Eng. Sci. 88, 428–438 (1913).

106. Geuchies, J. J. Connecting the dots: Shedding light on the self-assembly of semiconductor nanocrystals with synchroton X-ray scattering techniques. (2017).

107. Moreels, I. et al. Composition and Size-Dependent Extinction Coefficient of Colloidal PbSe Quantum Dots. Chem. Mater. 19, 6101–6106 (2007).

108. Geuchies, J. J. et al. In situ study of the formation mechanism of two-dimensional superlattices from PbSe nanocrystals. Nat. Mater. 15, 1248–1254 (2016).

This chapter is based on:

Synthesis of 2D superstructures with square or honeycomb nanoperiodicity by interfacial self-assembly and oriented attachment of PbSe nanocrystals;
Carlo van Overbeek, Joren E. Vos, Joep L. Peters, Marijn A. van Huis, Daniel Vanmaekelbergh;
In preparation.

Chapter 2

Methodology: synthesis of two-dimensional superstructures with square or honeycomb nanoperiodicity by interfacial self-assembly & oriented attachment of PbSe nanocrystals

Abstract 53

1.1. Introduction 53

1.2. Methodology

1.2.1. PbSe nanocrystal synthesis, purification & analysis **54**

1.2.2. Two-dimensional superstructure assembly & analysis *54*

56

1.3. Results 57

1.4. Discussion 60

1.5. Conclusions & Outlook 62

References 63

2.1

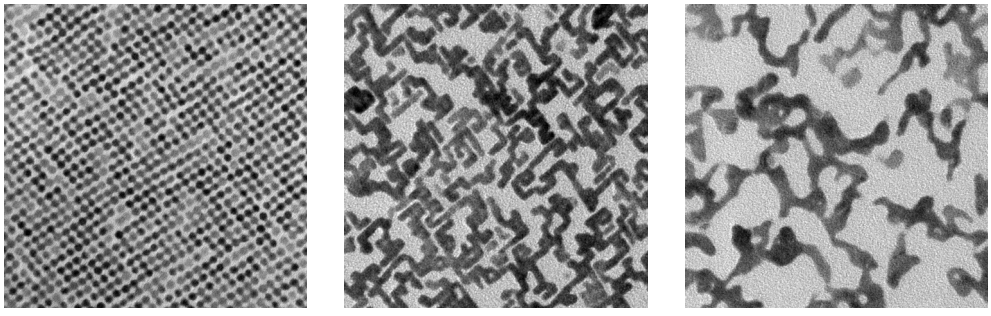

The synthesis of PbSe nanocrystal superstructures is highly susceptible to variations in the atmosphere where the reaction takes place. Particularly ligand stripping agents, such as oxygen, can have a profound detrimental effect.

Abstract

We discuss the synthesis of two-dimensional superstructures with a square or honeycomb nanoperiodic geometry by self-assembly and sequential oriented attachment of 5.5 nm PbSe nanocrystals. In a nitrogen-purged glovebox, the PbSe building blocks are synthesized via the hot injection method and drop casted onto an immiscible ethylene glycol substrate. Although the hot injection method is by now well established and the drop casting comes in a rather facile protocol, the method presented below is still hard to execute successfully. This is so because its outcome is very susceptible to changes in experimental conditions, mostly the atmosphere. We will discuss multiple sub-optimal outcomes and how to overcome them. Furthermore, it will be shown that the formation of small domains of honeycomb geometry superstructures can be promoted over square formation by lowering the amount of lead oleate and oleic acid but increasing the amount of toluene during the assembly. Particularly these honeycomb geometry superstructures are predicted to have optoelectronic properties that hold great promise for application in future electronics.

2.1. Introduction

Nanomaterials are extensively being studied, because of their envisioned applications in electronics, lighting and catalysis (1). In the present manuscript, we discuss the formation of atomically coherent NC superstructures by a facile drop casting protocol of NC suspension. The product of the assembly and oriented attachment are two-dimensional (2D) superstructures with a square or honeycomb nanoperiodic geometry (2). Tight-binding calculations on the optoelectronic properties of these materials predict that they can exhibit both semiconducting and Dirac-type charge carrier behavior (3), which is a very interesting combination of properties for future electronics.

The protocol towards making these 2D superstructures is a bottom-up method that can roughly be divided in two steps. First, 5.5 nm PbSe nanocrystals (NCs) are colloidally synthesized via the hot injection method (4). Second, the NC dispersion in toluene is drop casted onto an immiscible ethylene glycol substrate (5). At the end of the evaporation of the toluene, the NCs spontaneously start to self-assemble at the liquid-air interface and finally performs oriented attachment to form a 2D superstructures (6). In this way, materials can be formed with a periodic unit smaller than 10 nm. Such a small periodic length scale is hardly feasible by lithography, but is needed for the materials to have their envisioned optoelectronic properties.

Although the protocol towards making these 2D superstructures is relatively facile, creating the right conditions for it to happen with an appreciable yield, purity and

reproducibility is actually quite challenging. Therefore, we will provide an ample amount of sub-optimal experimental outcomes that we regularly observed, a detailed discussion what causes them and, most importantly, experimental procedures how to overcome them.

2.2. Methodology

2.2.1. PbSe nanocrystal synthesis, purification & analysis

Although nanocrystal synthesis via the hot injection method (4, 9) is not the focus of this manuscript, creating PbSe nanocrystals with a good quality is of pivotal importance to this research. Therefore, a synthesis protocol (7, 8) of these particles will be detailed below.

To synthesize a lead precursor, add 4.8 g of lead(II) acetate trihydrate, 10.35 g of oleic acid, 39.75 g of octadecene and a magnetic stirring to a round-bottom flask with a ground glass joint. Connect the flask to a Schlenk line and put it on a heating/stirring plate. Start stirring and gently apply vacuum. The mixture should start bubbling, this should stop after a couple of minutes. After the bubbling has stopped or has gotten much less vigorous, heat the mixture to 120 °C. The mixture should start bubbling again as the temperature rises. The bubbling under heating should stop after approximately 6 h. The lead-precursor is then finished. It should be a viscous liquid, clear to slightly yellow. Put the lead precursor under nitrogen and transfer it to a nitrogen-purged glovebox.

Note: From this point onwards, all chemicals should not come into contact with oxygen or water. Consequently, all subsequent steps should be performed at a Schlenkline or in a nitrogen-purged glovebox, unless stated otherwise.

To synthesize a selenium precursor, add 3.5 g of selenium, 0.41 mL of diphenylphosphine, 46.5 mL of trioctylphosphine and a stirring bar to an Erlenmeyer flask in a nitrogen-purged glovebox. Put the flask on a heating/stirring plate. Stir and gently heat (~75 °C) the mixture until all chemicals have dissolved, this typically takes a little less than an hour. The resulting selenium precursor should be a clear viscous liquid. Let the selenium precursor cool down to room temperature.

To synthesize the PbSe nanocrystals, add 20.5 mL of the lead precursor and a stirring bar to a 3-neck round-bottom flask. Connect the three necks of the flask with a stopper, a Vigreux cooler and a thermometer through a septum, respectively. Put the flask on a heating/stirring plate. Heat the lead precursor to 180 °C while stirring. When the precursor is at 180 °C, start stirring vigorously, and swiftly inject 15 mL of the selenium. The mixture should turn black within a few seconds. Keep the mixture at ~145 °C for 45 s. Swiftly add 40 mL of butanol under vigorous stirring and remove the heating. The

resulting crude PbSe nanocrystal solution should be a deep black liquid with a slight milky shine. Wait ~5 min.

Note: the temperature of the mixture is now still above that of the boiling point of methanol (65 °C), it is advisable to wait until the temperature has dropped below that. Otherwise, be mindful of overboiling.

To wash the nanocrystal solution, add 10 mL of methanol to the PbSe nanocrystal solution. The mixture should instantly turn milky in appearance if it isn't already. Transfer the liquid to centrifuge tubes or vials. Centrifuge the liquid at 1,200 g for 10 min. Decant the liquid supernatant and disperse the residual PbSe nanocrystals in toluene. Repeat the washing procedure from, depending on the oriented attachment results. The particles used in this chapter were washed 4 times.

To analyze the PbSe nanocrystals by infrared spectroscopy, take an aliquot of 15 µL of the nanocrystal solution and dry this under vacuum. Solvate the dried PbSe nanocrystals in 4 mL of tetrachloroethylene. Measure an absorption spectrum of the sample from 2000 to 1000 nm.

Note: To get a good spectrum, exact values of the previous two steps may vary depending on the concentration of the PbSe nanocrystal stock solution.

Fit a Gaussian on a linear background function through the first exciton peak. PbSe nanocrystals that are monodisperse enough for the rest of this procedure should have a full width at half maximum of around 65 meV. The peak position of the Gaussian function can yield the average diameter of the PbSe nanocrystals through the function below. An ideal particle size for the following oriented attachment procedure is 5.5 nm.

Eq.2.1 $$NC\ size\ (nm) = 3.81212 * \frac{\sqrt{peak\ (eV) + 4.02279} - 1.71329 * \sqrt{peak\ (eV) - 0.278}}{\sqrt{peak\ (eV) - 0.278}}$$

The integral of the Gaussian function can yield the concentration of the PbSe nanocrystals in the sample volume through the function:

Eq.2.2 $$NC\ concentration\ (\mu mol/L) = \frac{integral\ (eV * a.u.)}{NC\ size\ (nm)^{0.9} * 0.31 * pathlength\ (m)}$$

Calculate the concentration in the stock solution depending on the dilution factors of the measured dispersion.

To analyze the PbSe nanocrystals by TEM, drop cast one droplet of a dilute solution of the nanocrystals on a TEM grid. The dilute solution used for IR-spectroscopy is often fine. Transfer the TEM grid to a TEM. At a magnification of 90,000 times, the nanocrystals should appear as ~5.5 nm spheres packed in hexagonally ordered patches.

2.2.2. Two-dimensional superstructure assembly & analysis

To degas the ethylene glycol, add 1 L of ethylene glycol and a stirring bar to a round-bottom flask with a glass-ground joint. Connect the flask to a Schlenk line and put it on a heating/stirring plate. Start stirring and gently apply vacuum. The mixture should start bubbling, this should stop after a couple of minutes. After the bubbling has stopped or has become much less vigorous, heat the mixture to 100 °C. The mixture should start bubbling again as the temperature rises. Leave the degassing to proceed overnight. Allow the flask to cool down, set it under nitrogen and transfer it to a nitrogen-purged glovebox.

Note: The following procedure is extremely sensitive to atmospheric conditions, particularly oxygen can devastate an experiment. All subsequent steps should be performed in a nitrogen-purged glovebox with <1 ppm oxygen and water, unless stated otherwise. Also, as reproducibility is hard to achieve when starting out with these procedures, it is advisable to run multiple experiments simultaneously to be sure that obtained results are representative.

Assembly of 2D superstructures with honeycomb symmetry

Put a 29 mm diameter glass Petri dish on a heating/cooling plate and set it to 20 °C. Add 6.5 mL of degassed ethylene glycol to the Petri dish. Take an aliquot of the PbSe NC dispersion and dilute it to a concentration of 0.3 μmol/L with toluene. Gently drop cast 700 μL of the diluted NC suspension onto the degassed ethylene glycol liquid substrate. Allow the solvent to evaporate.

Dark brown patches should form on the liquid/air interface during this time. The solvent evaporation should take approximately 3 h. Whether all solvent has evaporated can be checked with a time-lapse from a webcam. Scoop the surface with a TEM grid where brown superstructure patches are visible by eye. Remove residual ethylene glycol by putting the TEM grid under vacuum.

Assembly of 2D superstructures with square symmetry

Put a 29 mm diameter glass Petri dish on a heating/cooling plate and set it to 22 °C. Add 6.5 mL of degassed ethylene glycol to the Petri dish. Gently drop cast 5.5 μL of a 2.5 μL/mL oleic acid in ethylene glycol suspension onto the degassed ethylene glycol liquid substrate. Take an aliquot of the PbSe NC dispersion and dilute it to a concentration of 0.6 μmol/L with toluene. Add 15 μL of a 10 mg/mL lead(II)oleate in toluene solution to the diluted NC dispersion. Gently drop cast 350 μL of the diluted NC suspension onto the liquid substrate. (Note that less toluene is used here compared to the honeycomb formation protocol.) Allow the solvent to evaporate.

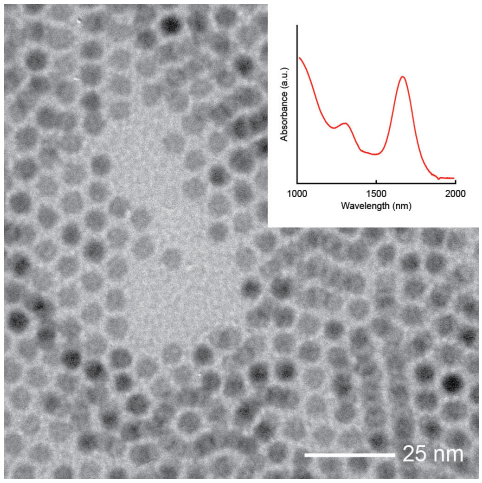

Figure 2.1: TEM image and IR-absorption spectrum (inset) of PbSe NCs used.
Both methods confirm that the NCs are approximately 5.5 nm in size and have a polydispersity of less than 10%. Both properties are a prerequisite for assembling good quality 2D superstructures.

• • • •

Dark brown patches should form on the liquid/air interface during this time. The solvent evaporation should take approximately 1 h. Whether all solvent has evaporated can be checked with a time-lapse from a webcam. Set the heating/cooling plate to 45 °C for 20 min. Scoop the surface where there are brown patches with a TEM grid. Remove residual ethylene glycol by putting the TEM grid under vacuum.

Analysis of 2D superstructures by TEM

Remove sample TEM grids from vacuum after complete evaporation of residual ethylene glycol, this is most conveniently achieved overnight. Transfer sample grids to a TEM. Dark superstructure patches should appear at a magnification of 1,000 times. Zooming in to 90,000 times should reveal the symmetry of the superlattices of the attached NCs.

2.3. Results

Although the focus of the present manuscript is the assembly of 2D superstructures, for completeness we also show a good example of the prerequisite PbSe NCs. Figure 2.1 shows a TEM image and an IR-absorption spectrum of such NCs. The particles are 5.66±0.30 nm in size as determined by IR-spectroscopy (8) and 5.34±0.34 nm by TEM.

At the end of the laboratory procedure, dark brown flakes should have formed on the liquid ethylene glycol substrate. Scooping these onto a TEM grid, letting them dry under vacuum and investigating them by TEM should ideally reveal 2D nanoperiodic superstructures with a square or honeycomb geometry, as displayed in Figure 2.2. The inset of each image in Figure 2.2 displays a selected area electron diffraction (SAED) pattern of the sample area. The spots visible in the SAED patterns and their orientation with respect to the TEM image prove that all constituent NCs are facing each other

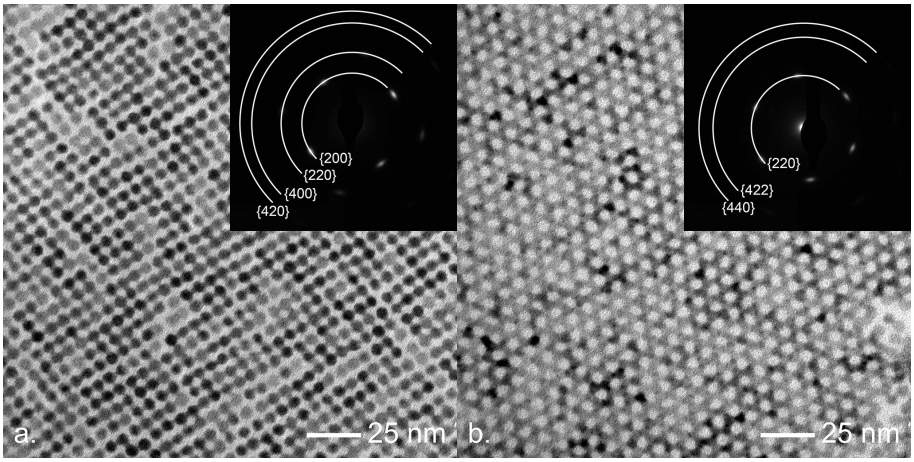

2.3

Figure 2.2: TEM images of the two 2D superstructures with (a) square and (b) honeycomb geometry, insets shows SAED patterns corresponding to the respective sample image.
The clear contrast between the NCs, i.e. the connecting necks, in the TEM images and the spots in the diffractogram prove that the NCs have performed oriented attachment with their in-plane {100} facets.

with their in-plane {100} facets. Furthermore, the NCs have a {100} or {111} facet facing up in the square or honeycomb geometry, respectively. The atomic alignment plus the clearly observable necks between the NCs proves that oriented attachment has taken place resulting in an atomically coherent superstructure. This is somewhat harder to observe directly by TEM for honeycomb samples. Below some extra information on distinguishing attached and unattached honeycombs will be provided, but in the end only high-resolution TEM tomography and electron diffraction can truly prove attachment in 2D honeycomb superstructures (10).

Sample patches of a coherent 2D superstructure up to a few micrometers in size can be synthesized with this protocol. It is, however, also common that smaller or overlapping patches are formed due to inhomogeneous spreading of the NCs during the solvent evaporation. Figure 2.3a displays an example image of overlapping NC patches on a microscopic scale and the different superstructure phases it can produce. The unequal spreading usually results in double square layers as a by-phase when preparing 2D square superstructures, as can be seen in Figure 2.3b. When preparing honeycombs, unequal spreading is far more common and results in low-density phases with line superstructures and high-density phases with interlaced honeycomb and zigzag superstructures. Smaller sample patches can also form or start overlapping as an artifact from breaking bigger superstructures by scooping the sample, a clear example of this effect is displayed in Figure 2.4a.

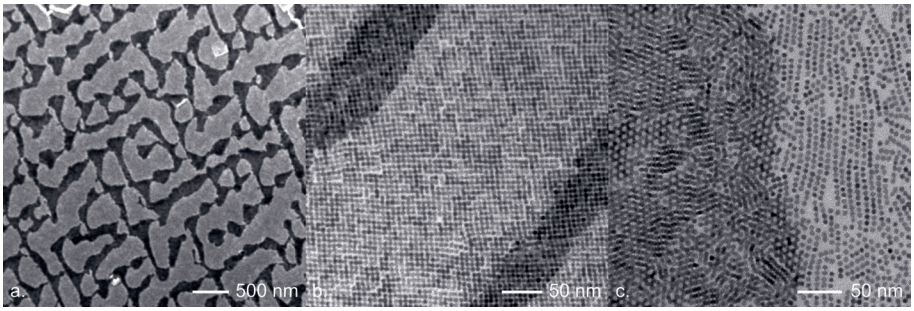

Figure 2.3: TEM images of often encountered mesoscopic irregularities in the 2D superstructures.
(A) Inhomogeneous distribution of the NCs during solvent evaporation caused the formation of drying patterns on a mesoscopic scale. (B) Nanoscopic inspection of such regions reveals that the system has monolayers, bilayers and sometimes phases with different geometries. (C) In this example image, we see a few small honeycomb patches intertwined by a linear zigzag phase and bordering rod-like systems.

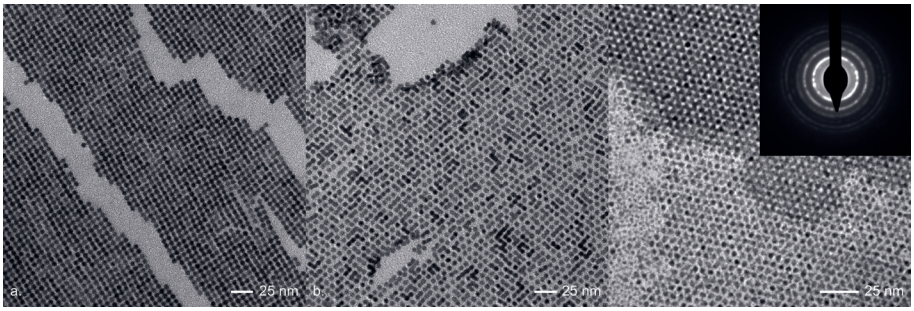

Figure 2.4: TEM images of regularly encountered artefacts and other undesired experimental outcomes.
(A) TEM image of sample area that was shattered by sample scooping (see experimental procedure step 2.2.7 and 2.3.10). Note how the sample edges would perfectly fit if they would be brought together. This observation proves the explanation that this is an artefact induced by scooping. (B) TEM image of mostly unattached NCs in a pseudo-square ordering. (C) TEM image of unattached NC multilayers creating a moiré pattern that resembles a honeycomb superstructure. The image inset shows the SAED pattern corresponding to this sample region. The absence of spots in the SAED and unattached NCs in the image prove that no oriented attachment has taken place and the observed moiré pattern is not a true 2D NC superstructure with honeycomb geometry.

Some sample patches or even whole PbSe NC batches might form ordered 2D superlattices without performing oriented attached. Figure 2.4b shows an example of an oblique, pre-square(6), phase where only very few NCs have attached. Sometimes these unattached patches overlap each other, giving the impression that attachment has taken place. Figure 2.4c shows overlapping layers of hexagonally ordered NC superlattices.

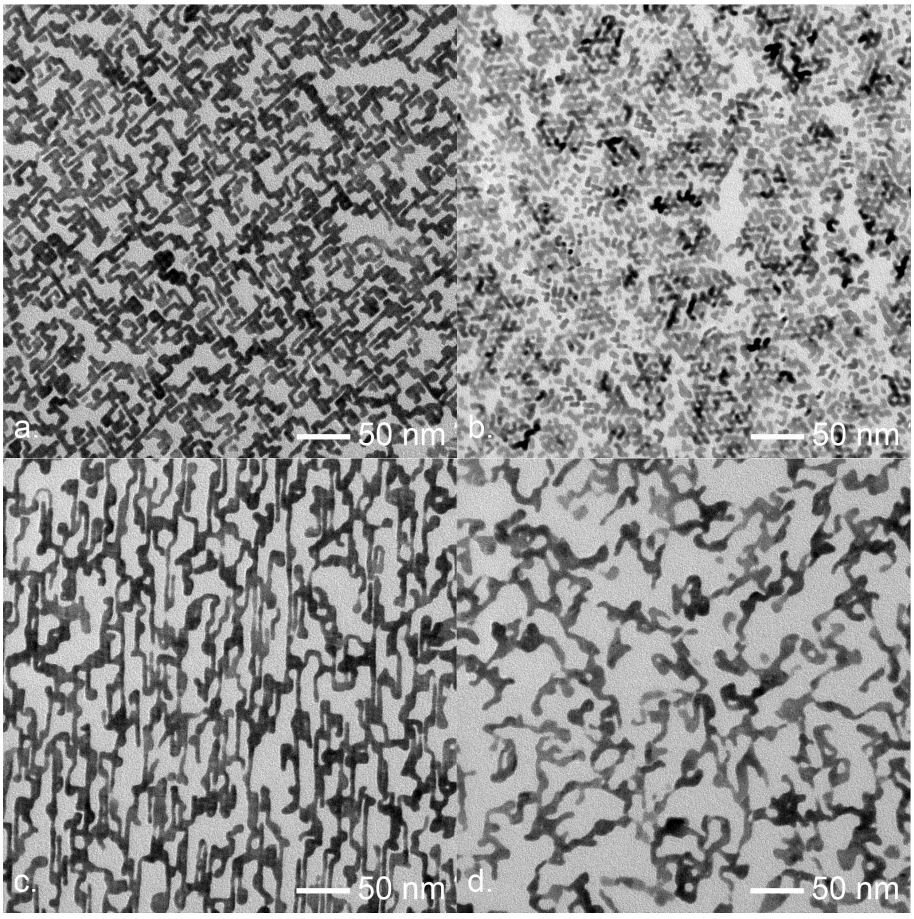

Figure 2.5: TEM images of NCs that performed irreversibly oriented attachment in an atmosphere with a >1 ppm of oxygen.
Under even small amounts of oxygen, the NCs become so reactive that oriented attachment occurs before the formation of a 2D well-ordered superlattice with unbound NCs. This results in irregular, "open", structures. (A - C) TEM images of samples which were clearly on their way towards forming square, honeycomb and linear symmetry superstructures, respectively. (D) TEM image of a sample where oriented attachment was so fast that no NC order is observable.

Their projected moiré pattern in the middle of the image strongly resembles a 2D honeycomb superstructure. Here, the SAED pattern inset shows no spots but rings. This proves that the sample is not atomically coherent and therefore the NCs in the patch are unattached. Sometimes, NCs ordered in a moiré pattern even display atomic coherency in SAED, but might still be unattached. Loose NCs always seem to lay next to such patches with a commensurate periodicity to the NCs in the moiré pattern. This can also clearly be seen in Figure 2.4c.

On the other hand, some sample patches or NC batches perform oriented attachment much too readily. The NCs in Figure 2.5a-c were clearly self-assembling towards square, honeycomb and linear superstructures, respectively, when oriented attachment took place and locked the NCs in a sub-optimal position. Sometimes the oriented attachment takes place before any self-assembly has happened, this results in the formation of fractal-like structures displayed in Figure 2.5d. Note that in all images in Figure 2.5 the edges of the structures have smoothed out and the original shape of the NCs cannot be distinguished anymore. This also happens when 2D superstructures are post-treated with heating to form percolated networks (11), which can be explained by realizing that both stripping the ligands with oxygen (12) and heating the system should enhance the NC surface reactivity. This in turn leads to a higher surface moiety mobility.

2.4. Discussion

Superstructure samples can in principle be scooped off the liquid substrate with any solid substrate. This makes the sample preparation for investigating the superstructure's properties with different techniques relatively facile (10, 11, 13, 14). In the present manuscript, checking the success of the procedure is solely done by TEM and SAED, because this is the most straightforward method to do so. The cracks in sample patches induced by scooping, as displayed in Figure 2.4a, can be reduced by gently stamping the liquid surface with a solid substrate instead of scooping it. Working with a less viscous liquid substrate should also reduce these artefacts. The results obtained from assembly experiments on different liquid substrates are, however, too preliminary to discuss into more detail.

The first prerequisite for making the 2D superstructures presented above is having PbSe NCs which are shaped like strongly truncated cubes (15–17) and have a minimal size and shape dispersity (18). Differently shaped or too polydisperse particles will not perform the self-assembly. The optimal particle size for the assembly procedure is ~5.5 nm. Small (<5 nm) particles tend to be more polydisperse and big (>7.5 nm) ones sometimes do not perform oriented attachment. Also, the NCs need to have a surface not damaged by oxygen or other reactive agents (19). Synthesizing the PbSe NCs in an atmosphere with >10 ppm oxygen often resulted in NC batches which could self-assemble, but did not perform oriented attachment. However, not performing oriented attachment can also be the result of residual octadecene from synthesis in the NC solution or the NCs having too many ligands on their surface. This can easily be remedied by washing the NC batch (protocol section 1.4) one or more times and trying the attachment procedure again.

The assembly process resulting in 2D geometric superlattices with unbound NCs and the oriented attachment should be considered as really two different steps. The assembly process of the 2D superstructures is very susceptible to variations in the atmosphere and should therefore be carried out preferably in a nitrogen-purged glovebox dedicated to self-assembly research. Oxygen and other ligand stripping agents (12, 19–21) are particularly detrimental to the process. If these are present, irreversible attachment speeds up to a much faster pace than the NC self-assembly. Then the system cannot form long-range or even short-range order anymore, examples of which are shown in Figure 2.5.

The self-assembly of the NCs can be tuned to go slower and therefore resulting in more order by adding a very small amount of oleic acid (step 2.3.3) and/or lead oleate (step 2.3.5). Oleic acid also facilitates a more homogeneous spreading of the NC solution over the ethylene glycol substrate. This decreases the amount of undesired by-phases, which are displayed in Figure 2.3. Oleic acid and lead oleate also inhibit the oriented attachment. Therefore, it is usually necessary to heat the sample after synthesis (step 2.3.9), if oleic acid and lead oleate were added, to make sure oriented attachment takes place. However, these chemicals also seem to favor the formation of the square superstructure. When following the procedure for making honeycomb samples, but with the addition of oleic acid or lead oleate, the sample will usually turn out to consist of square superstructures. This makes it harder to effectively tune the honeycomb assembly to a yield and purity as good as the square superstructures. Our group is currently researching towards tackling this problem.

A slightly different method towards preparing 2D NC superstructures published in literature (13) separates the self-assembly and the oriented attachment step by washing the NCs after synthesis with acetonitrile instead of the more aggressive ligand stripping methanol. This way oriented attachment is suppressed during the NC self-assembly, but is induced at a later stage by adding a ligand stripping amine. A good aspect of this procedure is that it should result in structures with a higher nanoperiodicity as the NCs have infinite time to self-assemble, because no attachment takes place to lock them in position. However, no synthesis of honeycomb superstructures has yet been reported using this method. Also, the oriented attachment is induced by drop casting of a ligand stripping agent after NC self-assembly, which disturbs the NC film and causes rapid inhomogeneous oriented attachment over the sample. Both effects should be detrimental to the final quality of the produced superstructures.

Following a procedure with aspects from both of the two methods should be done with care. First, the second method takes place in a Teflon cell rather than a glass petri dish as in the present manuscript. This has no effect on the self-assembly and oriented attachment on the interface of the ethylene glycol. However, toluene preferentially wets Teflon instead of glass or ethylene glycol. Therefore, when using more than 10 μL/cm2

of toluene during the drop casting, the NCs tend to agglomerate at the Teflon edge of the substrate which leads to an uncontrollable amount of NCs on the ethylene glycol surface. Conversely, using such a low amount of toluene in the present protocol usually results in all NCs uncontrollably agglomerating on the substrate's center. Another difference when comparing with the other protocol is that a lid is put over the Teflon cell. This cannot be done in the present protocol as the petri dishes are filled with ethylene glycol to the brim. Lowering this amount would curve the surface of the substrate, as the ethylene glycol wets the glass very well. The induced curvature unhomogeneously spreads the NCs over the liquid substrate causing undesired by-phases.

The oriented attachment of the NCs happens through a process called necking: atoms from the NC surface rearrange to form necks between neighbors (10, 22). At some point, of course, surface atoms available for this process run out and then no more connections with neighboring NCs can be made. In Figure 2.2a it is clearly visible that not all NCs are connected. Furthermore, the necking is an irreversible process and the NCs have a finite polydispersity. Both cause disorder in the final 2D superstructures (23), i.e. the crystal orientation of a single NC does not propagate further than a few building blocks (6). The crystalline disorder and missing necks may reduce the optoelectronic coupling in superstructures (11, 13, 14), a property which is vital to their envisioned applications (3). Recently, first steps towards addressing the issue of the missing necks have been made (24).

2.5. Conclusions & Outlook

We described the assembly of two-dimensional superstructures with a square or honeycomb nanoperiodic geometry. This was done by drop casting a colloidal dispersion of 5.5 nm PbSe nanocrystals in toluene onto an immiscible ethylene glycol substrate in a nitrogen-purged glovebox. By tuning the evaporation rate and the wetting of the toluene phase the formation of either square or honeycomb superstructures could be stimulated. Square superstructures could be made with an excellent purity, whereas honeycombs usually formed concommitantly with other linear or multilayer structures. Future research should be dericted towards improving superstructure sample purity and tackling the issues involved with oriented attachment of the nanocrystals, namely: missing necks and disorder in superstructure's crystal structure.

References

1. Kovalenko, M. V et al. Prospects of Nanoscience with Nanocrystals. ACS Nano 9, 1012–1057 (2015).

2. Evers, W. H. et al. Low-Dimensional Semiconductor Superlattices Formed by Geometric Control over Nanocrystal Attachment. Nano Lett. 13, 2317–2323 (2013).

3. Kalesaki, E. et al. Dirac Cones, Topological Edge States, and Nontrivial Flat Bands in Two-Dimensional Semiconductors with a Honeycomb Nanogeometry. Phys. Rev. X 4, 11010 (2014).

4. Murray, C. B., Norris, D. J. & Bawendi, M. G. Synthesis and characterization of nearly monodisperse CdE (E = sulfur, selenium, tellurium) semiconductor nanocrystallites. J. Am. Chem. Soc. 115, 8706–8715 (1993).

5. Dong, A., Chen, J., Vora, P. M., Kikkawa, J. M. & Murray, C. B. Binary nanocrystal superlattice membranes self-assembled at the liquid-air interface. Nature 466, 474–7 (2010).

6. Geuchies, J. J. et al. In situ study of the formation mechanism of two-dimensional superlattices from PbSe nanocrystals. Nat. Mater. 15, 1248–1254 (2016).

7. Steckel, J. S., Yen, B. K. H., Oertel, D. C. & Bawendi, M. G. On the mechanism of lead chalcogenide nanocrystal formation. J. Am. Chem. Soc. 128, 13032–3 (2006).

8. Moreels, I. et al. Composition and Size-Dependent Extinction Coefficient of Colloidal PbSe Quantum Dots. Chem. Mater. 19, 6101–6106 (2007).

9. Manthiram, K., Beberwyck, B. J., Talapin, D. V & Alivisatos, a P. Seeded Synthesis of CdSe/CdS Rod and Tetrapod Nanocrystals. J. Vis. Exp. e50731 (2013). doi:10.3791/50731

10. Boneschanscher, M. P. et al. Long-range orientation and atomic attachment of nanocrystals in 2D honeycomb superlattices. Science (80-.). 344, 1377–1380 (2014).

11. Evers, W. H. et al. High charge mobility in two-dimensional percolative networks of PbSe quantum dots connected by atomic bonds. Nat. Commun. 6, 8195 (2015).

12. Choi, J. J. et al. Controlling Nanocrystal Superlattice Symmetry and Shape-Anisotropic Interactions through Variable Ligand Surface Coverage. J. Am. Chem. Soc. 133, 3131–3138 (2011).

13. Whitham, K. et al. Charge transport and localization in atomically coherent quantum dot solids. Nat. Mater. 15, 557–563 (2016).

14. Alimoradi Jazi, M. et al. Transport Properties of a Two-Dimensional PbSe Square Superstructure in an Electrolyte-Gated Transistor. Nano Lett. acs.nanolett.7b01348 (2017). doi:10.1021/acs.nanolett.7b01348

15. Houtepen, A. J., Koole, R., Vanmaekelbergh, D., Meeldijk, J. & Hickey, S. G. The hidden role of acetate in the PbSe nanocrystal synthesis. J. Am. Chem. Soc. 128, 6792–3 (2006).

16. Bertolotti, F. et al. Crystal symmetry breaking and vacancies in colloidal lead chalcogenide quantum dots. Nat. Mater. 15, 987–994 (2016).

17. Peters, J. L. et al. Ligand-Induced Shape Transformation of PbSe Nanocrystals. Chem. Mater. 29, 4122–4128 (2017).

18. Campos, M. P. et al. A Library of Selenourea Precursors to PbSe Nanocrystals with Size Distributions near the Homogeneous Limit. J. Am. Chem. Soc. 139, 2296–2305 (2017).

19. Baumgardner, W. J., Whitham, K. & Hanrath, T. Confined-but-Connected Quantum Solids via Controlled Ligand Displacement. Nano Lett. 13, 3225–3231 (2013).

20. Zhang, H. et al. Surfactant ligand removal and rational fabrication of inorganically connected quantum dots. Nano Lett. 11, 5356–5361 (2011).

21. Sandeep, C. S. S. et al. Epitaxially connected PbSe quantum-dot films: Controlled neck formation and optoelectronic properties. ACS Nano 8, 11499–11511 (2014).

22. Li, D. et al. Direction-specific interactions control crystal growth by oriented attachment. Science 336, 1014–8 (2012).

23. Savitzky, B. H. et al. Propagation of Structural Disorder in Epitaxially Connected Quantum Dot Solids from Atomic to Micron Scale. Nano Lett. 16, 5714–8 (2016).

24. Treml, B. E. et al. Successive Ionic Layer Absorption and Reaction for Postassembly Control over Inorganic Interdot Bonds in Long-Range Ordered Nanocrystal Films. ACS Appl. Mater. Interfaces 9, 13500–13507 (2017).

This chapter is based on:

Interfacial self-assembly and oriented attachment in the family of PbX (X = S, Se, Te) nanocrystals; Carlo van Overbeek, Joep L. Peters, Susan A. P. van Rossum, Marc Smits, Marijn A. van Huis and Daniel Vanmaekelbergh; in preparation.

Chapter 3

Interfacial self-assembly and oriented attachment in the family of PbX (X = S, Se, Te) nanocrystals

Abstract **69**

3.1. Introduction **69**

3.2. Experimental methods **70**

3.3. Results and discussion **71**

3.3.1. Size, shape and surface facets of nanocrystals in the lead chalcogenide family *71*

3.3.2. Comparison of the reactivity and superstructure assembly conditions for the lead chalcogenides *72*

3.3.3. Geometrical analysis of the lead chalcogenide superstructures *74*

3.3.4. Mechanistic aspects of interfacial nanocrystal self-ssembly *77*

3.3.5. Mechanistic aspects of neck formation *80*

3.4. Conclusions **82**

3.S. Supporting information **83**

References **88**

3.1

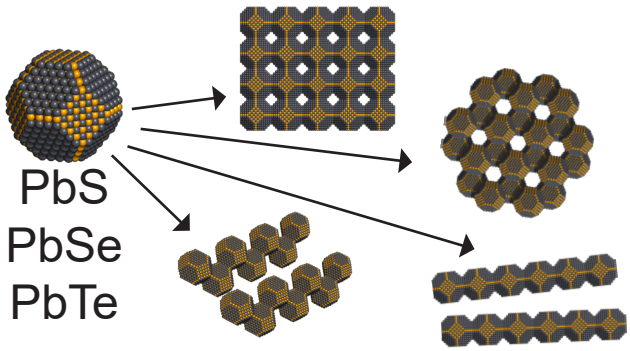

By sequential interfacial self-assembly and oriented attachment lead oleate capped ~5.5 nm nanocrystals of lead sulfide, lead selenide and lead telluride, i.e. lead chalcogenides, can form the same four nanoperiodic superstructures: squares, honeycombs, lines and zigzags.

Abstract

The realization of materials with new optoelectronic properties draws much scientific attention towards the field of nanocrystal superstructures. Low-dimensional superstructures created by interfacial assembly and oriented attachment of PbSe nanocrystals are a striking example, since theory showed that PbSe sheets with a honeycomb geometry possess non-trivial flat bands and Dirac cones in the valence and conduction bands. Here, we report on the formation of 1D linear and zigzag structures, and 2D square and honeycomb structures for the entire lead chalcogenide family: PbX (X = S, Se, Te). We observe that PbTe, with a lower bulk melting temperature and enthalpy of formation than PbSe, shows a higher nanocrystal surface reactivity, such that the surface must be passivated and the reaction conditions moderated to obtain reasonably ordered superstructures. The present findings constitute a step forwards in the realization of a larger family of atomically coherent 2D superstructures with variable IV-VI and II-VI composition, and with electronic properties dictated by the nanogeometry.

3.1. Introduction

3.1

Nanocrystals (NCs) are currently being extensively studied by the scientific community, because of their unique size-tunable properties caused by their nanoscale dimensions (1). Colloidal NCs also form the basis of solid materials, in which the properties are dictated by the interactions between the individual NC building blocks. When NCs with their original organic capping ligands are directly used in colloidal crystallization, the interaction between the NCs is weak, and the electronic conductivity low. Applications in photovoltaics and electronics therefore necessitated the development of ligand exchange chemistry that improves the electronic coupling between the NCs (2).

Almost three decades ago it was found that crystal growth does not always strictly proceed via monomer-by-monomer addition (3, 4). For example, NC nuclei can form larger crystallites by directly fusing together by a process called oriented attachment (5). Oriented attachment implies that two identical crystal facets face each other and rearrange some of their constituent atoms such that a neck grows between them (6). In this way, the crystallites fuse in such a neat manner that the resulting structure is singly crystalline (7).

More recently, it was reported that, with PbSe NCs, oriented attachment could be employed to create 2D superstructures (SSs) in which the NC building blocks are atomically connected to each other (8) and are therefore also electronically coupled (9). Moreover, it was found that the oriented attachment of PbSe NCs could be combined

with their interfacial self-assembly. In this way, low-dimensional SSs with a linear, square or honeycomb geometry can be created (10). These systems show long-range periodicity at the nm scale (i.e. the geometry) (11) and strict atomic crystallinity over a few NC units (12). Tight-binding calculations predict that this nanoscale ordering gives rise to truly novel band structures and hence properties that cannot be derived from the individual building blocks (13). Although the exact mechanism of formation of such 2D SSs is not yet fully understood, the first steps towards unravelling its chemistry (14) and physical chemistry (15) have just been reported.

In the present study, the preparation by interfacial self-assembly of four low-dimensional SSs, namely lines, squares, zigzags and honeycombs, is reported for NCs from the entire lead chalcogenide family: PbS, PbSe and PbTe (PbX). Successful synthesis of these SSs with different members of the PbX family opens the pathway to further tailoring SS properties towards specific ends. By also employing cation exchange as a post-treatment (10, 16), the synthesis of for example broad bandgap SSs of CdX compounds or SSs with high spin-orbit coupling (e.g. HgX compounds) might become possible. We remark that all PbX NCs have a rock salt crystal structure, a similar truncated cubic shape, and Pb-oleate ligands. However, the PbX compounds differ in their bulk lattice properties, such as melting temperature and enthalpy of formation. We, therefore, endeavored into a comparative study of the reaction conditions and compared the SSs that have been formed.

3.1

3.2. Experimental methods

Nanocrystal Synthesis

All PbX NCs in this study have been prepared via adaptations of the hot injection method (17). PbS, PbSe and PbTe NCs have respectively been produced according to Abel et al. (18), Steckel et al. (19) and Urban et al. (20) Furthermore, the PbTe particles were capped with additional chloride ligands according to Woo et al. (21) to slow down their intrinsically fast attachment; more discussion will be given in the Results and Discussion section. See Supporting Information for the full experimental conditions of the NC syntheses.

Nanocrystal analysis

All NCs were analyzed by transmission electron microscopy (TEM), using a FEI TECNAI 10/12, and IR-spectroscopy (Perkin Elmer, Lambda 950 UV/VIS/IR absorption spectrophotometer) to determine their size monodispersity and/or concentration. Although sizing curves for each of the PbX NCs have been published in literature (20, 22, 23), the way these sizing curves were established vary for each member in the PbX family. In order to have a better comparable estimate of the size of the NCs, the TEM images were analyzed in the program ImageJ by performing a background subtraction and particle detection.

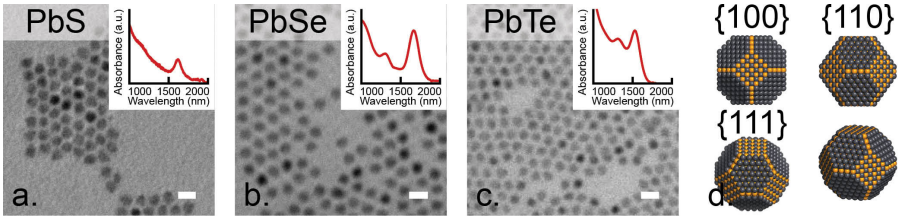

Figure 3.1: TEM and IR-spectroscopy (insets) characterization of the PbX building blocks used in the present study (a, b, c) and their atomistic models (d).
The scale bar denotes 10 nm in all images. All NCs are approximately 5 nm in size and appear as nearly spherical particles in TEM due to their strongly truncated cubic shape. Image (d) shows the NC's atomic structure as proposed by literature, grey denotes a lead atom and yellow denotes a chalcogenide atom (S, Se or Te). The right-bottom image in (d) shows a perspective view of the NCs, whereas the rest of the models in (d) are displayed with a specific surface crystal facet facing up. There is still debate in literature whether the {110} facets are exposed at the NCs' surface or not. All oriented attachment in this study happens through atomic connection of the {100} facets.

• • • •

To determine the concentration of the PbX NCs, IR-spectroscopy was used (22, 23). However, no such procedure exists in the literature for PbTe NCs. Therefore, the procedure for concentration determination of PbSe NCs was also used for PbTe NC. This procedure proved to work well enough for obtaining good and comparable results with the oriented attachment procedures. These concentrations were used to calculate the experimental surface area per NC values (= inverse NC density).

Superstructure assembly via oriented attachment

All PbX SSs in this study have been prepared via adaptations of the oriented attachment method described by Evers et al. (10) and Boneschanscher et al. (11) In a nitrogen-purged glovebox a dilute PbX NC suspension in an apolar liquid is drop casted onto an ethylene glycol substrate. After the solvent is completely evaporated, a sample is scooped with a TEM grid and analyzed by TEM. The surface area per NC and bonds per NC values in resulting SSs were manually obtained. See Supporting Information for more experimental details on the SS assembly.

3.3. Results and discussion

3.3.1. Size, shape and surface facets of nanocrystals in the lead chalcogenide family

Figure 3.1 displays TEM images of the PbX NCs that were synthesized and used for the assembly of the SSs through oriented attachment. Using automated particle detection, the NC sizes were determined from these TEM images assuming a spherical particle shape (see experimental methods for more details). It was found that the particle

sizes for the PbS, PbSe and PbTe NCs are respectively 5.2±0.6 nm (sample size: 124), 5.5±0.5 nm (sample size: 465), and 4.8±0.5 nm (sample size: 2254). These three sizes are sufficiently close, such that a comparative study of the influence of the surface chemistry in SS formation is possible. Furthermore, for each PbX compound, several NC suspensions were used, and the results were reproducible enough to be able to indicate and discuss meaningful differences between the three PbX compounds.

All PbX NCs were synthesized with a capping layer of Pb-oleate ligands that stabilizes the NC colloidal dispersions and passivates the NC surfaces, mostly the {111} crystal facets (24). The PbTe NCs were capped with additional Cl-ligands, which had a profound effect on their stability in ambient air, as was already found for PbS NCs (21). Also, the chloride ligands slightly reduced their reactivity during the oriented attachment procedure, which was usually necessary to obtain well-ordered PbTe SSs.

All PbX NCs possess the rock salt crystal structure. Their shape can be well described by a cube, which is strongly truncated in the <111> directions (25–28) and some works also suggests some cantillation in the <110> directions (29–31). This exposes the {100} and {111} (and possibly {110}) facets on the NC's surface and gives especially the small (<10 nm) particles the appearance of a sphere when observed by TEM, as can be seen in Figure 3.1.

We remark that the magnitude of the surface energy of the {100} facets is considerable lower than that of the {110} and {111} facets (30). This is in line with recent findings of Peters et al. showing that oleate and Pb-oleate moieties are weakly bound to the {100} facets (24).

All oriented attachment in the present study occurs at the {100} facets, which reminisce a checkboard of lead and chalcogenide atoms. As a result, all NC bond angles are approximately 90° or 180°. This coincides well with the literature on oriented attachment of PbSe NCs at liquid interfaces (10, 14, 32). PbS and PbSe NCs have only been observed to attach with other facets in reaction conditions that resemble those of the NC synthesis (8, 33).

3.3.2. Comparison of the reactivity and superstructure assembly conditions for the lead chalcogenides

Figure 3.2 shows an overview of models, TEM images and selected area electron diffraction (SAED) patterns of the formed SSs: 1D linear and zigzag SSs, and 2D square and honeycomb SSs were observed for each PbX. The most comparable reaction conditions at which these SSs have been synthesized are listed in Table 3.1. It might be hard to see in Figure 3.2 that the NCs have actually performed oriented attachment. Figure 3S.4 shows a close-up image in which each of the PbX NCs are clearly attached. This proves that the NCs have the propensity to perform oriented attachment.

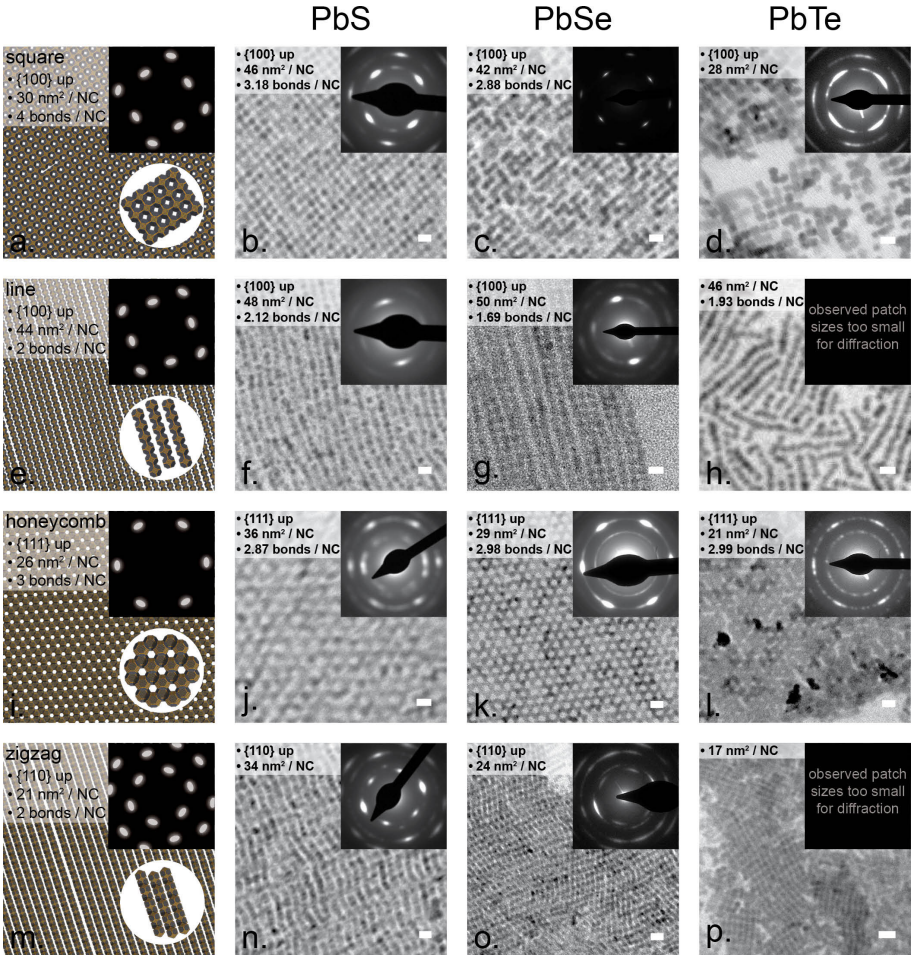

Figure 3.2: Overview of the SSs formed by interfacial self-assembly and oriented attachment of NCs from the PbX family.
Atomic models are displayed in the left column and TEM images are displayed in the right three columns. All three PbX NCs produced the same four types of SSs: squares (a - d), lines (e - h), honeycombs (i - l) and zigzags (m - p). All scale bars denote 10 nm. Inset images display the SAED pattern of the SSs. Inset text specifies for each SS which crystallographic facet its constituent NCs have facing up, its surface area per constituent NC (i.e. inverse NC density) and how much bonds each NC has on average with its neighbors in the SS. The latter two were measured on similar SSs displayed in Figure 3S.2.

When comparing the three members of the PbX family, it was found that each formed SSs at mostly similar reaction conditions: all on an ethylene glycol substrate, all with a reaction time on the order of 1 hour, all dispersed in a volatile apolar solvent, all with a size of ±5 nm NCs and all with an area of a few ten nm²/NC (i.e. inverse NC density). This can be explained by the similar material properties in the PbX family of

Table 3.1. Most comparable reaction conditions used to create the PbX SSs, similar conditions mean co-existing structures.

	PbS				PbSe				PbTe			
	square	*line*	*HC*	*ZZ*	*square*	*line*	*HC*	*ZZ*	*square*	*line*	*HC*	*ZZ*
Substrate	*ethylene glycol*											
Solvent	*hexane*				*toluene*				*hexane*			
NC size (nm)	*5.1±0.6*				*5.5±0.5*				*4.8±0.5*			
Temperature (°C)	*30*				*Room temperature (~26 °C)*				*Room temperature (~22 °C)*			
Ligands	*Pb-oleate*				*Pb-oleate*				*Pb-oleate + PbCl*			
Added surfactant (oleic acid/Å²)	*0*				*0*				*1.67*	*1.67*	*1.89*	*1.11*
Surface area per NC (nm²/NC)	*42*	*33*	*33*	*40*	*18*	*15*	*18*	*18*	*40*			
Reaction time (min)	*60*	*60*	*60*	*30*	*60*				*60*			

materials. NCs of the three compounds all have the rock salt crystal structure and a very similar shape.

3.3

The strong similarities in reaction conditions aside, the temperature, NC passivating ligands and oleic acid concentrations do vary slightly between PbS, PbSe and PbTe. This was done to compensate for the fact that at reaction conditions ideal for creating PbSe SSs, the PbS NCs sometimes only performed oriented attachment at a slightly increased temperature that speeds up oriented attachment. In contrast, PbTe NCs would sometimes perform uncontrolled agglomeration under ideal PbSe attachment conditions. An image of such suboptimal attachment is presented in Figure 3S.5. To prevent this, the PbTe NCs had to be capped with additional chloride ligands and oleic acid was added to the substrate. These measures have been proven to inhibit NC surface oxidation and moderate the process of oriented attachment, respectively (10, 21).

These observations are indicative of a higher surface reactivity of the PbTe NCs and a lower reactivity of the PbS ones, compared to PbSe NCs. This follows the trend of a decrease in the binding energy of the PbX lattice from PbS to PbTe, which is reflected in the bulk melting temperature of the materials, 1113, 1078 and 924 °C respectively, and their formation enthalpies, -100.4, -102.9 and -70.7 kJ/mol (34). Moreover, PbTe NCs are exceptionally prone to surface deterioration, exemplified in their enhanced propensity for surface oxidation (35). More evidence that the NC surface reactivity follows the trend PbS < PbSe < PbTe will be presented below in the section on neck formation between the NCs.

3.3.3. Geometrical analysis of the lead chalcogenide superstructures

The atomic geometry of and NC alignment in the SSs can be derived from atomic models of the constituent PbX NC cores (22, 31, 36), this is depicted in the left column of Figure 3.2. The geometries and alignments can also be deduced from the SAED data shown in the TEM image insets of Figure 3.2. By overlaying the TEM images with the SAED patterns in Figure 3.2, it becomes clear that each SS geometry is indeed identical for each member in the PbX family.

Square and linear superstructures

The square SSs made from PbS and PbTe NCs have the same structure as those of PbSe, which was already reported (10). The SAED patterns in Figures 3.2a-3.2d show that all constituent NCs in square SSs have a <100> crystallographic direction perpendicular to the sample substrate and up to four connections with neighboring NCs through in-plane <100> directions, i.e., NC-NC bonds oppose each other or roughly have a 90° angle with respect to each other (15). Thus square PbS and PbTe structures have the same atomic structure as square PbSe SSs (10, 14, 32).

The linear SSs made from PbS and PbTe NCs also have a similar structure to those reported for PbSe (10). The SAED patterns in Figures 3.2e-3.2h show that all constituent NCs in linear SSs have a <100> crystallographic direction perpendicular to the sample substrate and are attached through opposing {100} facets in the image plane. In this respect, linear SSs can be seen as 1D sections of the square SSs.

Note that the SAED patterns of linear SSs have less pronounced peaks and generally coincide less well with their predicted diffraction pattern than the other SSs. The reason for this is rather trivial: once a linear structure is formed by oriented attachment, it can still be positioned in different ways on the TEM grid, while 2D SSs do not have this freedom and zigzag SSs are generally too densely packed for such rotations.

Honeycomb and zigzag superstructures

The scientific literature on experimental realization of the honeycomb NC SSs is limited (10, 11), despite the extensive theoretical studies published predicting interesting non-trivial optoelectronic properties due to the honeycomb geometry (13, 37–39). This is probably due to the fact that the honeycombs are much harder to make with an appreciable yield and reproducibility than the other SSs. In this manuscript, the synthesis of small domains of epitaxially connected NCs with the silicene honeycomb geometry is reported for all three PbX compound NCs. The domain size and reproducibility is most pronounced in the case of PbSe.

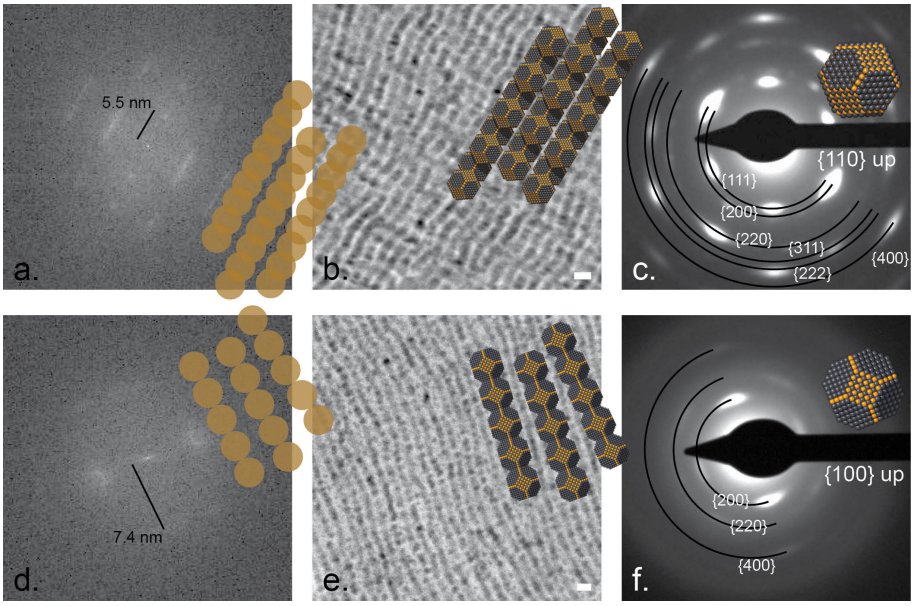

Figure 3.3: Comparison between zigzag and line SSs for PbX NCs.
All scale bars in the TEM images denote 10 nm. Although zigzags (b) and lines (e) are both 1D SSs their exact geometry differs. Fourier transformations (a, d) of the TEM images show periodicity at the NC scale for linear SSs and periodicity at a slightly shorter length scale for zigzag SSs. Both these periodicities are depicted as insets to the Fourier transforms. The spots in the SAED patterns (c, f) prove that the NCs are oriented as shown by the inset models of the SAED patterns. By combining the information of the real images, their Fourier transforms and the SAED patterns it becomes clear that lines are a straight chain of {100} attached NCs that all have a {100} facet pointing up; in zigzags all NCs have a {110} facet pointing up and are connected through {100} facets in 90° angles. These geometries are displayed as insets to the TEM images.

3.3

The TEM images and SAED data acquired on the honeycomb SSs are similar for all PbXs, as can been seen in Figure 3.2i-3.2l. Each NC in the honeycomb SS has a <111> crystallographic direction up and is atomically connected to up to three NCs. Not directly visible in these images, but already established in the literature, is that the NCs in these SSs are arranged in a quasi-bilayer also called the silicene structure (11). This bilayer structure is depicted in perspective view in Figure 3.4b.

The zigzag SSs, displayed in Figures 3.2m-3.2p, have so far not been described in the literature. An unattached PbS NC superlattice very reminiscent of the zigzag SS has been reported by Novák et al (40). Cho et al. have also described zigzagging SSs made by oriented attachment of PbSe NCs (11), however the latter SSs clearly differ from the ones presented in the present study as those are made from much larger, octahedrally-

shaped NCs. Moreover, those SSs are attached in their <111> crystallographic directions in contrast to the <100> attachment that is observed in this study.

A more thorough geometrical analysis will be provided for the zigzag SSs as these can sometimes closely reminisce line SSs when observed by TEM, for example the zigzags displayed in Figure 3S.2n. In Figure 3.3 the 1D SSs are further analyzed by Fourier transformation and SAED. Particularly SAED can differentiate well between the two SSs, as the <110> up orientation of NCs in zigzags allows for reflections from their {111} planes to be visible in their SAED patterns. In contrast, lines are oriented <100> up, so {111} planes are not at their Bragg angle with the incoming electron beam and thus their reflections are not visible in their SAED patterns. These differences in SAED pattern can be seen in Figures 3.3c and 3.3f.

Furthermore, TEM images of zigzags show lighter and darker regions within each line of zigzagging NCs. By Fourier transforming the images of the SSs, it follows that zigzags are periodic at the length scale one would expect for two NCs connected through their {100} facets in a 90° angle out of the image plane. In contrast, linear structures show the periodicity at the NC scale. Adding up these two observations we conclude that zigzag SSs are shaped as illustrated in Figure 3.4a and 3.4c: the NCs are ordered in a zigzag fashion and form a quasi-bilayer in the image plane. The NCs in zigzags are sometimes attached to each other in the image plane and most likely also in their zigzagging directions. In this respect, zigzag SSs can be seen as 1D sections of the honeycomb SSs, as was also the case for linear SSs with respect to squares.

We remark that some images of the zigzag SS deviate from the idealized schematics in the present manuscript. In reality honeycomb and zigzag structures are more like the extremes of a continuous span of possible structures. Very NC dense regions, such as can be seen in Figures 3S.2n and 3S.2p, match the presented zigzag structure perfectly. Intermediate density patches look more wiggly in the image plane, as can be seen in Figures 3.2n and 3.2o. In low density regions those wiggles coherently break open into a honeycomb structure.

Even though the NC ordering between honeycombs and zigzags appears to be rather fluid, the NC orientation in them is not. This is clearly visible in the accompanying SAED patterns. All NCs in a honeycomb have a {111} facet pointing up and all NCs in a zigzag have a {110} facet pointing up. This is the reason we made a clear distinction between the two structures.

These observations make it tempting to speculate that both SSs originate from a common pre-phase, but more in-situ research on the formation of these SSs should be performed to verify such a statement.

3.3.4. Mechanistic aspects of interfacial nanocrystal self-assembly

NC adsorption and assembly at the toluene/air interface

A striking observation on the samples is that SSs never overlap. Even when looking at larger sample patches, such as those displayed in Figure 3S.3, NC densities fluctuate but the SS domains do not overlap. This observation of non-overlapping SSs is most peculiar for the lines, examples of which can be seen in Figures 3.2n-3.2p and Figures 3S.1n-p, 3S.2n-p & 3S.3. This is in contrast with the results of Cho et al., where oriented attachment presumably takes place in the bulk solution (i.e. without a liquid substrate and at reaction conditions reminiscent of PbX NC synthesis) (8).

This indicates that all SSs discussed in the present study are formed at the liquid/gas interface, as was already proven for the square SSs in ref. (15). For square PbSe SSs it was found that the NCs adsorb to the toluene-air interface with a random orientation at first. After 30 minutes, the toluene is (almost) evaporated and the NCs form a single hexagonal layer at the liquid/gas interface. Over the course of a few minutes the NC layer starts to contract and slowly reforms itself to a square geometry, during this transformation the NCs gradually orient their {100} facets towards each other. Finally, the NCs attach via their {100} facets. From the non-overlapping SS domains, it can safely be concluded that linear, square, zigzag and honeycomb structures also originate all from an adsorbed NC (sub)monolayer at the interface.

Formation of superstructure domains

By further analyzing the geometry of the formed SSs in Figure 3S.2 it was found that the NC density and the amount of bonds per NC can deviate strongly from the 'geometrically perfect' models in Figure 3.2a, 3.2e, 3.2i and 3.2m. The deviations in NC density can be attributed to the relatively broad NC size distribution (±10% by TEM) (12). Deviations in the amount of bonds per NC can be attributed to exhaustion of mobile surface atoms needed to form crystalline necks (41), the NCs preferably form robust necks with a few neighbors instead of weaker necks with all of them.

The observation of rather extended domains of one type of SS despite fluctuations in defining parameters (i.e. NC density and bonds/NC) indicates that, once a given SS has been nucleated under the right conditions, its further growth is quite robust. This aspect resembles classic monomer-by-monomer crystal growth of atomic or molecular building blocks.

Can we understand the concomitant formation of multiple superstructures?

Although the NC density for each SS fluctuates per domain, it does generally follow the geometrically predicted trend: lines < squares < honeycombs < zigzags. Furthermore, on a microscopic scale, NC density fluctuations reminiscent of patterns caused by

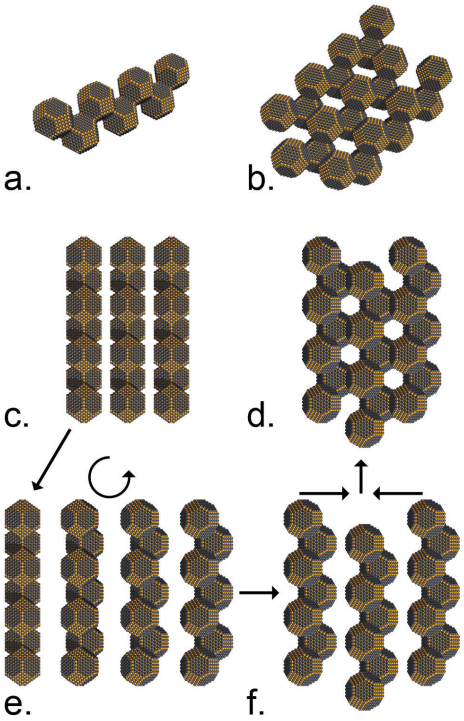

Figure 3.4. Models of the zigzag and honeycomb SSs and their geometric relations, please note that this is not a presumed mechanism of formation for the honeycomb SSs.
(a) and (b) show a perspective view of the zigzag and honeycomb SSs respectively, both are quasi-2D structures that have an atomically connected bottom and top layer. Images (c) to (f) show how the zigzag and honeycomb SSs are geometrically related to each other: (c) shows a top view of a zigzag SS, (e) shows how one zigzag line is rotated 35° around its linear axis, which results in lines that zigzag both in and out of the image plane. (f) by connecting these zigzags through their {100} facets that point from the top to bottom the bottom layer (and vice versa) results in a honeycomb SS, depicted in (d).

• • • •

solvent flow have often been observed. These variations in the NC density at the liquid/air interface may arise from irregular flows during the evaporation of the toluene, see Supporting Information 3.3 for more details. This might indicate that local fluctuations in the density of NCs at the toluene/air interface are important in the type of SS that is formed.

Figure 3S.3a and 3S.3b respectively show examples of the observation that domains of line and square SSs, and domains of zigzag and honeycomb SSs often form nearby each other or even interlace each other. This indicates that the formation of these sets of SSs have a common origin and that the local NC density on the liquid/air interface finally decides between linear and square structures, or between zigzag and honeycomb structures, respectively.

In fact, squares can simply be formed by sideways attachment of line strands, also zigzag and honeycomb SSs are very close in geometry. As the latter might be hard to picture at first, this is illustrated in Figure 3.4: a honeycomb structure results when tilting zigzag strands by 35°, shifting them by the length of less than a NC and then connecting them together. Local NC surface density during SS formation therefore seems the most defining difference between the squares and lines, as well as between honeycombs and zigzags.

However, why square and honeycomb SSs formed concomitantly and can be observed on the same TEM grid is not very clear. It could indicate that the free energy of the pre-attached phases of these SSs (i.e. a 2D NC superlattice attached to the toluene/air interface) is similar. Soligno et al. have recently studied the effect of the toluene surface tension on the orientation of the NCs at the toluene surface, and found that in most cases the energy for adsorption with the [100] axis upright (square SSs) or the [111] axis upright (honeycomb SSs) is similar (42).

Formation of 1-dimensional superstructures

Both the line and zigzag SSs clearly show a preference for attachment propagating in one direction while orthogonal binding sites are seemingly fully available. In both SSs the NCs attach via their {100} facets, but their direction of propagation differs: lines propagate in a <100> direction and zigzags in a <110> direction. Presumably, attaching {100} NC facets such that a corner or T-split in the 1D SSs is formed, should be just as favorable as attaching them in a linear fashion, but this is apparently in contrast with linear structures consisting of many NC units. The propensity of NCs to preferentially form 1D SSs is hard to rationalize at the moment.

Finally, we would like to remark that 1D SSs often contain far more bends, kinks or wiggles along their direction of propagation than 2D SSs, examples of which can clearly be seen in Figures 3.2f, 3.2h, 3.2o, 3.3b and 3.3e. This jitter in morphology is probably caused by the fact that oriented attachment is not a reversible process; the first attachment of two NC cores will lock them together, even if their connection is not perfect. The interfacial NC self-assembly prior to attachment is reversible. During the formation of 2D SSs the NCs are in a stronger self-assembled scaffold, causing the 2D SSs to be less prone to irregularities in the final attachment. In fact, Savitzky et al. have shown that a scaffold of NC SSs increases the long-range ordering in overlaying SSs (12).

3.3.5. Mechanistic aspects of neck formation

General aspects

The last step in the formation process of the PbX SSs is oriented attachment of the NCs. We remark that it is essential for the formation of highly periodic SSs that the self-assembly and oriented attachment processes are separated in time. This was indeed observed for the square formation (15).

The oriented attachment of the NCs happens through a process called necking. Necking implies that atoms from the two attaching crystallites solidify into a bridge between two opposing similar crystal facets, {100} facets in the present study (6). This follows from the fact that in the SSs the center-to-center distance is always larger than the original size of the NCs (11). Note that the process of necking requires vast atomic

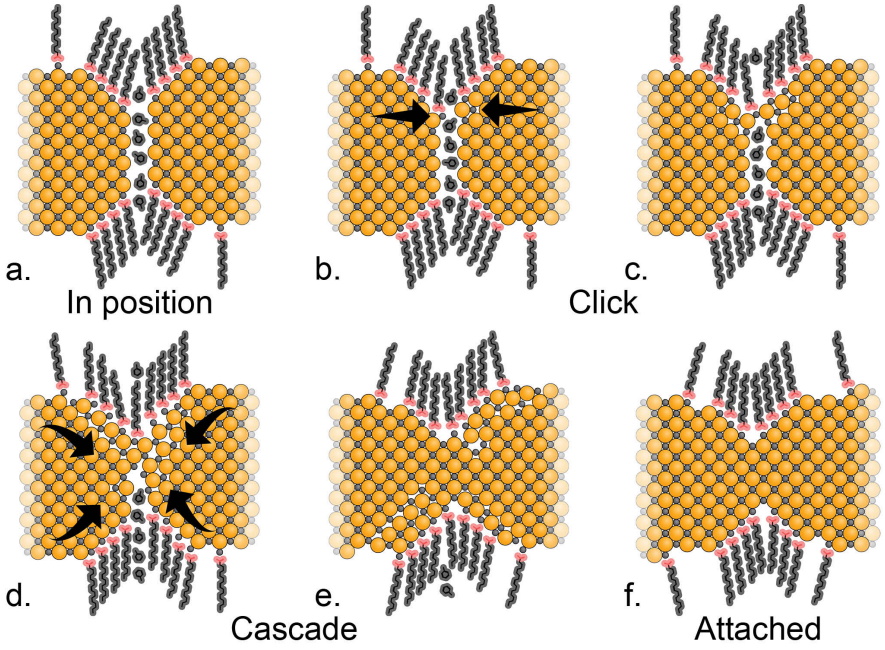

Figure 3.5: Model images of how PbX NCs are presumed to perform oriented attachment through a 'click and cascade' necking model.
(a) at very short range, attractive Coulombic forces between the NCs start to dominate their interactions, however the last few solvent molecules cannot leave the bordering area all at the same time, so the NCs cannot attach directly facet-to-facet. (b, c) atoms at the NC corner sites are expected to be the most labile as they have the lowest coordination number. Therefore, they will be the most mobile surface atoms at the NC surface, so they will find atoms from the other NC first by random thermal motion and 'click' to form a first connection. (d, e) the site of the first click forms an ideal nucleus for other labile surface atoms to find a more stable position with a higher coordination number. Finally, these surface atoms start to 'cascade into the NCs' bordering area. (f) after thorough surface reconstructions a neck is formed between the two NCs.

3.3

motion of the atoms in crystallites, as multiple layers of material have to solidify between two attaching NCs. This process is most likely a rearrangement of surface atoms (30, 43), finally resulting in a more extended single crystal.

We present a tentative model for a step-by-step necking process in Figure 3.5. Initially, a couple of atoms 'click' together by random thermal motion and thereby form the nucleus of a bridge, as depicted in Figure 3.5b and 3.5c. This will create a 'cascade' of surface atoms that move to an energetically more favorable position. This cascading process is illustrated in Figure 3.5d and 3.5e. After further reconstructions of the atoms on the surface, a neck is fully formed between the NCs as depicted in Figure 3.5f.

This 'click and cascade' model that attaches NCs like a zipper can also explain why crystallites that perform oriented attachment form necks in the first place. NCs cannot

simply click together two opposing facets, as the last bits of solvent cannot move out of the way all at once. This residual solvent layer, blocking direct facet-to-facet attachment of two NCs, is depicted in Figure 3.5a. With the proposed necking model, the residual solvent molecules can gradually diffuse out of the bordering area to make space for the neck.

Of course, Figure 3.5 depicts a highly idealized image projected in two dimensions the of NC attachment, which in reality must be more complex and occurs in three dimensions. Both HR-TEM observations and modelling studies show that the surface atoms of PbX NCs are at non-crystallographic positions due to surface reconstructions or random thermal motion (24, 30). Still the general idea of the proposed model holds even then. Atoms from the 'cloud' of loosely bound surface atoms meet and form a nucleus for further neck growth.

Comparison of neck formation in the PbX family

Although the SSs formed by oriented attached of PbX NCs showed mostly similarities in geometry, some subtle differences can be identified upon closer scrutiny. The observed differences are increasing disorder in attachment, thicker neck formation and preferential 2D SS formation, all with increasing atomic weight of the anions, i.e. PbS < PbSe < PbTe.

3.3

The first two differences can best be discussed together as both are related to the neck formation process itself. First, when comparing Figures 3.2n-p it can be seen that the lines formed by PbTe NCs are less straight than those formed by PbS and PbSe. Second, neighboring PbTe NCs in a SS generally formed thicker necks between each other, two examples of this thicker necking can be seen in Figures 3S.2d and 3S.2l.

Both these observations can be explained by looser binding of the surface atoms to the NC core. Particularly the Pb-oleate moieties at the {100} facets are expected to be highly mobile as these do not have to stabilize the underlying surface facet, such as ligands bound to a {111} facet. In this way, the ligands at {100} facets can easily move out of the way and let the NCs attach faster. Faster attachment makes reversible reconfigurations more difficult. Hence, this results into less nicely ordered SSs as observed in the more wiggly PbTe lines.

Also, looser binding of the ligands allows for a more rigorous reformation of the structure's surface towards a thermodynamic minimum, which is bulk PbX. Thicker necks between NCs, as we observe for PbTe, is the closest to the bulk geometry that the system can come by reordering the surface moieties.

The last observed difference in SS formation between the PbXs is that PbS NCs showed a preference for forming 1D SSs, whereas PbTe showed a preference for forming 2D SSs. The 1D SSs need at least two bonds to form whereas the 2D SSs need at least

three. It seems therefore likely that more reactive species would prefer forming 2D SSs instead of 1D ones.

As was already discussed above, the slight optimizations of the reaction conditions also show a trend that coincides well with the binding energy in the different PbX lattices, as reflected in their bulk melting temperatures and formation enthalpies. The subtle differences in the neck formation corroborate that the surface reactivity trend is indeed PbS < PbSe < PbTe.

3.4. Conclusions

In this study a synthetic self-assembly route towards four (quasi) 2D SSs, namely squares, honeycombs, zigzags and lines, from PbX NCs is described in detail, their common features but also their differences are highlighted. The geometry of the SSs made with different PbXs show mostly similarities, which coincides well with the fact that their constituent NCs all have the rock salt crystal structure and Pb-oleate capping ligands leading to similar colloidal behavior and a similar surface chemistry. Therefore, also the reaction conditions at which the SSs formed show mostly similarities. It was deduced that all these SSs form at a liquid/gas interface. The surface reactivity of the NC cores increases slightly when going from PbS to PbSe and greatly when going from PbSe to PbTe, which coincides well with their bulk melting temperatures and enthalpies of formation. Finally, a 'click and cascade' model of PbX oriented attachment was proposed that explains neck formation as a process to remove solvent molecules from the area between two attaching NCs.

Full reproducibility and comparability of the reaction conditions towards these SSs could not be reached, because the exclusive formation of a single kind of SS requires very fine tuning of the nanoscopic NC density at the liquid/air interface during the experiment, but this is hampered by surface liquid flow during the solvent evaporation. Future research should focus on homogenizing the NC density throughout the experiment and on further exploring the parameter space in which the SSs are formed to allow quantitative research into the microscopic parameters (NC, ligand and surfactant concentrations) for finding fully reproducible parameters towards each of the desired PbX NC SSs.

3.S. Supplementary information

3.S.1 Nanocrystal synthesis

Lead sulfide nanocrystal synthesis (18)

To produce a lead-precursor 0.39 g Pb(II)acetate trihydrate (99.999%, Sigma-Aldrich), 1.28 ml oleic acid (90%, Sigma-Aldrich), 2 mL trioctyl phosphine (90%, Sigma-Aldrich) and 12.5 mL octadecene (90%, Sigma-Aldrich) were added to an erlenmeyer in a nitrogen-purged glovebox. This mixture was transported

to a Schlenkline where it was left to react under vacuum at 130 °C for 1.5 hours. The resulting mixture was cooled down to room temperature and transported to a nitrogen-purged glovebox. There it was transferred to a three-neck flask and heated to 120 °C after which 16 µL of bis(trimethylsilyl)sulfide (synthesis grade, Sigma-Aldrich) was rapidly added under vigorous stirring. After two minutes at a constant temperature of 120 °C the heating was removed and the reaction mixture was allowed to cool down at room temperature. The mixture was quenched by adding 20 mL of acetone (anhydrous, Merck) when it reached a temperature of 65 °C. The resulting NCs were then centrifuged, the solvent decanted and residue NCs dispersed in 4 mL hexane (99%, Sigma-Aldrich). To this dispersion 15 mL methanol (99.8%, Sigma-Aldrich) was added, the resulting mixture was centrifuged, solvent decanted and residue dispersed in 4 mL hexane. To this dispersion 15 mL methanol and 400 µL oleic acid were added, the resulting mixture was again centrifuged, decanted and dispersed in 4 mL hexane.

Lead selenide nanocrystal synthesis (19).

To produce a Se-precursor, 2.487 g selenium powder (99.999%, Alfa-Aesar) was dissolved in 32.83 mL trioctyl phosphine (90%, Sigma-Aldrich) and 0.289 mL diphenylphosphine (98%, Sigma-Aldrich) in a nitrogen-purged glovebox. To produce a Pb-precursor 4.80 g Pb(II)acetate trihydrate (99.999%, Sigma-Aldrich), 10.35 g oleic acid (90%, Sigma-Aldrich) and 40.73 g octadecene (90%, Sigma-Aldrich) were added to an erlenmeyer. This mixture was left to react under vacuum at 120 °C at a Schlenkline for 5 hours. The resulting mixture was cooled down to room temperature and transported to a nitrogen-purged glovebox. There 20.5 mL of the Pb-precursor was transferred to a three-neck flask and heated to 180 °C after which 15 mL of the Se-precursor was rapidly added under rigorous stirring. The mixture was left to react at 150 °C for 80 seconds and then quenched by adding 20 mL butanol (99.8%, Sigma-Aldrich) and 10 mL of methanol (99.8%, Sigma-Aldrich) after 5 more minutes. The NC were then sedimented by centrifugation and the solvent removed by decantation. The NCs were washed again by adding 20 mL methanol, centrifugation, decantation. Finally, the NCs were dispersed in 20 mL toluene (99.8%, Sigma-Aldrich).

3S

Lead telluride nanocrystal synthesis (20, 21)

To produce a Te-precursor 0.194 g telluride powder (99.997%, Sigma-Aldrich) was dissolved in 3 mL trioctyl phosphine (90%, Sigma-Aldrich) in a nitrogen-purged glovebox. To produce a lead-precursor 1.138 g Pb(II)acetate trihydrate (99.999%, Sigma-Aldrich), 3.3 ml oleic acid (90%, Sigma-Aldrich) and 8 mL octadecene (90%, Sigma-Aldrich) were added to an erlenmeyer. This mixture was left to react under vacuum at 130 °C at a Schlenkline for 3 hours. The resulting mixture was cooled down to room temperature and transported to a nitrogen-purged glovebox. There it was transferred to a three-neck flask and heated to 170 °C after which the Te-precursor was rapidly added under rigorous stirring. The mixture was left to react at 140 °C for three minutes and then quenched by adding 3 mL hexane (95%, Sigma-Aldrich). The mixture was then brought to 60 °C after which 1 mL 0.161 M NH_4Cl (99.99%, Sigma-Aldrich) in methanol (99.8%, Sigma-Aldrich) was added and left to react for 15 minutes. Then the mixture was washed twice by adding 5 mL ethanol (96%, Alfa-Aesar), centrifugation, decantation and dispersion in 5 mL hexane.

3.S.2 Superstructure assembly (10, 11)

All methods listed here are performed in a nitrogen-purged glovebox dedicated to oriented attachment research only. Performing oriented attachment in a glovebox which is also used for NC synthesis can yield detrimental results. Oxygen and molecules used in some syntheses share the ability to strip ligands from the surfaces of the NCs (32, 44–46), thereby speeding up attachment to such a rapid pace that long-range or even short-range order is not preserved anymore. A few ppm of oxygen in the atmosphere during the oriented attachment procedure can already devastate an experiment, such results are shown in Figure 3S.1.

Irreproducibility caused by chemical pollution in the attachment atmosphere could be greatly reduced by working in a dedicated oriented attachment glovebox in which extra care was taken never to let the

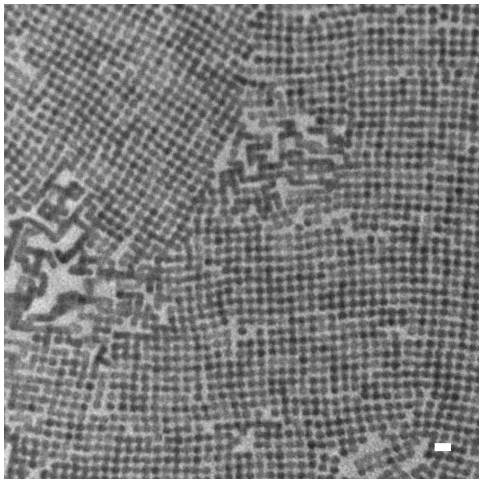

Figure 3S.1: TEM image of a square SS synthesized in a glovebox with a few ppm oxygen present. Note the patches of distorted NC attachment. Scale bar denotes 10 nm.

oxygen and water levels rise above 1 ppm. Also, heating the ethylene glycol at 100 °C under reduced pressure for 3 hours or until no more bubbles were visible in order to remove residual water prior to use greatly improved reproducibility over different batches of oriented attachment experiments.

Below NC concentrations are mentioned, as those can actually be used in experiments. In the main article NC surface density or surface area per NC is used, as it was found that those values influence the SS formation process more directly. Below, all substrate dimensions are mentioned, so concentration and surface density values can easily be converted by those who wish to reproduce our results.

3.S

Lead sulfide superstructure assembly.

A dispersion of ~6.6 x 10^{-8} M PbS NCs (see results and discussion in the main article for exact numbers) in hexane was prepared by dilution. A liquid substrate was prepared by adding 1 mL of ethylene glycol to a glass vial with a diameter of 10 mm. The liquid substrate was heated to 30 °C after which 50 µL of the PbS NC dispersion was carefully drop casted onto it. This system was left to react for 1 hour after which the surface was scooped with a TEM grid. Residual liquid substrate was removed by vacuum. The sample was then removed from the glovebox and analyzed by TEM.

Lead selenide superstructure assembly.

A dispersion of ~1.5 x 10^{-7} M PbSe NCs (see results and discussion in the main article for exact numbers) in toluene was prepared by dilution. A liquid substrate was prepared by adding 6.5 mL of ethylene glycol to a glass petri dish with a diameter of 27 mm. Then 350 µL of the PbSe NC dispersion was carefully drop casted onto it. This system was left to react for 1 hour at room temperature (around 26 °C) after which the surface was scooped with a TEM grid. Residual liquid substrate was removed by vacuum. The sample was then removed from the glovebox and analyzed by TEM.

Lead telluride superstructure assembly.

A dispersion of ~6.8 x 10^{-8} M PbTe NCs (see results and discussion in the main article for exact numbers) in hexane was prepared by dilution. A liquid substrate was prepared by adding 6.6 mL of ethylene glycol to a glass petri dish with a diameter of 27 mm, onto which ~15 µL of a dilute oleic acid dispersion (10 µL oleic acid in 3 mL ethylene glycol) was drop casted. Then 350 µL of the PbTe NC dispersion was carefully drop casted onto it. This system was left to react for 1 hour at room temperature (~22 °C) after which the surface was scooped with a TEM grid. Residual liquid substrate was removed by vacuum. The sample was then removed from the glovebox and analyzed by TEM.

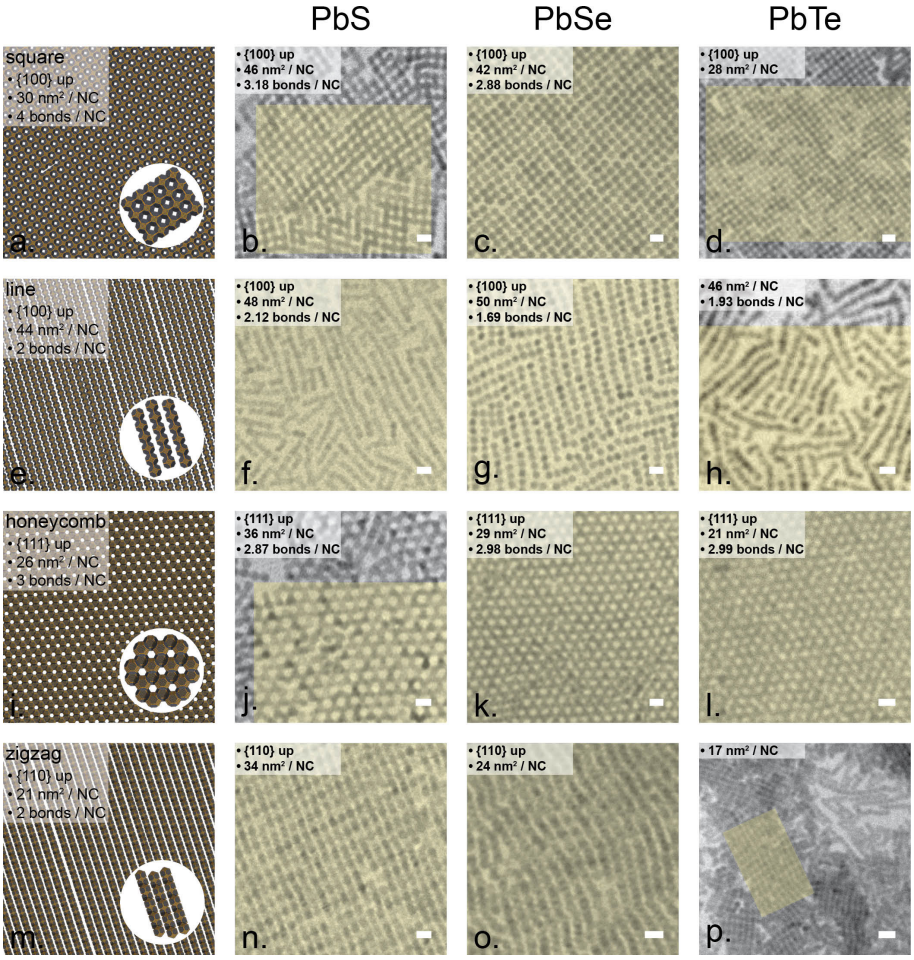

Figure 3S.2: Same models and SSs as Figure 2 in the main article, but these TEM images have been used for measuring the amount of nm²/NC and bonds/NC.
The image quality of the TEM data in Figure 3.2 is not good enough for such analysis. The areas where was measured are highlighted in yellow. All scale bars denote 10 nm.

• • • •

3.S.3 Solvent flow causes fluctuations in local nc density

The reaction conditions for creating SSs are not only very reminiscent between the members of the PbX family, also the reaction conditions towards each SS within one member of the PbX family are very similar. In fact, on some occasions several or even all SSs can be observed in only a few tens of nanometers in proximity, as can be seen in Figures 3S.3a and 3S.3b. These observations are most likely caused by local fluctuations in NC surface density, which are in turn caused by solvent evaporation flow during SS formation. Many observations on a micrometer scale have been made of sample morphologies, examples of which can be seen in Figures 3S.3c and 3S.3d, that reminisce literature results on particle ordering affected by fluid flow (46–50).

Solvent flow causing the formation smaller SS domains with a geometry that does not match the NC concentration of the experimentally used value of course hampers the reproducibility of synthesizing a single desired SS. Hence, to avoid this problem in the future, fluid flow should be stopped, possibly by extremely slow evaporation of the solvent.

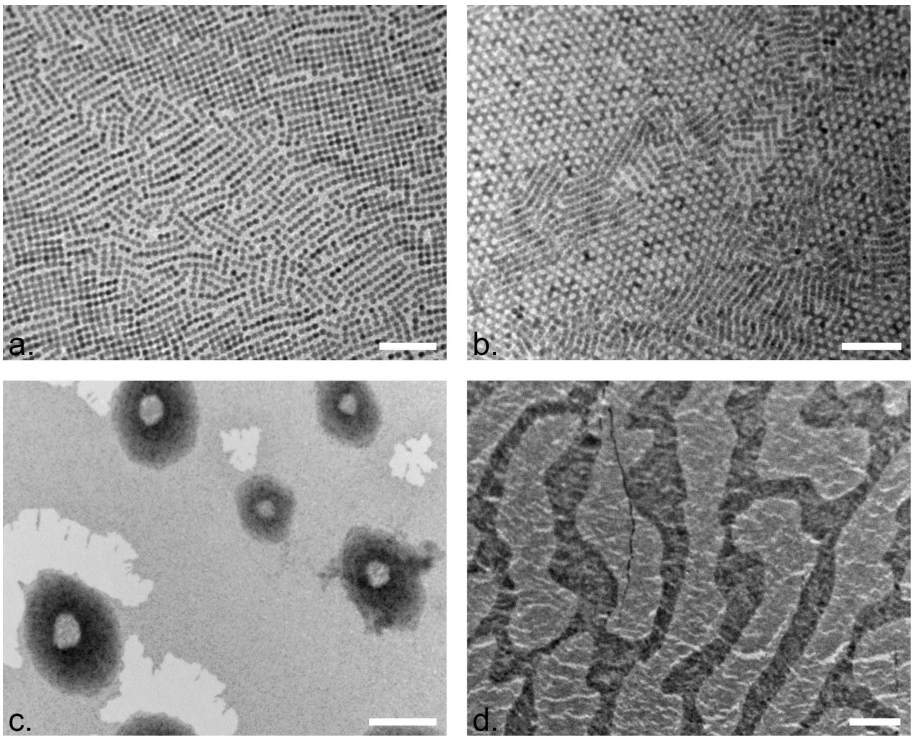

Figure 3S.3: TEM images of NC surface density fluctuations on nanoscopic (a, b) and microscopic (c, d) scale.
This behavior is probably caused by liquid flow during the experiments due to solvent evaporation. Note that the SS geometry changes when the local NC density changes. Scale bars denote 50 nm and 0.5 µm in images (a, b) and (c, d), respectively.

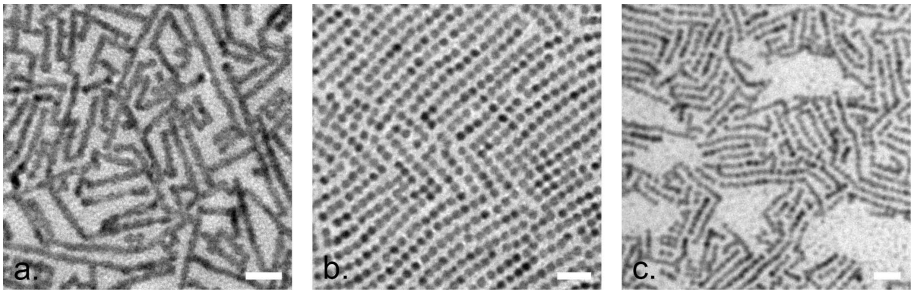

Figure 3S.4: TEM images of linear SSs of respectively (a) PbS, (b) PbSe and (c) PbTe NCs. The dark contrast between the NCs shows that a neck has formed between the particles during oriented attachment. Scale bars denote 20 nm.

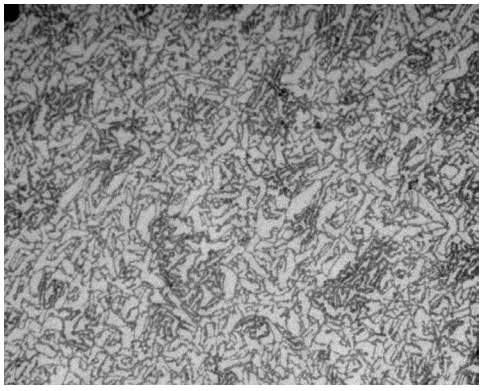

Figure 3S.5: TEM image of PbTe NCs that have undergone the oriented attachment procedure without additional Cl-ligands and oleic acid.

3S

References

1. Kovalenko, M. V et al. Prospects of Nanoscience with Nanocrystals. ACS Nano 9, 1012–1057 (2015).

2. Nag, A. et al. Metal-free Inorganic Ligands for Colloidal Nanocrystals: S 2– , HS – , Se 2– , HSe – , Te 2– , HTe – , TeS 3 2– , OH – , and NH 2 – as Surface Ligands. J. Am. Chem. Soc. 133, 10612–10620 (2011).

3. Bailey, J. K., Brinker, C. J. & Mecartney, M. L. Growth Mechanisms of Iron Oxide Particles of Differing Morphologies from the Forced Hydrolysis of Ferric Chloride Solutions. J. Colloid Interface Sci. 157, 1–13 (1993).

4. Banfield, J. F., Welch, S. A., Zhang, H., Ebert, T. T. & Penn, R. L. Aggregation-Based Crystal Growth and Microstructure Development in Natural Iron Oxyhydroxide Biomineralization Products. Science (80-.). 289, 751–754 (2000).

5. Liao, H.-G., Cui, L., Whitelam, S. & Zheng, H. Real-time imaging of Pt3Fe nanorod growth in solution. Science 336, 1011–4 (2012).

6. Li, D. et al. Direction-specific interactions control crystal growth by oriented attachment. Science 336, 1014–8 (2012).

7. De Yoreo, J. J. et al. Crystallization by particle attachment in synthetic, biogenic, and geologic environments. Science (80-.). 349, aaa6760-aaa6760 (2015).

8. Cho, K.-S., Talapin, D. V, Gaschler, W. & Murray, C. B. Designing PbSe nanowires and nanorings through oriented attachment of nanoparticles. J. Am. Chem. Soc. 127, 7140–7 (2005).

9. Evers, W. H. et al. High charge mobility in two-dimensional percolative networks of PbSe quantum dots connected by atomic bonds. Nat. Commun. 6, 8195 (2015).

10. Evers, W. H. et al. Low-Dimensional Semiconductor Superlattices Formed by Geometric Control over Nanocrystal Attachment. Nano Lett. 13, 2317–2323 (2013).

11. Boneschanscher, M. P. et al. Long-range orientation and atomic attachment of nanocrystals in 2D honeycomb superlattices. Science (80-.). 344, 1377–1380 (2014).

12. Savitzky, B. H. et al. Propagation of Structural Disorder in Epitaxially Connected Quantum Dot Solids from Atomic to Micron Scale. Nano Lett. 16, 5714–8 (2016).

13. Kalesaki, E. et al. Dirac Cones, Topological Edge States, and Nontrivial Flat Bands in Two-Dimensional Semiconductors with a Honeycomb Nanogeometry. Phys. Rev. X 4, 11010 (2014).

14. Walravens, W. et al. Chemically Triggered Formation of Two-Dimensional Epitaxial Quantum Dot Superlattices. ACS Nano 10, 6861–6870 (2016).

15. Geuchies, J. J. et al. In situ study of the formation mechanism of two-dimensional superlattices from PbSe nanocrystals. Nat. Mater. 15, 1248–1254 (2016).

16. Rivest, J. B. & Jain, P. K. Cation exchange on the nanoscale: an emerging technique for new material synthesis, device fabrication, and chemical sensing. Chem. Soc. Rev. 42, 89–96 (2013).

17. Murray, C. B., Norris, D. J. & Bawendi, M. G. Synthesis and characterization of nearly monodisperse CdE (E = sulfur, selenium, tellurium) semiconductor nanocrystallites. J. Am. Chem. Soc. 115, 8706–8715 (1993).

18. Abel, K. A., Shan, J., Boyer, J. C., Harris, F. & van Veggel, F. C. J. M. Highly photoluminescent PbS nanocrystals: The beneficial effects of trioctylphosphine. Chem. Mater. 20, 3794–3796 (2008).

19. Steckel, J. S., Yen, B. K. H., Oertel, D. C. & Bawendi, M. G. On the mechanism of lead chalcogenide nanocrystal formation. J. Am. Chem. Soc. 128, 13032–3 (2006).

20. Urban, J. J., Talapin, D. V, Shevchenko, E. V & Murray, C. B. Self-Assembly of PbTe Quantum Dots into Nanocrystal Superlattices and Glassy Films. 3248–3255 (2006).

21. Woo, J. Y. et al. Ultrastable PbSe Nanocrystal Quantum Dots via in Situ Formation of Atomically Thin Halide Adlayers on PbSe(100). J. Am. Chem. Soc. 136, 8883–8886 (2014).

22. Cademartiri, L. et al. Size-Dependent Extinction Coefficients of PbS Quantum Dots. J. Am. Chem. Soc. 128, 10337–10346 (2006).

23. Moreels, I. et al. Composition and Size-Dependent Extinction Coefficient of Colloidal PbSe Quantum Dots. Chem. Mater. 19, 6101–6106 (2007).

24. Peters, J. L. et al. Ligand-Induced Shape Transformation of PbSe Nanocrystals. Chem. Mater. 29, 4122–4128 (2017).

25. Kaushik, A. P. & Clancy, P. Explicit all-atom modeling of realistically sized ligand-capped nanocrystals. J. Chem. Phys. 136, 114702 (2012).

26. Petkov, V., Moreels, I., Hens, Z. & Ren, Y. PbSe quantum dots: Finite, off-stoichiometric, and structurally distorted. Phys. Rev. B 81, 241304 (2010).

27. Zherebetskyy, D. et al. Hydroxylation of the surface of PbS nanocrystals passivated with oleic acid. Science (80-.). 344, 1380–1384 (2014).

28. Anderson, N. C., Hendricks, M. P., Choi, J. J. & Owen, J. S. Ligand Exchange and the Stoichiometry of Metal Chalcogenide Nanocrystals: Spectroscopic Observation of Facile Metal-Carboxylate Displacement and Binding. J. Am. Chem. Soc. 135, 18536–18548 (2013).

29. Fang, C., van Huis, M. a, Vanmaekelbergh, D. & Zandbergen, H. W. Energetics of Polar and Nonpolar Facets of PbSe Nanocrystals from Theory and Experiment. ACS Nano 4, 211–218 (2010).

30. Schapotschnikow, P., van Huis, M. a, Zandbergen, H. W., Vanmaekelbergh, D. & Vlugt, T. J. H. Morphological Transformations and Fusion of PbSe Nanocrystals Studied Using Atomistic Simulations. Nano Lett. 10, 3966–3971 (2010).

31. Bertolotti, F. et al. Crystal symmetry breaking and vacancies in colloidal lead chalcogenide quantum dots. Nat. Mater. 15, 987–994 (2016).

32. Baumgardner, W. J., Whitham, K. & Hanrath, T. Confined-but-Connected Quantum Solids via Controlled Ligand Displacement. Nano Lett. 13, 3225–3231 (2013).

33. Schliehe, C. et al. Ultrathin PbS sheets by two-dimensional oriented attachment. Science 329, 550–3 (2010).

34. Haynes W. M. CRC Handbook of Chemistry and Physics, 97th Edition. CRC Handbook of Chemistry and Physics (2017).

35. Piveteau, L. et al. Structure of Colloidal Quantum Dots from Dynamic Nuclear Polarization Surface Enhanced NMR Spectroscopy. J. Am. Chem. Soc. 137, 13964–13971 (2015).

36. Murphy, J. E. et al. PbTe colloidal nanocrystals: Synthesis, characterization, and multiple exciton generation. J. Am. Chem. Soc. 128, 3241–3247 (2006).

37. Delerue, C. From semiconductor nanocrystals to artificial solids with dimensionality below two. Phys. Chem. Chem. Phys. 16, 25734–25740 (2014).

38. Delerue, C. & Vanmaekelbergh, D. Electronic band structure of zinc blende CdSe and rock salt PbSe semiconductors with silicene-type honeycomb geometry. 2D Mater. 2, 34008 (2015).

39. Beugeling, W. et al. Topological states in multi-orbital HgTe honeycomb lattices. Nat. Commun. 6, 1–7 (2015).

40. Novák, J. et al. Site-Specific Ligand Interactions Favor the Tetragonal Distortion of PbS Nanocrystal Superlattices. ACS Appl. Mater. Interfaces 8, 22526–33 (2016).

41. Treml, B. E. et al. Successive Ionic Layer Absorption and Reaction for Postassembly Control over Inorganic Interdot Bonds in Long-Range Ordered Nanocrystal Films. ACS Appl. Mater. Interfaces 9, 13500–13507 (2017).

42. Soligno, G., Dijkstra, M. & van Roij, R. Self-Assembly of Cubes into 2D Hexagonal and Honeycomb Lattices by Hexapolar Capillary Interactions. Phys. Rev. Lett. 116, 258001 (2016).

43. Yalcin, A. O. et al. Atomic Resolution Monitoring of Cation Exchange in CdSe-PbSe Heteronanocrystals during Epitaxial Solid–Solid–Vapor Growth. Nano Lett. 14, 3661–3667 (2014).

44. Choi, J. J. et al. Controlling Nanocrystal Superlattice Symmetry and Shape-Anisotropic Interactions through Variable Ligand Surface Coverage. J. Am. Chem. Soc. 133, 3131–3138 (2011).

45. Zhang, H. et al. Surfactant ligand removal and rational fabrication of inorganically connected quantum dots. Nano Lett. 11, 5356–5361 (2011).

46. Sandeep, C. S. S., Azpiroz, J. M., Evers, W. H. & Boehme, S. C. Epitaxially Connected PbSe Quantum-Dot Films : Controlled Neck Formation and Optoelectronic Properties. ACS Nano 8, 1–7 (1930).

46. Adachi, E., Dimitrov, A. S. & Nagayama, K. Stripe Patterns Formed on a Glass Surface during Droplet Evaporation. Langmuir 11, 1057–1060 (1995).

47. Ge, G. & Brus, L. Evidence for Spinodal Phase Separation in Two-Dimensional Nanocrystal Self-Assembly. J. Phys. Chem. B 104, 9573–9575 (2000).

48. Rabani, E., Reichman, D. R., Geissler, P. L. & Brus, L. E. Drying-mediated self-assembly of nanoparticles. Nature 426, 271–274 (2003).

49. Prevo, B. G. & Velev, O. D. Controlled, Rapid Deposition of Structured Coatings from Micro- and Nanoparticle Suspensions. Langmuir 20, 2099–2107 (2004).

50. Ball, P. In Retrospect: the physics of sand dunes. Nature 457, 1084–1085 (2009).

This chapter is based on:

In situ study of the formation mechanism of two-dimensional superlattices from PbSe nanocrystals; Jaco J. Geuchies, Carlo van Overbeek*, Wiel H. Evers, Bart Goris, Annick De Backer, Anjan P. Gantapara, Freddy. T. Rabouw, Jan Hilhorst, Joep L. Peters, Oleg Konovalov, Andrei V. Petukhov, Marjolein Dijkstra, Laurens D.A. Siebbeles, Sandra Van Aert, Sara Bals and Daniel Vanmaekelbergh; Nat. Mater. 15, 1248–1254 (2016).*

**These authors contributed equally.*

Chapter 4

In-situ study of the formation mechanism of two-dimensional superstructures from PbSe nanocrystals

Abstract **95**

4.1. Introduction **95**

4.2. Results and discussion **96**
4.2.1. Time-evolution investigation of the nanocrystal superlattice by in-situ scattering experiments *99*
4.2.2. Confirming atomic coherency by ex-situ high-resolution electron microscopy *100*
4.2.3. Superstructure formation hypothesis *102*
4.2.4. Checking the formation hypothesis with Monte Carlo simulations *102*

4.3. Conclusions and outlook **105**

4.S. Supporting information **106**
4.S.1. Methods *106*
4.S.2. Additional data and analysis *109*

References **112**

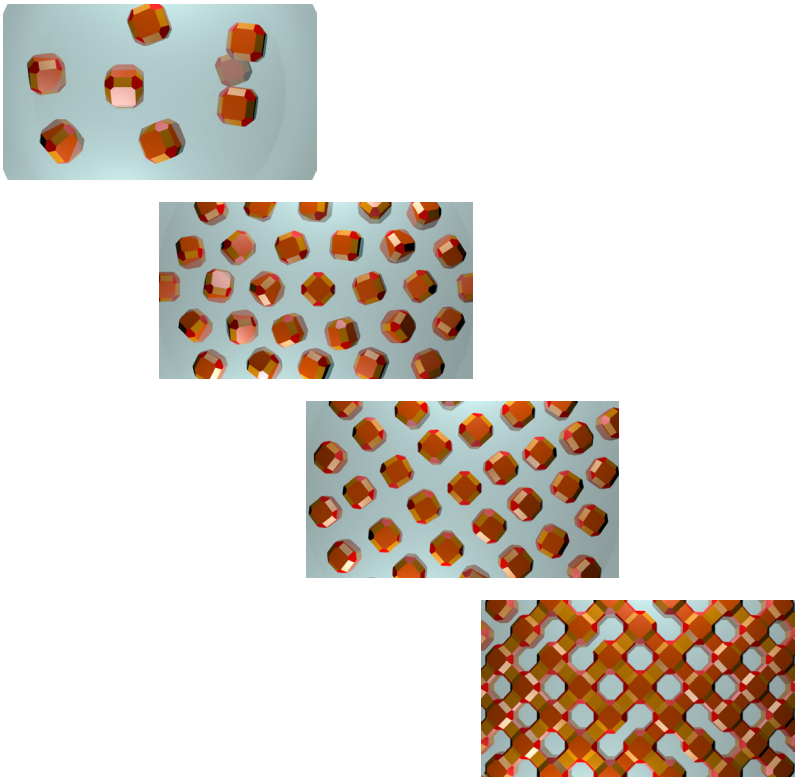

4.1

In-situ and ex-situ studies show that nanoperiodic superstructures made with PbSe nanocrystals perform multiple phase changes at the liquid interface before final oriented attachment.

Abstract

Oriented attachment of PbSe nanocubes can result in the formation of two-dimensional (2D) superstructures with long-range nanoscale and atomic order (1, 2). This questions the applicability of classic models in which the structure grows by first forming a nucleus, followed by sequential irreversible attachment of nanocrystals (3, 4), as one misaligned attachment would disrupt the 2D order beyond repair. Here, we demonstrate the formation mechanism of 2D PbSe superstructures with square geometry by using in-situ grazing-incidence X-ray scattering (small-angle and wide-angle), ex-situ electron microscopy, and Monte Carlo simulations. We observed nanocrystal adsorption at the liquid/gas interface, followed by the formation of a hexagonal nanocrystal monolayer. The hexagonal geometry transforms gradually through a pseudo-hexagonal phase into a phase with square order, driven by attractive interactions between the {100} planes perpendicular to the liquid substrate, which maximize facet-to-facet overlap. The nanocrystals then attach atomically via a necking process, resulting in 2D square superstructures.

4.1. Introduction

Oriented atomic attachment of colloidal nanocrystals (NCs), i.e. the formation of a single crystal by atomic connection of smaller crystals, is an important process in geology (5-8), and recently gained much attention as a preparation tool in semiconductor nanoscience (9, 10). We reported a method to prepare 2D atomically coherent PbSe superstructures, starting from a suspension of PbSe NCs (1, 2). The NCs have the shape of a truncated cube, consistent with the rock salt crystal structure of PbSe. A suspension of these NCs is cast onto a surface of an immiscible liquid, ethylene glycol, and the solvent is evaporated at room temperature. During the evaporation, extended sheets are formed with a thickness of one NC monolayer (1).

The 2D structure shows a nanoscale geometry with square periodicity with, to some extent, also atomic coherency. In this so-called square geometry, all NCs are directed with a <100> axis perpendicular to the 2D plane, and are laterally connected via the in-plane {100} facets. This means that two out of six {100} facets, namely those at the top and the bottom of the 2D sheet, are not used for attachment.

Nanocrystal self-assembly and atomic attachment forms a unique route to prepare 2D semiconductors with a superimposed geometry on the nanometer scale that influences the band structure and can result in semiconductors with Dirac-type valence and conduction bands and high charge carrier mobility (10-14). Although superstructures with a square geometry are slightly disordered on the atomic scale, they show amazing

long-range ordering on the nanoscale. A better understanding of the formation process is required for further progress in the synthesis of these systems. The 2D long-range ordering cannot be explained in terms of the classic nucleation and growth model (3, 4). In this model the interactions between a crystal (nucleus) and building blocks are supposed to be relatively weak, in the order of a few k_BT. As a result, the building blocks can bind and unbind to an existing crystal, until the optimal binding geometry is found, resulting in ordering over long distances. In the case of superstructure formation by oriented attachment of NCs this mechanism cannot be operative, because per NC-NC connection, chemical bonds are formed between tens of atoms on opposing crystal facets. The corresponding energy change is orders of magnitude larger than the thermal energy, and oriented attachment should therefore be irreversible. Thus 'incorrect' irreversible attachments should lead to disruption of the long-range nanoscale order in the superstructure.

Here, we present a real-time study of the growth of 2D superstructures with a square periodicity. We monitor the reactive self-assembly in real time and in-situ by simultaneous grazing-incidence small-angle and wide-angle X-ray scattering (GISAXS and GIWAXS), see Figure S1. Moreover, we scoop the structures formed at different stages of the process for analysis with ex-situ Transmission Electron Microscopy (TEM).

Previous work on self-assembly of NCs has either focused on only monitoring the long-range order on the NC scale using GISAXS (15), ex-situ measurements using GISAXS and GIWAXS (16-19) and time resolved GISAXS and GIWAXS on the 3D self-assembly of PbS nanocrystals, showing an FCC-to-BCC phase transition (20). We find that oriented attachment of the nanocrystals by neck formation is preceded by a remarkable sequence of processes: nanocrystal adsorption at the liquid/air interface with the preservation of the rotational degrees of freedom, formation of a dense hexagonal NC phase, finally followed by a phase transition from hexagonal into square order in the NC monolayer in which the rotations become entirely frozen.

4.2. Results and discussion

In Figure 4.1 we follow the formation of the square superstructure starting from individual NCs, combining ex-situ TEM and electron diffraction (ED) with in-situ GISAXS and GIWAXS. The TEM and X-ray scattering measurements show the same stage in the NC assembly process. However, TEM data should be interpreted with care as a structure extracted at a given time during the self-assembly process may undergo changes during drying.

In the initial stages of the self-assembly process (16 minutes after the start of solvent evaporation), it is not clear whether the NCs are still dispersed or already adsorbed at the toluene/air interface (Figure 4.1b, 4.1c); but any long-range positional order (Figure 4.1a, 4.1b) or atomic orientation (Figure 4.1c) is lacking.

After 27 minutes, diffraction rods appear in the GISAXS pattern (Figure 4.1e), at scattering vectors of 0.80 nm^{-1}, 1.39 nm^{-1} and 1.61 nm^{-1}, consistent with a 2D hexagonal superlattice at the liquid-gas interface. We were not able to isolate this lattice ex-situ (Figure 4.1d), demonstrating the importance of the in-situ scattering measurements. The corresponding GIWAXS pattern in Figure 4.1f still shows the PbSe {200} and {220} diffraction rings, with no sign of a preferential crystallographic orientation or attachment of the NCs. We conclude that at this stage the NCs behave as hard spheres. Indeed, hard sphere interactions between NCs confined on a 2D interface leads to entropically driven packing into a hexagonal lattice (21, 22). Our difficulty in isolating this phase ex-situ indicates that short-range repulsive contributions from the solvent may be important to the hard sphere-like interaction potential.

At longer times, a complete monolayer of NCs is adsorbed at the interface. The NCs form a 2D pseudo-hexagonal close-packed layer (Figure 4.1g), with bond-angles deviating from the 60° of a perfect hexagonal structure. In the corresponding ED pattern the {111} and {222} rings are missing, meaning that all NCs have a {100} facet pointing upwards. Moreover, the ED pattern shows diffraction arcs rather than full rings, indicating that the NCs have a preferred crystallographic orientation in the 2D plane. The width of the arcs reflects the remaining in-plane rotational freedom of the NCs. In the GISAXS pattern obtained 30 minutes after the start of the experiment (Figure 4.1i) the first diffraction rod has moved further from the origin, indicating that the average NC–NC distance has decreased compared to Figure 4.1e. The diffraction peaks are broader than before, consistent with a peak splitting due to deviations of the superlattice symmetry from perfectly hexagonal. An alternative explanation for the broadening of the GISAXS reflections could be the increase of superlattice disorder due to evaporation of residual solvent (23, 24). However, we point out that we scooped a sample of this exact sample and confirmed the formation of the square superstructure (see Figure 4S.3), supporting the former interpretation of the scattering data. In the corresponding GIWAXS pattern (Figure 4.1j) we observe the first indications of spots of increased intensity on the atomic diffraction rings, indicative for NC orientation with a <100> axis perpendicular to the liquid-gas interface. In Figure 4.1h many NC–NC atomic connections have formed, but not yet all NCs make the maximum number of four NC–NC bonds with their in-plane {100} facets. The diffraction arcs in the ED pattern have further narrowed, since the rotational freedom has decreased with respect to the pseudo-hexagonal phase of Figure 4.1g.

Finally, the NCs attain a square ordered structure (Figure 4.1k, 4.1l) with the <100> direction pointing upward and orientational order in the 2D plane (inset Figure 4.1k). Furthermore, the NCs attach, as evidenced not only in the TEM image (Figure 4.1k), but also from the narrowing of the {200} diffraction spot in the horizontal direction in the GIWAXS pattern (Figure 4.1m). This is confirmed by later TEM measurements on the structure formed during the in-situ measurement (Figure 4S.3).

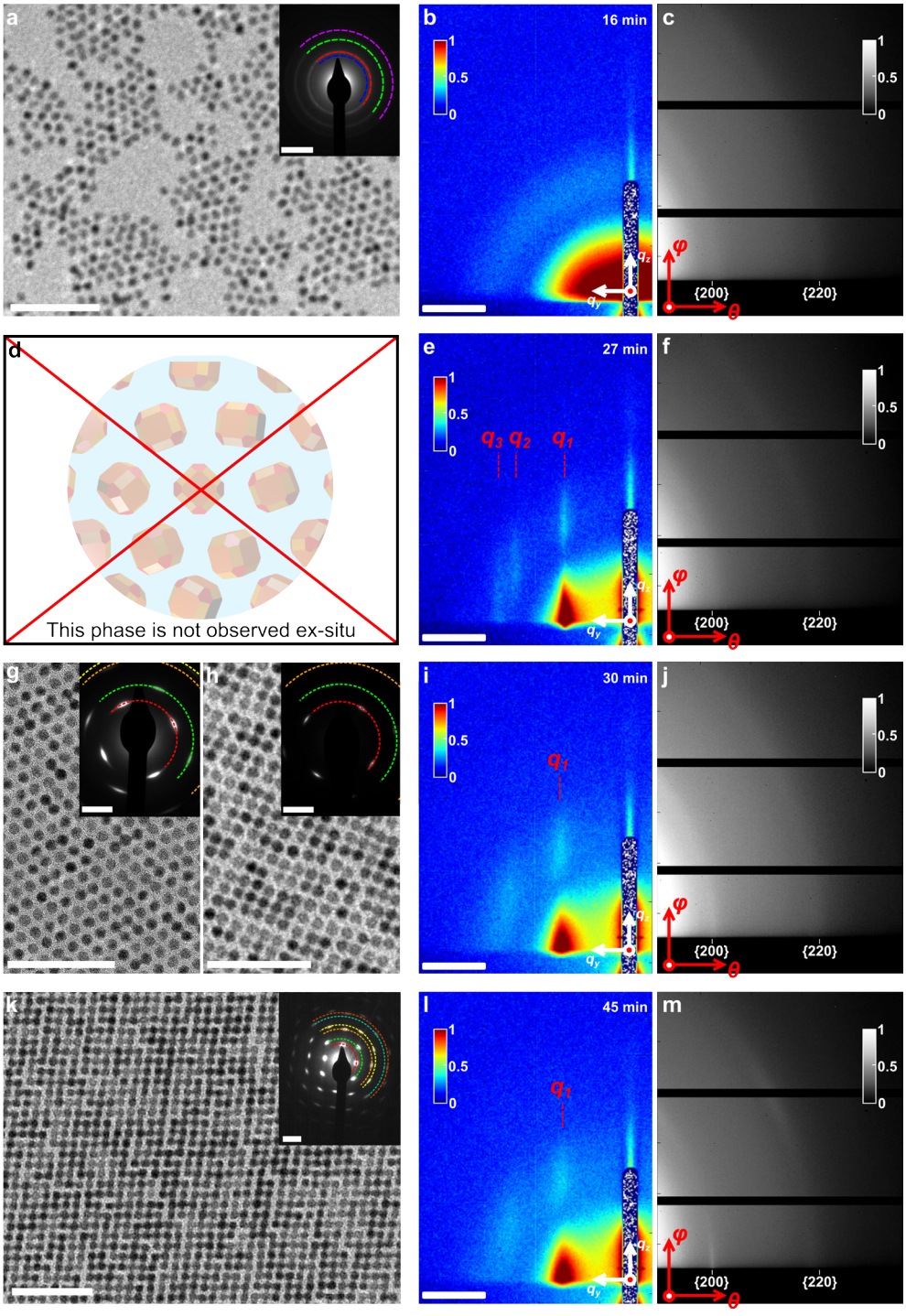
a
b
16 min
c
1
0.5
0
q_z
q_y
φ
θ
{200}
{220}
d
This phase is not observed ex-situ
e
27 min
q_3 q_2 q_1
f
g
h
i
30 min
q_1
j
k
l
45 min
m

4.2

Figure 4.1: The different stages of the self-assembly process towards an oriented attached PbSe NC superstructure.
Ex-situ TEM images and in-situ X-ray scattering data are taken at different stages in the hexagonal-to-square phase transition. Top to bottom rows show the different phases over time. (a) TEM image of the disordered NCs, obtained by scooping immediately after drop casting on ethylene glycol. Inset shows the corresponding ED pattern, where diffraction rings indicate random orientations of the NCs, i.e. they have rotational freedom. (b) At the initial stage, we observe form factor scattering in GISAXS, indicating the presence of NCs without long-range positional order. (c) The GIWAXS pattern shows the full {200} and {220} diffraction rings of PbSe, indicating rotational freedom. (d) No hexagonal phase could be isolated ex-situ. (e) GISAXS pattern showing the presence of a hexagonal nanocrystal monolayer at the interface, with (f) the corresponding GIWAXS pattern. (g) TEM image of the pseudo-hexagonal phase, obtained when scooping the NCs just before toluene has completely evaporated. Inset: in ED the rings transformed into arcs. (h) TEM image of the initial square phase, before complete attachment of all NCs. Inset: the arcs in the ED have narrowed. (i) GISAXS pattern of the corresponding phase. Note that all peaks have broadened. (j) GIWAXS pattern corresponding to (i). (k) TEM image of the final square phase. Inset: the ED pattern now consists of distinct spots, visible at least up to the {600} reflection. (l) GISAXS pattern of the final square phase, with (m) the corresponding GIWAXS pattern. Note how the diffraction rings have spots superimposed. The {200} diffraction has a narrower width in the 2θ-direction than before (compare j), indicating that the NCs have attached in this direction. All TEM scale bars correspond to 50 nm. The ED scale bars denote 20 nm^{-1}. The colored rings in the ED patterns display the position of the diffraction rings: blue = {111}, red = {200}, green = {220}, purple = {222}, orange = {400}, yellow = {420}, turquoise = {440}, brown = {600}. All GISAXS scale bars denote 1 nm^{-1}.

• • • •

4.2.1. Time-evolution investigation of the nanocrystal superlattice by in-situ scattering experiments

We now investigate in more detail the structural changes observed in the in-situ experiments. We calculate the time-evolution of the nanoscale lattice spacing from the position of the first diffraction rod in GISAXS (see Figure 4.2a). The fitted peak position in reciprocal space (left axis) increases from 0.74 nm^{-1} to 0.83 nm^{-1}. Realizing that the initial structure has hexagonal symmetry while the final structure is square, this corresponds to a contraction of the NC-NC distance by 17%, from 9.1 nm after 1200 s after injection, to 7.6 nm at 2700 s.

The initial NC–NC distance of 9.1 nm is as expected in a hexagonal monolayer of NCs of 5.7±0.6 nm core diameter separated by oleic acid ligands (roughly 2 nm in length). In the final oriented attached square structure, however, the NC–NC distance of 7.6 nm is 34% larger than the original PbSe NC core diameter. This shows that necking takes place during the atomic attachment, i.e. the formation of a crystal bridge between opposed {100} facets (2, 5, 25).

The increase of the average atomic coherence length during the formation can be extracted from the width of the horizontal atomic {200} reflections in GIWAXS (see Figure 4.2b). The FWHM of the {200} peak of individual NCs in dispersion equals 1.1

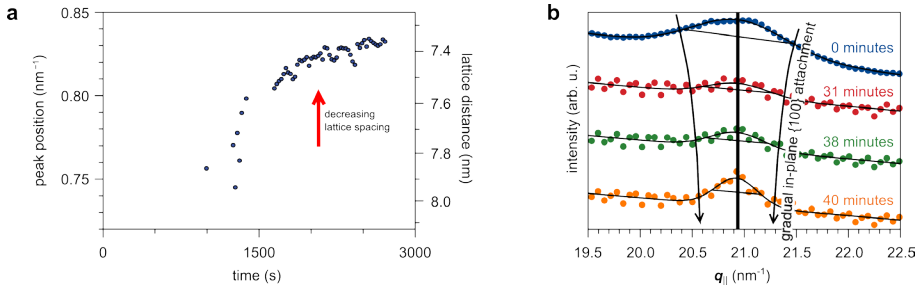

Figure 4.2: Quantitative analysis of the GISAXS and GIWAXS data.
(a) Fitted peak positions of the first diffraction rod q_1 in the horizontal scattering direction from the in-situ GISAXS measurements depicted in Figure 4.1. From the position of the diffraction rod the lattice spacing is calculated. (b) Evolution of the peak width of the in-plane {200} atomic reflection in the horizontal scattering direction $q_{||}$ over time as measured with GIWAXS. The black line is the calculated position of the {200} reflection for a rock salt PbSe crystal structure with a lattice vector of 6 Å.

nm^{-1}, corresponding to an average crystalline domain size of 5.9 nm, consistent with the NC sizes measured with TEM. During the in-situ experiments, the FWHM decreased to a value of 0.7 nm^{-1} after 31 minutes and 0.5 nm^{-1} after 40 minutes. These values correspond to crystalline domain sizes of 9.1 nm and 13.2 nm in the horizontal <100> direction. We conclude that when NCs attach atomically, the size of single-crystalline domains grows to on average to a lower limit of two to three NC diameters, which agrees with the TEM sample obtained from the same experiment (Figure 4S.3).

4.2.2. Confirming atomic coherency by ex-situ high-resolution electron microscopy

4.2

In order to study the degree of atomic coherency inside the superstructure, we performed aberration corrected high angle annular dark field (HAADF) scanning transmission electron microscopy (STEM) measurements to investigate the atomic lattice. First, Figure 4.3a shows an overview of part of a square sheet, showing that the square nanogeometry is present over many unit cells. In the atomically resolved image of Figure 4.3b, we observe atomic connections between the nanocrystals that are fully coherent, and some defective connections as well. These defective connections and the natural dispersion in the nanocrystal size must affect the perfectness of the square geometry, i.e. lead to some variation in the translation vectors. In SI Figure 4S.4, we show that the overall square periodicity (although with its intrinsic variation) is essentially preserved when it is considered over different length scales. From the HAADF-STEM image we extract the number of atoms in each projected atomic column using atom

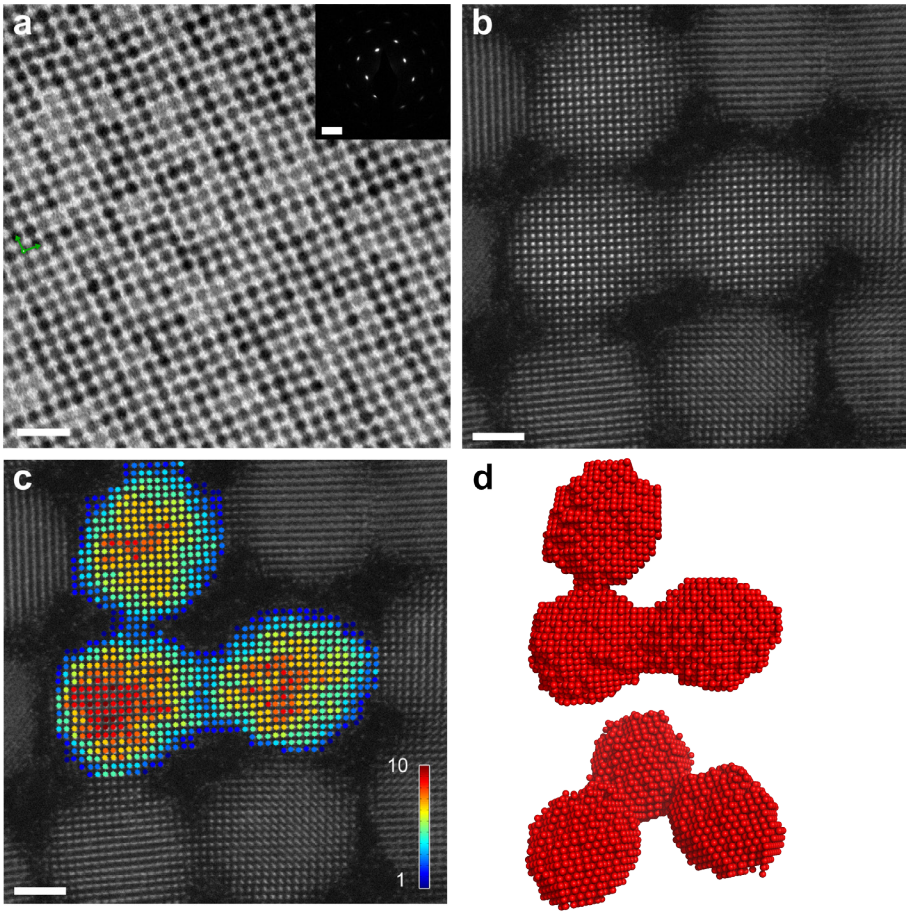

Figure 4.3: HAADF-STEM and atom counting reconstruction on the attached NCs.
(a) Typical overview bright-field TEM image on a square superstructure. Inset shows the corresponding ED pattern. (b) More detailed HAADF-STEM image on NCs attached in a square superstructure, showing truly epitaxial connections and connections with crystal defects. (c) Results from the atom counting procedure, using (b) as an input image. The colorbar represents the number of detected atoms in the column. (d) Topview and sideview of the reconstructed atomic model. Scale bars equal 20 nm in a (20 nm^{-1} in the ED inset) and 2 nm in b and c.

counting (Figure 4.3c) (26, 27). These numbers can then be used as an input for an iterative energy minimization scheme in order to obtain a 3D model for the investigated superstructure as illustrated in Figures 4.3d (28, 29). More experimental details are provided in the SI Methods section.

4.2.3. Superstructure formation hypothesis

Combining all information from the in-situ and ex-situ experiments, we postulate a model for the reactive self-assembly of PbSe nanocubes into the square oriented attached superstructure.

Figure 4.4 shows cartoons of the different phases occurring in the reactive self-assembly. For clarity, we omitted the oleic acid ligands from the image. During the toluene evaporation the NCs adsorb at the liquid-gas interface without long-range order, as illustrated in (a). As the NC concentration at the interface increases, they start to form a hexagonally packed monolayer at the interface, (b). The NCs still behave similar to hard spheres, as any anisotropic interaction is screened by the oleate ligands. Possibly, oleate ligands weakly attached to the {100} facets (30), detach and are absorbed in the ethylene glycol phase. The particles align one of their <100> directions perpendicular to the liquid-gas surface. The rotational freedom in plane is gradually reduced, in favor of electrostatic and Van der Waals interactions between opposed {100} facets. This also results in a reduced NC–NC distance, (c). Due to the directionality of these in-plane {100} attractions, the superlattice has to change its symmetry from hexagonal to square. A similar transition between hexagonal and square symmetry has been predicted from Monte Carlo simulations for a monolayer of hard truncated nanocubes confined at an interface (31). Once the NCs are in close proximity, crystalline bridges grow between neighboring NCs (d). This necking has also been observed in a chemically distinct case of NC attachment (8, 32, 33).

4.2.4. Checking the formation hypothesis with Monte Carlo simulations

To test the postulated model, we investigated the formation of superlattices from PbSe NCs adsorbed at the liquid-gas interface using Monte Carlo simulations with periodic boundary conditions in the canonical ensemble, i.e. we fixed the number of particles N, the volume V, and the temperature T of the system. We model the NCs by cantellated cubes as depicted in Figure 4.5a. The cubes are confined to a 2D plane and are oriented such that the {100} facet points upwards. The nanocrystals are allowed to move freely in this plane.

The ligand-free {100} facets lead to an attractive driving force that attempts to position the nanocrystals with their vertical {100} facets face-to-face. This directional driving force is mimicked in the simulations by introducing small patches on the center of the vertical {100} facets. We assume the cantellated cubes to interact as hard particles, but with the attractive patchy interaction between the {100} facets. The patchy interaction is modelled as a square patch that interacts with an attractive square-well potential (34, 35). The patch size is defined by the ratio of the length of the patch P_x and

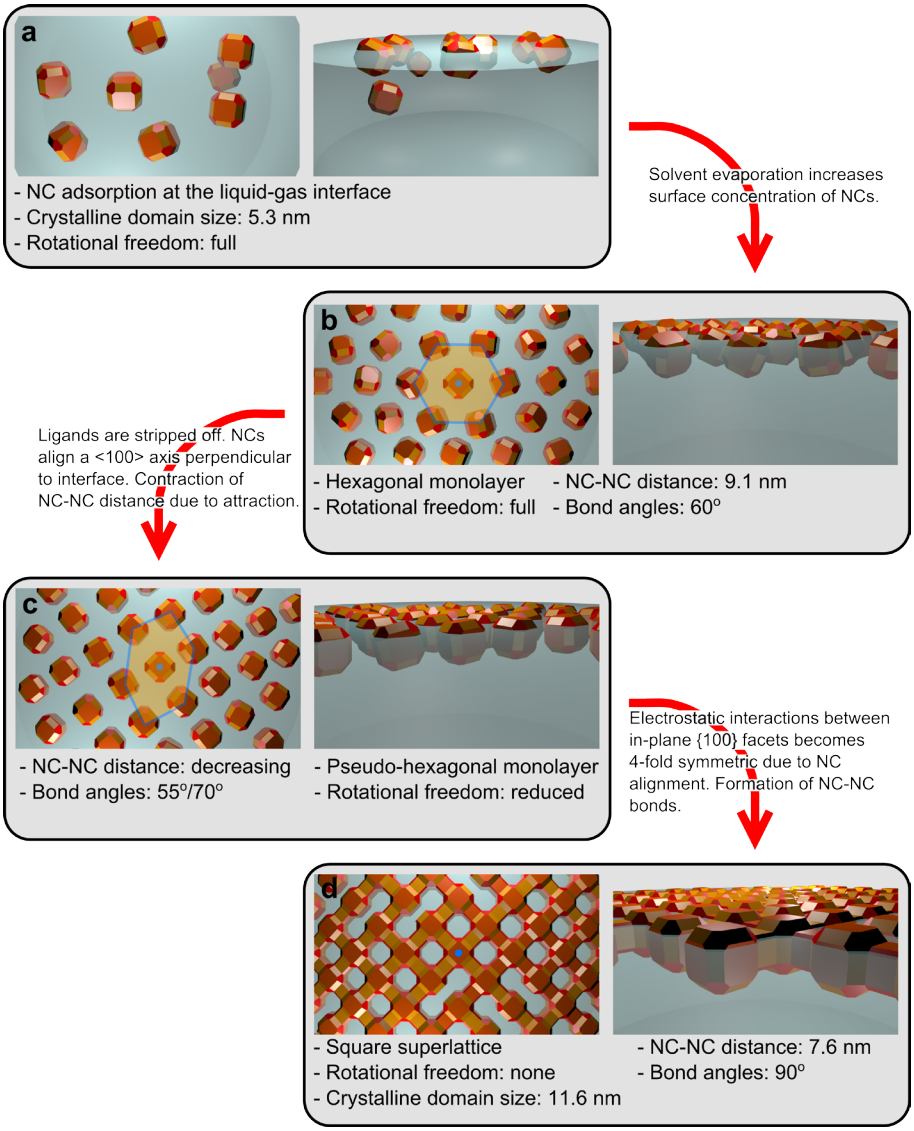

Figure 4.4: Schematic mechanism of the consecutive phase transitions during the reactive self-assembly of the PbSe NCs.

Left image shows top views, right image side views. (a) As the solvent evaporates, the concentration of the NCs increases, and the particles adsorb at the liquid-gas interface. (b) The central NC is indicated with a blue dot. The increase in NC concentration forces the particles to form a hexagonally packed monolayer. (c) The ligands on the {100} facets stabilizing the particles in the toluene slowly dissolve in the ethylene glycol substrate, thus increasing the {100} facet-to-facet attractive interaction and decreasing the NC-NC distance. Due to the directionality of the in-plane {100} attractions, the superlattice transforms into a pseudo-hexagonal lattice. (d) Once the particles are sufficiently close, they connect atomically via necks; the superstructure obtains a square geometry.

• • • •

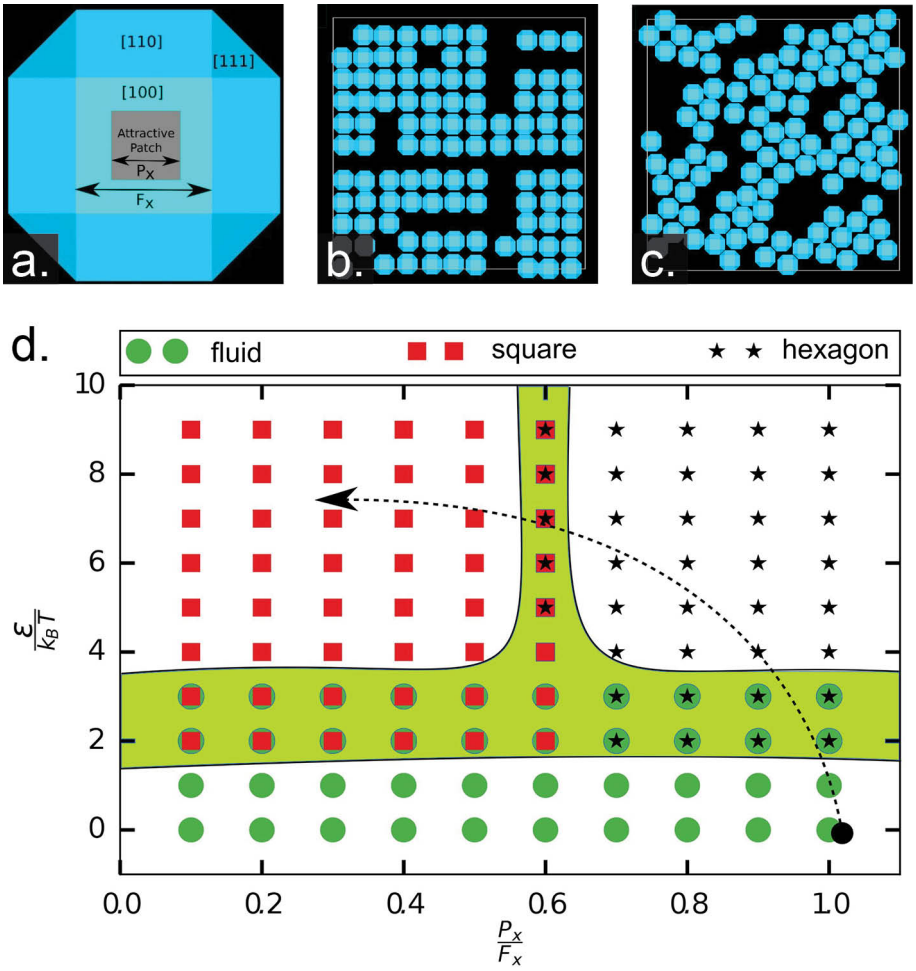

42

Figure 4.5: Monte Carlo simulations on the cantellated nanocubes confined to a 2D plane. (a) Model of the cantellated nanocube used in our NVT simulations. Different facets are indicated along with the attractive patch on the [100] facets. Dimension of the patch Px and the [100] facet Fx are also indicated. (b) Square phase (P_x/F_x = 0.1, ε/k_BT = 6) and (c) hexagonal/pseudo-hexagonal phase (P_x/F_x = 0.8, ε/k_BT = 6) obtained for different sizes of the attractive patches on the {100} facets. (d) State diagram for the truncated cubes with attractive {100} facets as a function of the relative attractive patch size on a {100} facet P_x/F_x, and the square-well interaction strength ε/k_BT between the attractive patches. The arrow depicts a possible route that describes the different phases observed in our experiments. The green shaded area shows regions where multiple phases coexist.

the length of the {100} facet F_x, i.e., P_x/F_x, and the attraction strength is given by ε/k_BT with k_B Boltzmann's constant. We simulate the self-assembled structures of the NCs as a function of the size of the attractive patch and the attraction strength in order to shed

light on the contraction and symmetry change of the hexagonally packed layer towards the square superlattice, as shown in Figure 4.1g to 4.1k and Figure 4.4.

In Figure 4.5b and 4.5c, we show two typical configurations of the self-assembled structures for the cantellated cubes with different patch size. We clearly find that the self-assembled structure depends sensitively on the patch size, which determines the directionality of the attractive interaction. For a stronger directionality, i.e. smaller patch size, we observe a square symmetry for the superlattice (see Figure 4.5b) whereas for a less directional interaction, i.e. a larger patch size, the superlattice shows hexagonal symmetry (see Figure 4.5c). In Figure 4.5d, we present the state diagram of the nanocrystals as a function of the patch size P_x/F_x, and attraction strength ε/k_BT. We observe that the particles self-assemble into a superlattice for attraction strengths > $4\,k_BT$, even with very small attractive patch sizes. The results corroborate our interpretation of the experimental data that the directional electrostatic and Van der Waals interactions between the vertical {100} facets drive the phase transition from hexagonal to square NC ordering and keep the {100} facets face-to-face, finally enabling an atomic necking process and growth of attached nanocrystals that form single crystalline domains.

4.3. Conclusions and outlook

In conclusion, we have shown that the formation of 2D superstructures with a square nanogeometry from PbSe NCs involves multiple phases and transitions. We could directly observe this remarkable behavior with in-situ GISAXS and GIWAXS experiments.

The acquired data showed that the NCs have no preferential ordering or orientation after drop casting onto the immiscible liquid substrate of ethylene glycol, i.e. the NCs are in a liquid-like state just as they were in the toluene dispersion. After 27 minutes, the NCs have formed monolayers at the liquid/air interface and are arranged in a hexagonal superlattice. In these monolayer superlattices, the NCs are still separated and show no preferential orientation. Over the next 15 minutes, the NCs start to show a preferential {100} up orientation with respect to the plane of the interface and come closer together, causing the monolayer to contract to a pseudo-hexagonal superlattice. Finally, the monolayer fully contracts to a square lattice and the NCs form the final square superstructure by oriented attachment of their in-plane {100} facets.

Ex-situ HAADF-STEM experiments showed that the PbSe NCs form necks between their {100} facets with their constituent atoms upon attachment. Monte Carlo simulations showed that the hexagonal to square geometry phase change can be induced by an increasingly directional interaction of the NC {100} facets.

The fact that it is possible to monitor in-situ the adsorption of colloidal particles at a liquid surface and to reveal the ensuing structural transformations of the particle

monolayer will further our understanding of the mechanisms of interfacial self-assembly processes and the differences with self-assembly in three dimensions. This may result in bottom-up routes towards a diversity of 2D electronic or photonic materials based on nanocrystals or (anisotropic) polymer-type colloids. We remark that improvements in the atomic coherency are desired for high quality 2D optoelectronic materials. In such a way, colloid self-assembly can become a feasible alternative for top-down lithography based methods.

4.S. Supporting information

4.S.1. Methods

Nanocrystal synthesis

The PbSe nanocrystals used for the oriented attachment experiments in this study were prepared using the method described by Steckel et al. (36). The synthesis was performed in a glovebox with a water and oxygen free environment. (a) 4.77g of lead acetate trihydrate (99.999% Aldrich), 10.35g of oleic acid (OA, 90% Aldrich) and 39.75g octadecene (ODE, 90% Aldrich) were heated to 130°C under low pressure (10^{-3} bar) for approximately 4 hours. (b) A second mixture containing 3.52g Se (99.999% Alfa Aesar), 46.59 mL trioctylphosphine (TOP, 90% Fluka) and 0.41mL diphenylphosphine (DPP, 98% Aldrich) was prepared by dissolving the Se. Subsequently solution (a) was heated in a three-necked round-bottom flaks to 180°C after which 15mL of solution (b) was rapidly injected. The particles were grown for approximately 60 seconds, after which the reaction was quenched with 20mL butanol. After the solution was cooled down to approximately 50°C, 10 mL methanol was added to induce precipitation of the nanocrystals. The resulting suspension was centrifuged at 2500 rpm for 10 minutes, the supernatant was removed and the washed particles were redispersed in toluene. This washing procedure was repeated two times.

Oriented attachment of truncated PbSe nanocubes

The ex-situ oriented attachment was performed at 20°C inside a glovebox with <1ppm O_2 and <1ppm H_2O. A glass petri dish (Ø 27mm) was filled with 6.5 mL ethylene glycol. The nanocrystal (NC) solution with an initial concentration of 3.0×10^{-5}mol/L was diluted by adding 4µL of the NC solution to 800µL of toluene. A total volume of 350µL of this dispersion was drop cast gently on top of the ethylene glycol. The ethylene glycol serves as an immiscible liquid substrate for the NC solution. After drying the NC solution on top of the EG for 60 minutes, a sample was scooped from the ethylene glycol interface on a copper TEM grid and dried in vacuum to remove any residual ethylene glycol.

In-situ GISAXS/WAXS

The in-situ X-ray scattering experiments under grazing incidence were performed at beamline ID10 of the European Synchrotron Radiation Facility (ESRF), Grenoble. The energy of the incident X-ray beam was set at 10.0 keV, below the Pb and Se absorption edges to minimize beam damage. We optimized the grazing angle to 0.3° for the best signal-to-noise ratio on both GIWAXS and GIWAXS detectors. The scattering was recorded by two Pilatus detectors. The GIWAXS patterns were recorded on a Pilatus 300K detector with 619x487 pixels, each 172x172µm^2 in size, positioned approximately 25 cm from the sample. The GISAXS patterns were recorded on a Pilatus 300K-W detector with 1475x195 pixels, each 172x172µm^2 in size, positioned 0.578 m from the sample. Before drop casting the dispersion of NCs on top of the EG substrate, the x-ray beam was aligned to the surface. After drop casting and every three minutes the alignment was repeated in <10 sec to adjust for solvent evaporation. The oriented attachment was performed in a home-built liquid cell, which can be flushed with argon repeatedly to lower the oxygen and water levels (Figure S10). A Teflon petri dish (Ø 64 mm) was filled with 28 mL of ethylene glycol. To the ethylene glycol we added 10 µL of an OA solution (1% (v/v) OA in ethylene glycol). The cell was then flushed five times with

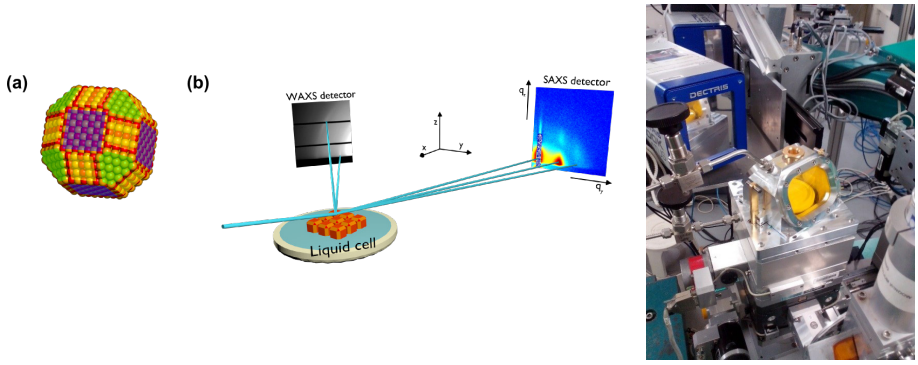

Figure 4S.1: Schematic and photograph setup used for the in-situ GISAXS/WAXS study of nanocrystal assembly at the liquid/air interface.
(a) An atomic model of the PbSe truncated nanocubes, showing the different facets of the NC. Blue indicates the {100} facets, yellow the {110} facets and green the {111} facets. (b) Schematic of the setup used for in-situ GISAXS/WAXS experiments. A dispersion of NCs in toluene evaporates in a liquid sample cell. We examine the process of assembly and attachment using grazing-incidence X-ray scattering, by simultaneously monitoring the atomic order on the wide-angle detector and nanoscale order on the small-angle detector.

• • • •

vacuum/argon cycles, and was filled with toluene saturated vapour (argon gas blown through hot toluene). Next, the PbSe NC solution (0.5 mL; 1.9×10^{-6} mol/L) was deposited on top of the liquid substrate. As the PbSe NCs proved to be sensitive to beam damage, we scanned the sample position in between the measurement, back and forth over a distance of 4 mm (in 21 steps) in the direction perpendicular to the incident X-ray beam. In this way, the dose of X-ray photons on each position of the sample was minimized. Each frame was recorded with a 10 s integration time, after which the position of the sample was changed. After each sequence of 21 positions, we returned to the starting position and repeated the procedure.

HAADF-STEM

The HAADF-STEM imaging and atom counting is performed using an aberration corrected FEI Titan microscope operated at 300 kV. By modelling images as a superposition of Gaussian functions located at the atomic columns, the volume under each peak can be estimated by fitting this model to the region of interest. These volumes are integrated intensities of electrons and thus correspond to scattering cross-sections. In a subsequent analysis, the distribution of scattering cross-sections of all atomic columns is decomposed into overlapping normal distributions, where the number of normal components is selected using an Integrated Classification Likelihood (ICL) approach (25, 26). Based on the analysis of the image shown in Figure 4.3, 10 components have been retrieved illustrating the presence of 1 up to a maximum of 10 atoms in a column. The number of atoms in each projected atomic column is then obtained by assigning the component which generates the experimental scattering cross-section with the highest probability. In this manner, a map reflecting the number of atoms in each column is retrieved as illustrated in Figure 4.3b. Based on the counting results, a starting 3D configuration is obtained by positioning all Pb atoms on a perfect crystal grid symmetrically arranged around a central plane. Next, the potential energy of this configuration is calculated using a Lennard-Jones potential and minimized using an iterative scheme. In each iteration step, one atomic column, selected by a Monte Carlo based approach, is shifted over one unit cell and the total energy is again calculated. The previous 3D configuration is replaced by the new one if the total energy is decreased. This procedure is repeated until convergence is reached.

	δ	β
PbSe	$1.292x10^{-5}$	$8.430x10^{-7}$
Toluene	$1.964x10^{-6}$	$1.750x10^{-9}$
Ethylene glycol	$2.539x10^{-6}$	$4.188x10^{-9}$

Table 4S.1: Values of the real (δ) and imaginary (β) part of the refractive-index decrement at 10keV for the materials used in these experiments, δ and β define refraction and absorption in a material accordingly.

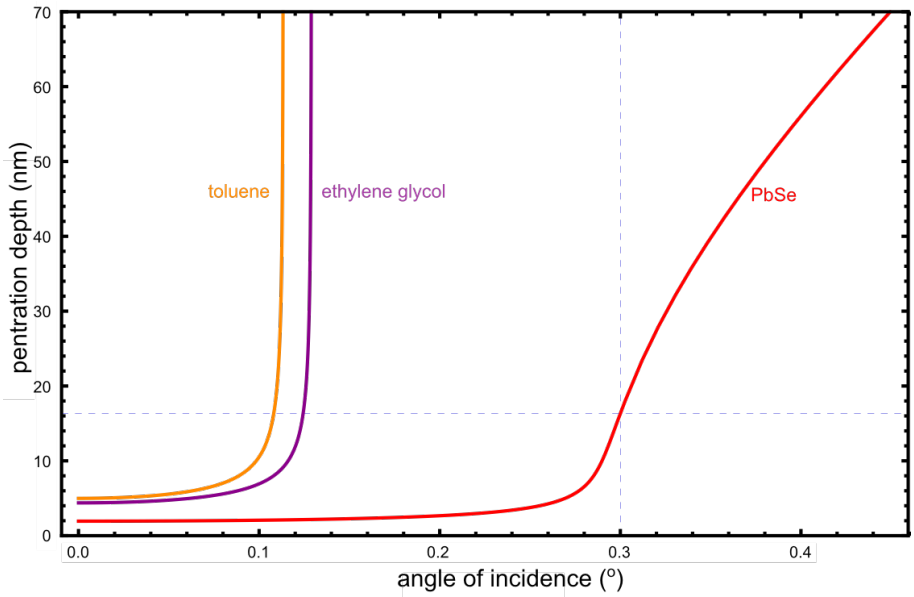

4S

Figure 4S.2: Calculation of the X-ray penetration depth as a function of incident angle.
The red, purple and orange lines depict the penetration depths as function of incident angle for PbSe, ethylene glycol and toluene respectively. The blue dashed lines show the incident angle of the experiments (0.3°) and the corresponding penetration depth for PbSe (16.3 nm). Working at the critical angle of either toluene or ethylene glycol would result in a minute penetration of the X-ray photons into the PbSe superstructure.

Calculation of the X-ray penetration depth

The incident X-ray energy of 10 keV corresponds to a wavelength $\lambda_0 = 0.124\ nm$ and a wavevector of magnitude $k_0 = 2\pi/\lambda_0 = 50.7\ nm^{-1}$ in air. For our experiments we used a grazing angle of incidence of 0.3°, slightly larger than the critical angle for total external reflection of bulk PbSe. Since the refractive index of any material is negative at X-ray frequencies ($n = 1-\delta+i\beta$), the wavevector inside the sample $k = nk_0$ is smaller than in air. Upon transmission of the beam into the sample, the wavevector component parallel to the air–sample interface $k_{||} = k_0 \cos(\alpha_i)$ is conserved. The wavevector component perpendicular to the sample is

Eq.4S.1
$$k_z = \sqrt{k^2 - k_{||}^2} = k_0\sqrt{n^2 - \cos^2(\alpha_i)}$$

Since n is complex, k_z is complex. The imaginary part of k_z describes how quickly the X-ray intensity decays when going deeper into the sample. The penetration depth d, defined as the depth at which the X-ray intensity is lower by a factor e than at the interface, is given by

Eq.4S.2
$$d = \frac{1}{2\,\mathrm{Im}(k_z)}$$

3.S.2. Additional data and analysis

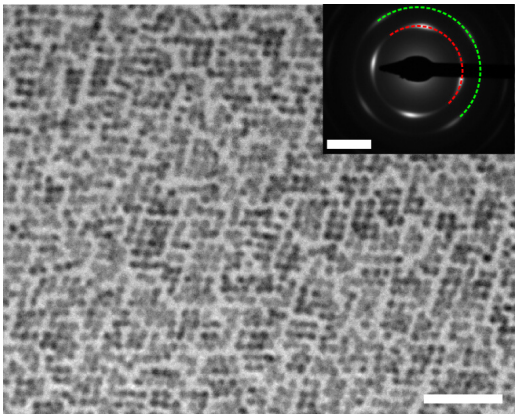

Figure 4S.3: Characteristic TEM image of the sample scooped from the surface in the in-situ experiments.
Note the resemblance to Fig. 4.1g. The micrograph shows that the NCs have assembled into a square superlattice. The NCs are atomically attached only in relatively small separate patches of 10-30 NCs, which could explain the peak broadening and absence of higher order diffraction rods in the GISAXS patterns. The electron diffraction pattern shows diffraction arcs, indicating atomic alignment of the NCs. The coloured rings index the diffraction spots: red = {200} and green = {220}. Scalebars denote 50 nm in the TEM image and 20 nm-1 in the diffraction pattern. We should remark here that the formation of rather small domains that are atomically aligned has to do with the conditions under which in-situ measurements are done. Under better controlled conditions µm-large atomically coherent domains are observed (see e.g. Figures 4S.4).

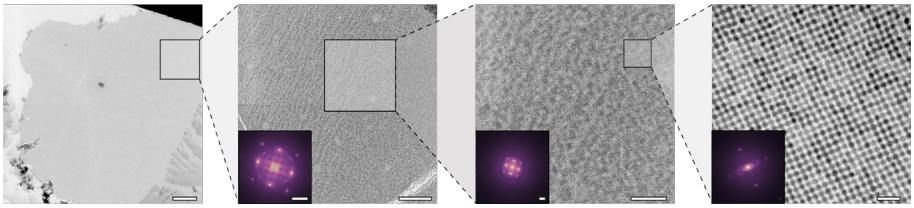

Figure 4S.4: Conservation of nanocrystalline order on mesoscopic length scales.
From left to right consecutive zoomed in TEM images are displayed, which show a very long-range periodicity. Even though the atomic coherency throughout the complete lattice is conserved over several NCs only, this does not perturb the long-range nanocrystalline order. From the widths of the {100}-superlattice reflections in the Fourier transforms we obtain nanocrystal coherence lengths for the superlattice of 39.3 nm, 34.3 nm and 35.9 nm from left to right. Scale bars from left to right images are 2µm, 500nm, 200nm and 20 nm respectively and 1 nm^{-1} for all Fourier transform insets.

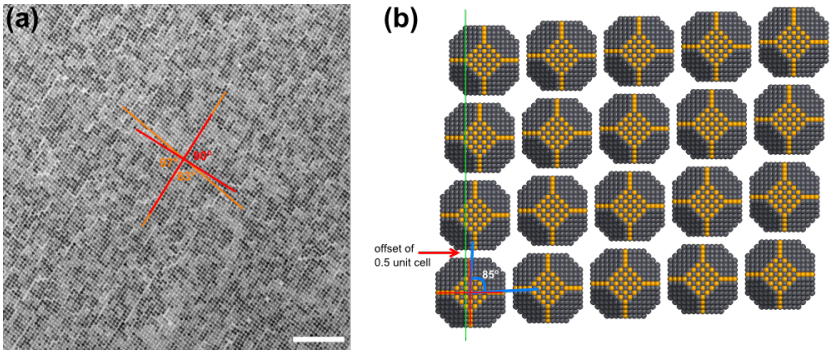

Figure 4S.5: Discussion on the bond-angles in the final square superstructures.
Due to the crystal structure of the individual PbSe nanocrystals, a shift of 0.5 unit cells in the two lateral directions is required to result in Pb-to-Se binding. The resulting bond angles would then be slightly larger or slightly smaller than 90°. (a) TEM image of a superstructure, where the deviation of the bond angles (83°/97°) with a perfect square lattice (90°) is clearly seen over longer distances. (b) Models of the PbSe nanocrystals in a square superlattice, where in both lateral directions the particles are shifted by half a unit cell. The scale bar in the TEM image equals 100 nm.

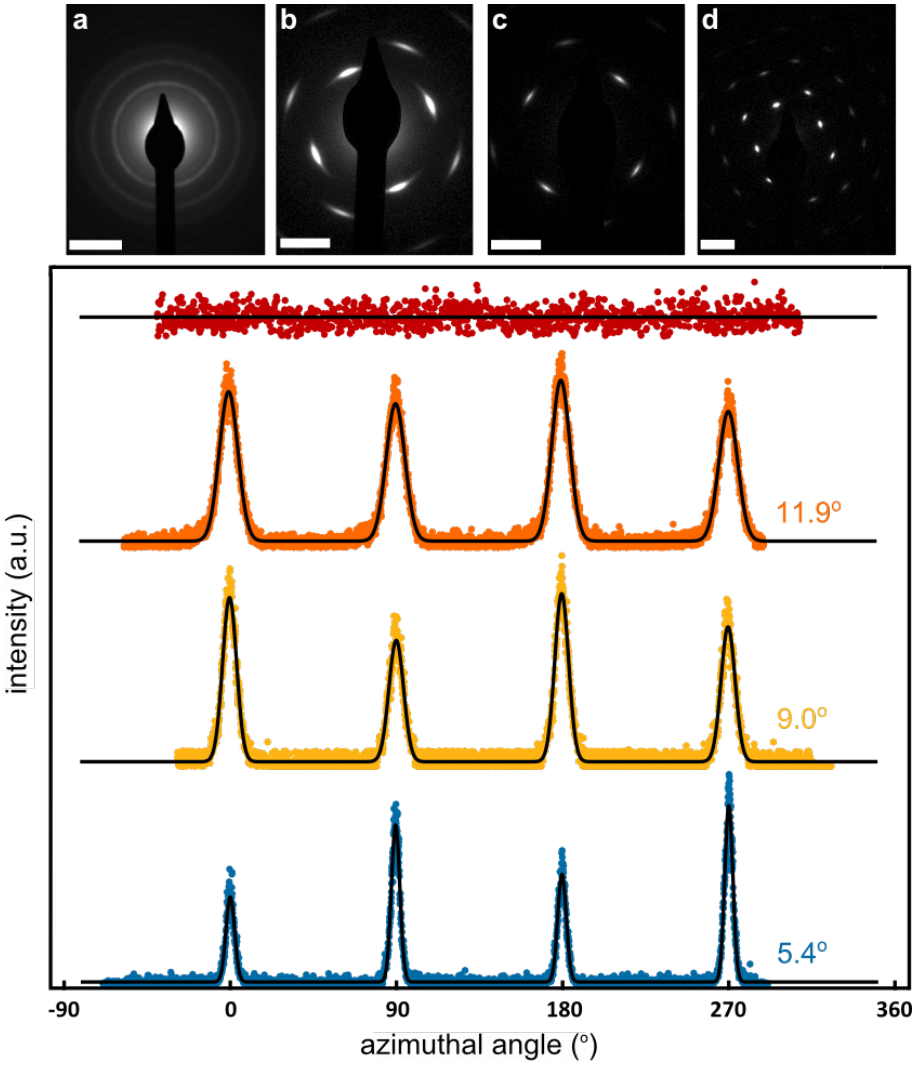

Figure 4S.6: azimuthal peak widths of the electron diffraction patterns during the self-assembly process.
ED patterns and azimuthal azimuthal traces over the {400} reflection from the electron diffraction patterns in the main text show a decrease in peak width, which indicates the loss of in-plane rotational freedom of the nanocrystals during the self-assembly process. Going from completely disordered NCs (a), to the square superlattice with attached nanocrystals (d), the peak widths of the {400} reflections decrease, showing that the nanocrystals have less in-plane rotational freedom with respect to each other. We should remark here that the data should not be interpreted in a quantitative way, as instrumental broadening is not taken into account here.

....

References

1. Evers, W. H. et al. Low-dimensional semiconductor superlattices formed by geometric control over nanocrystal attachment. Nano Lett. 13, 2317–2323 (2013).

2. Boneschanscher, M. P. et al. Long-range orientation and atomic attachment of nanocrystals in 2D honeycomb superlattices. Science 344, 1377-1380 (2014). doi:10.1126/science.1252642

3. Pound, G. M. & Mer, V. K. La. Kinetics of Crystalline Nucleus Formation in Supercooled Liquid Tin 1,2. J. Am. Chem. Soc. 74, 2323–2332 (1952).

4. LaMer, V. K. & Dinegar, R. H. Theory, Production and Mechanism of Formation of Monodispersed Hydrosols. J. Am. Chem. Soc. 72, 4847–4854 (1950).

5. Banfield, J. F. Aggregation-Based Crystal Growth and Microstructure Development in Natural Iron Oxyhydroxide Biomineralization Products. Science 289, 751–754 (2000).

6. Pacholski, C., Kornowski, A. & Weller, H. Self-assembly of ZnO: from nanodots to nanorods. Angew. Chem. Int. Ed. Engl. 41, 1188–1191 (2002).

7. Li, D. et al. Direction-specific interactions control crystal growth by oriented attachment. Science 336, 1014–1018 (2012).

8. Schliehe, C. et al. Ultrathin PbS sheets by two-dimensional oriented attachment. Science 329, 550–553 (2010).

9. Cho, K.-S., Talapin, D. V, Gaschler, W. & Murray, C. B. Designing PbSe nanowires and nanorings through oriented attachment of nanoparticles. J. Am. Chem. Soc. 127, 7140–7147 (2005).

10. Kalesaki, E., Evers, W. H., Allan, G., Vanmaekelbergh, D. & Delerue, C. Electronic structure of atomically coherent square semiconductor superlattices with dimensionality below two. Phys. Rev. B 88, 115431 (2013).

11. Kalesaki, E. et al. Dirac Cones, Topological Edge States, and Nontrivial Flat Bands in Two-Dimensional Semiconductors with a Honeycomb Nanogeometry. Phys. Rev. X 4, 011010 (2014).

12. Beugeling, W. et al. Topological states in multi-orbital HgTe honeycomb lattices. Nat. Commun. 6, 6316 (2015).

13. Evers, W. H. et al. High charge mobility in two-dimensional percolative networks of PbSe quantum dots connected by atomic bonds. Nat. Commun. 6, 8195 (2015).

14. Whitham, K. et al. Charge transport and localization in atomically coherent quantum dot solids. Nat. Mater. 15, 557–563 (2016).

15. Pietra, F. et al. Semiconductor nanorod self-assembly at the liquid/air interface studied by in situ GISAXS and ex situ TEM. Nano Lett. 12, 5515–5523 (2012).

16. Bian, K. et al. Shape-anisotropy driven symmetry transformations in nanocrystal superlattice polymorphs. ACS Nano 5, 2815–2823 (2011).

17. Li, R., Bian, K., Hanrath, T., Bassett, W. A. & Wang, Z. Decoding the superlattice and interface structure of truncate PbS nanocrystal-assembled supercrystal and associated interaction forces. J. Am. Chem. Soc. 136, 12047–12055 (2014).

18. Choi, J. J. et al. Controlling nanocrystal superlattice symmetry and shape-anisotropic interactions through variable ligand surface coverage. J. Am. Chem. Soc. 133, 3131–3138 (2011).

19. Choi, J. J., Bian, K., Baumgardner, W. J., Smilgies, D.-M. & Hanrath, T. Interface-induced nucleation, orientational alignment and symmetry transformations in nanocube superlattices. Nano Lett. 12, 4791–8 (2012).

20. Weidman, M. C., Smilgies, D.-M. & Tisdale, W. A. Kinetics of the self-assembly of nanocrystal superlattices measured by real-time in situ X-ray scattering. Nat. Mater. 15, 775–781 (2016).

21. Evers, W. H. et al. Entropy-driven formation of binary semiconductor-nanocrystal superlattices. Nano Lett. 10, 4235–4241 (2010).

22. Bodnarchuk, M. I., Kovalenko, M. V, Heiss, W. & Talapin, D. V. Energetic and entropic contributions to self-assembly of binary nanocrystal superlattices: temperature as the structure-directing factor. J. Am. Chem. Soc. 132, 11967–11977 (2010).

23. Hanrath, T., Choi, J. J. & Smilgies, D.-M. Structure/processing relationships of highly ordered lead salt nanocrystal superlattices. ACS Nano 3, 2975–88 (2009).

24. Narayanan, S., Wang, J. & Lin, X.-M. Dynamical self-assembly of nanocrystal superlattices during colloidal droplet evaporation by in situ small angle x-ray scattering. Phys. Rev. Lett. 93, 135503 (2004).

25. Simon, P. et al. Interconnection of nanoparticles within 2D superlattices of PbS/oleic acid thin films. Adv. Mater. 26, 3042–3049 (2014).

26. Van Aert, S., Batenburg, K. J., Rossell, M. D., Erni, R. & Van Tendeloo, G. Three-dimensional atomic imaging of crystalline nanoparticles. Nature 470, 374–347 (2011).

27. Van Aert, S. et al. Procedure to count atoms with trustworthy single-atom sensitivity. Phys. Rev. B 87, 064107 (2013).

28. Jones, L., MacArthur, K. E., Fauske, V. T., van Helvoort, A. T. J. & Nellist, P. D. Rapid estimation of catalyst nanoparticle morphology and atomic-coordination by high-resolution Z-contrast electron microscopy. Nano Lett. 14, 6336–6341 (2014).

29. Bals, S. et al. Atomic scale dynamics of ultrasmall germanium clusters. Nat. Commun. 3, 897 (2012).

30. Woo, J. Y. et al. Ultrastable PbSe Nanocrystal Quantum Dots via in Situ Formation of Atomically Thin Halide Adlayers on PbSe(100). J. Am. Chem. Soc. 136, 8883-8886 (2014).

31. Thapar, V. et al. Entropic self-assembly of freely rotating polyhedral particles confined to a flat interface. Soft Matter 11, 1481–1491 (2015).

32. Sandeep, C. S. S. et al. Epitaxially connected PbSe quantum-dot films: controlled neck formation and optoelectronic properties. ACS Nano 8, 11499–11511 (2014).

33. Baumgardner, W. J., Whitham, K. & Hanrath, T. Confined-but-connected quantum solids via controlled ligand displacement. Nano Lett. 13, 3225–3231 (2013).

34. Zhang, H., De Yoreo, J. J. & Banfield, J. F. A Unified Description of Attachment-Based Crystal Growth. ACS Nano 8, 6526,6530 (2014).

35. Zhang, H. & Banfield, J. F. Energy Calculations Predict Nanoparticle Attachment Orientations and Asymmetric Crystal Formation. J. Phys. Chem. Lett. 3, 2882–2886 (2012).

36. Steckel, J. S., Yen, B. K. H., Oertel, D. C. & Bawendi, M. G. On the mechanism of lead chalcogenide nanocrystal formation. J. Am. Chem. Soc. 128, 13032–13033 (2006).

This chapter is partly based on:

The adsorption geometry of PbSe nanocrystals at liquid/air interfaces;
Jaco J. Geuchies, Ellenor Geraffy, Giuseppe Soligno, Carlo van Overbeek, Federico Montanarella, Marlou R. Slot, Oleg Konovalov, Andrei V. Petukhov and Daniel Vanmaekelbergh; In preparation.

Chapter 5

Towards a full description of PbSe nanocrystal self-assembly behavior at liquid interfaces

Abstract 117

5.1. Introduction 117

5.2. Methods 118

5.3. Results 119
5.3.1. Scattering results 119
5.3.2. Oriented attachment results 123

5.4. Discussion 124
5.4.1. The adsorption geometry of PbSe nanocrystals at liquid interfaces 124
5.4.2. Forks in the path of interfacial self-assembly for PbSe nanocrystalss 126

5.5. Conclusions 131

5.6. Outlook 132

5.S. Supporting information 132

References 140

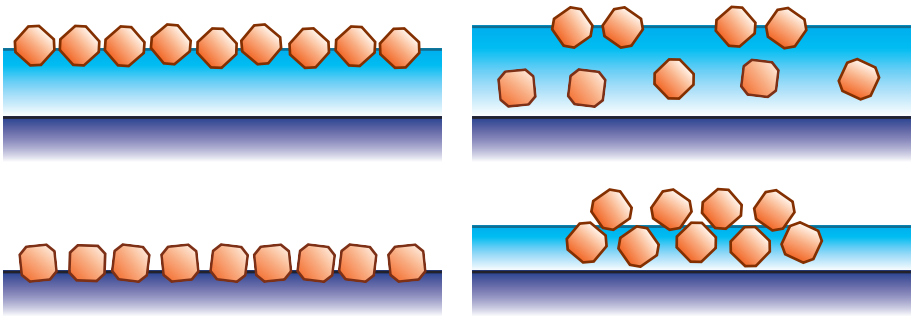

5.1

PbSe nanocrystals self-assembly at a liquid and subsequent superstructure formation is influenced by an interplay of multiple physical parameters. The wetting angle and local part particle density appear to be the most determining factors.

Abstract

The adsorption and self-assembly of PbSe nanocrystals at liquid/air interfaces has led to remarkable nanocrystal superlattices, which show long-range nanoscale order and sometimes even atomic bonding via oriented attachment. Our previous in-situ X-ray scattering experiments have unraveled the two-dimensional 'square' superstructure's mechanism of formation, which is governed by remarkable phase transitions. However, during these experiments the crystallographic orientation of the nanocrystals seemed to develop late in the process, contrary to predictions from simulations and results for big PbSe nanocrystals. In the present study, we therefore investigated the adsorption geometry of PbSe nanocrystals with varying sizes at the ethylene glycol/air interface. It was found that all particles shallowly penetrate the liquid substrate and indeed particles <7.3 nm adsorb without a preferred crystallographic orientation in hexagonal monolayers, whereas particles ≥7.3 nm adsorb with a <100> axis up in a two-dimensional analogue of a smectic phase. Furthermore, we combined these results with oriented attachment experiments in which mainly the toluene evaporation rate was varied. In this way, we can sketch a phenomenological picture of the self-assembly behavior of PbSe nanocrystals at liquid interfaces.

5.1. Introduction

The bottom-up fabrication of functional materials through the self-assembly of colloidal nanocrystals (NCs) currently attracts a lot of scientific attention. The self-assembly of colloidal NCs was pioneered by Murray et al. (1). Later the group of Murray also developed the NC assembly at the liquid/air interface by drop casting the NC suspension on diethylene glycol (acting as an immiscible liquid substrate). Solvent evaporation then resulted in the formation of thin-film NC superlattices (2). Upon gradual solvent evaporation, the NCs are forced to self-assemble at the liquid interface.

In our research group, Evers et al. managed to combine this process with sequential oriented attachment of PbSe NCs via their {100} facets (3). In this way, atomically connected 2D superstructures with long-range NC periodicity (4) and short-range atomic coherency (5) were created. The NC superstructure with a honeycomb geometry is of special interest, as calculations show that these structures can exhibit interesting optoelectronic behavior (6).

Recently, we managed to monitor in-situ the formation of the PbSe NC superstructure with a square geometry using grazing incidence small-angle and wide-angle X-ray scattering (GISAXS and GIWAXS) (7). We observed remarkable phase changes, the first phase was a hexagonal NC monolayer adsorbed at the liquid/air interface with

rotational freedom for the NCs, evolving into a contracted 2D oblique superlattice in which the NCs became oriented with their <100> axis up, to finally a monolayer superstructure in which the NCs are attached with their vertical {100} facets forming a square geometry. Work in other groups has shown that (partial) removal of the ligands promotes the oriented attachment of the NCs at their {100} facets (8, 9).

Although these are very promising first steps towards understanding the formation of 2D superstructures, a full picture is lacking and the reproducibility of most of their allotropes, particularly honeycombs, is still low. Calculations have shown that the NCs can have different adsorption geometries at liquid interfaces, depending on the NC truncation and relative surface energies (10). Choi et al. (11) have indeed shown a <111> and <100> up orientation at the toluene/air and the ethylene glycol/air interface respectively for large (≥10 nm) PbSe NCs, which do not perform oriented attachment. However, our own in-situ work mentioned above indicated that there was no preferred orientation for smaller NCs of a size of ~5 nm, until the last stage of the process, i.e. just before NC-NC attachment took place (7).

Here, we report on the size-dependence of the interfacial adsorption geometry of PbSe NCs. We studied the orientation of the nanocrystals at the ethylene glycol/air interface. We have chosen this interface because it doesn't evaporate, making it the most reproducible one to work with.

Furthermore, I will combine these scattering results with additional oriented attachment experiments in which mainly the toluene evaporation rate is varied. In this way, a phenomenological description of the full self-assembly path towards each of the observed 2D superstructures, namely lines, squares, honeycombs and zigzags, can be created

5.2. Methods

A brief outline of the experimental methods is given below, see the SI for a more detailed discussion.

Scattering experiments

5.1

PbSe NCs were synthesized with sizes of 4.3 nm (from now on referred to as small NCs, sNCs), 7.3 nm (medium-sized NCs, mNCs) and 8.2 nm (big NCs, bNCs) (12, 13). 100 µL of a 10 µL/mL dispersion of oleic acid in ethylene glycol was drop casted onto a 32 cm^2 ethylene glycol substrate to prevent oriented attachment of the NCs (3) and to enhance wettability of the substrate. 1 mL of a dilute (~0.5 µmol/L) dispersion of one particular size of NCs in toluene was drop casted on a substrate inside an inert atmosphere (7).

The subsequent self-assembly of the NCs at the liquid/air interface was observed with grazing incidence scattering techniques at the ESRF ID10. GIWAXS patterns were

recorded to obtain the crystallographic orientation of the NCs. GISAXS patterns were recorded to obtain the superlattice geometry of the NCs. XRR patterns were recorded to obtain the adsorption geometry of the NCs. See Figure 5S.3 for the experimental set-up and a schematic of how the experiments were performed.

Oriented attachment experiments

PbSe NCs with a size of 5.7 nm (from now on referred to as washed NCs, wNCs) were synthesized (12, 13) and thoroughly washed to promote oriented attachment (3, 14). In a nitrogen-purged glovebox, a 5.7 cm^2 ethylene glycol substrate is put in a closed set-up equipped with a temperature controller and a vacuum valve to regulate the evaporation rate of the toluene solvent. 5.5 µL of a 2.5 µL/mL oleic acid in ethylene glycol suspension were drop casted onto an ethylene glycol liquid substrate. 350 µL of a 0.6 µmol/L wNCs in toluene dispersion were drop casted onto the substrate and left to perform sequential self-assembly and oriented attachment under multiple evaporation rates. After the toluene is evaporated, the liquid surface is stamped with a TEM grid and brought to a TEM for analysis of the samples.

5.3. Results

5.3.1. Scattering results

The following data was acquired upon complete toluene, i.e. solvent, evaporation. First, GIWAXS and GISAXS signals were recorded simultaneously, after which XRR signals were recorded.

GIWAXS results: nanocrystal orientation

The crystallographic orientation of the NCs was obtained by measuring the diffraction from their atomic lattices in GIWAXS. These results are presented in Figure 5.1. The calculated GIWAXS patterns for NCs having a random orientation are drawn in Figure 5.1a as blue lines, the pattern for NCs all having a [100] axis perpendicular to the liquid-air interface are drawn as orange spots in the same figure. For completeness, we also calculated the patterns corresponding to NCs with axes up observed in other self-assembly studies (namely: [111] up (15) and [110] up (16)), these are shown in Figure 5S.5. However, the latter two orientations were not observed in our scattering experiments.

Figures 5.1b-d show the GIWAXS patterns corresponding to the small, medium-sized and big NCs (sNCs, mNCs and bNCs), respectively. For the sNCs, we observed powder rings in the GIWAXS pattern, which means that the sNCs do not have a preferential orientation at the liquid/air interface. The GIWAXS patterns of the mNCs and bNCs show a series of well-defined diffraction spots, which matches the calculated GIWAXS pattern for [100] up NCs very well. The diffraction spots originating from

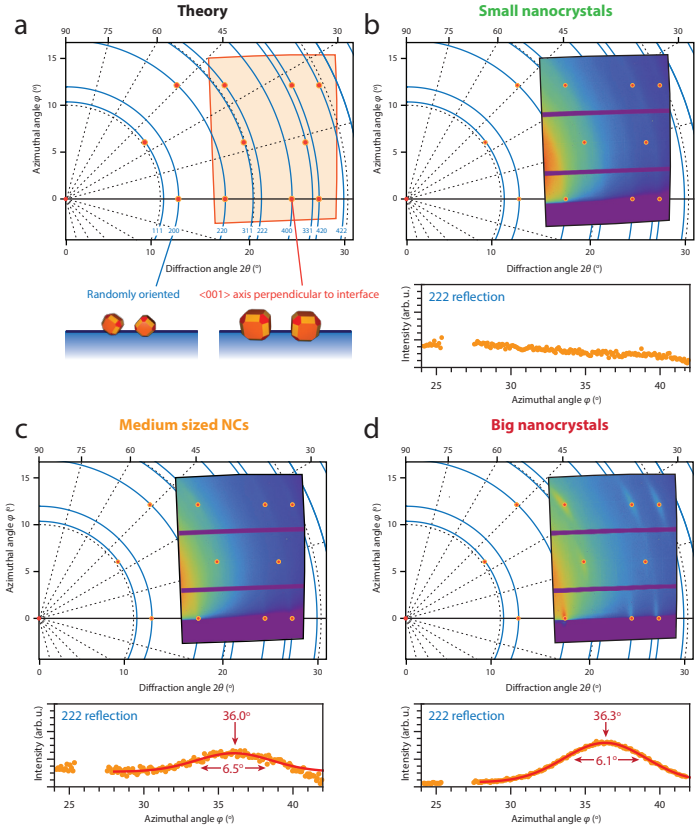

Figure 5.1: Calculated (a) and measured (b-d) GIWAXS patterns of the PbSe NCs at the ethylene glycol/air interface.
The detector plane is overlaid with a calculation in each image panel. Beneath each panel, intensity traces are shown of the {222} diffraction ring vs. the azimuthal angle φ with a fit to this data revealing the spread in NC orientation (when relevant). Note that the pattern for sNCs (a) shows rings meaning they have no preference in crystallographic orientation. The mNCs (c) and bNCs (d) patterns show spots corresponding to all NCs having a <100> axis up.

• • • •

the {222} planes have an azimuthal full-width half-maximum (FWHM) of 6.5° and 6.1° for mNCs and bNCs, respectively. This FWHM gives an indication of the spread in orientations of the NCs.

The average orientation of the NCs at the interface can also be verified by looking at intensity traces in the 2θ-direction along the scattering horizon (azimuthal angle equals ~1°), which are presented in Figure 5S.6. For the mNCs and bNCs, only reflections originating from {hk0} lattice planes are observed along the scattering horizon, corroborating that these NCs have a <100> axis up.

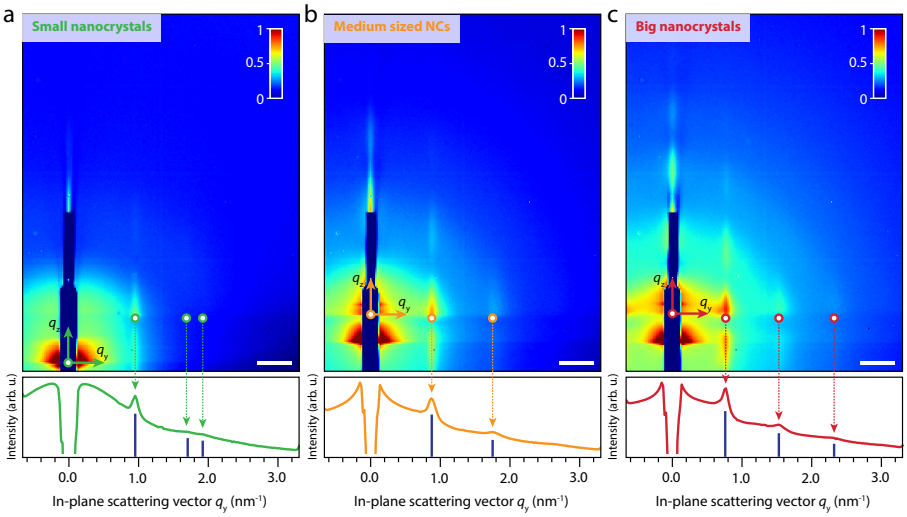

Figure 5.2: Measured GISAXS patterns of the PbSe NCs at the ethylene glycol/air interface. Corresponding intensity traces in the horizontal scattering direction q_y depicted below each image panel. Note that all patterns show rods rather than spots, meaning that a monolayer of particles is being observed. The relative positions of the Bragg rods in the horizontal scattering direction (depicted in bars under the intensity traces) indicate the formation of a hexagonally packed superlattice for sNCs (a) and a 2D smectic phase for mNCs and bNCs. Scalebars in the GISAXS patterns equal 0.5 nm^{-1}.

From the intensity traces in the 2θ-direction, we are also able to estimate the coherent crystalline size in the sample (7). The in-plane FWHM of the {400} reflections are used to this end. The insets in Figure 5S.3 show fits to the diffraction spots, Table S1 lists the corresponding FWHM's and coherent crystal domain size. All domain sizes match the size of the used NCs quite well.

GISAXS results: nanocrystal ordering

The NC superlattice geometry was found by measuring the diffraction from the NC lattice planes in GISAXS. These results are presented in Figure 5.2. All patterns show rods, rather than spots. This means that all NC samples formed 2D superlattices, i.e. a NC monolayer.

The GISAXS pattern for the sNCs, shown in Figure 5.2a, shows Bragg rods at positions of 0.94 nm^{-1}, 1.62 nm^{-1} and 1.88 nm^{-1} in the horizontal scattering direction q_y with a FWHM of 0.06 nm^{-1}. The peak positions relation 1:√3:2 indicates that the NCs are ordered in a 2D hexagonal lattice with a NC center-to-center distance of 7.7±0.4 nm, roughly the sNC's diameter plus two 'coronas' of oleate ligands.

The GISAXS pattern of the mNCs, shown in Figure 5.2b, shows Bragg rods at 0.86 nm^{-1} and 1.71 nm^{-1} in the q_y direction with a FWHM of 0.08 nm^{-1}. The 1:2 relative peak

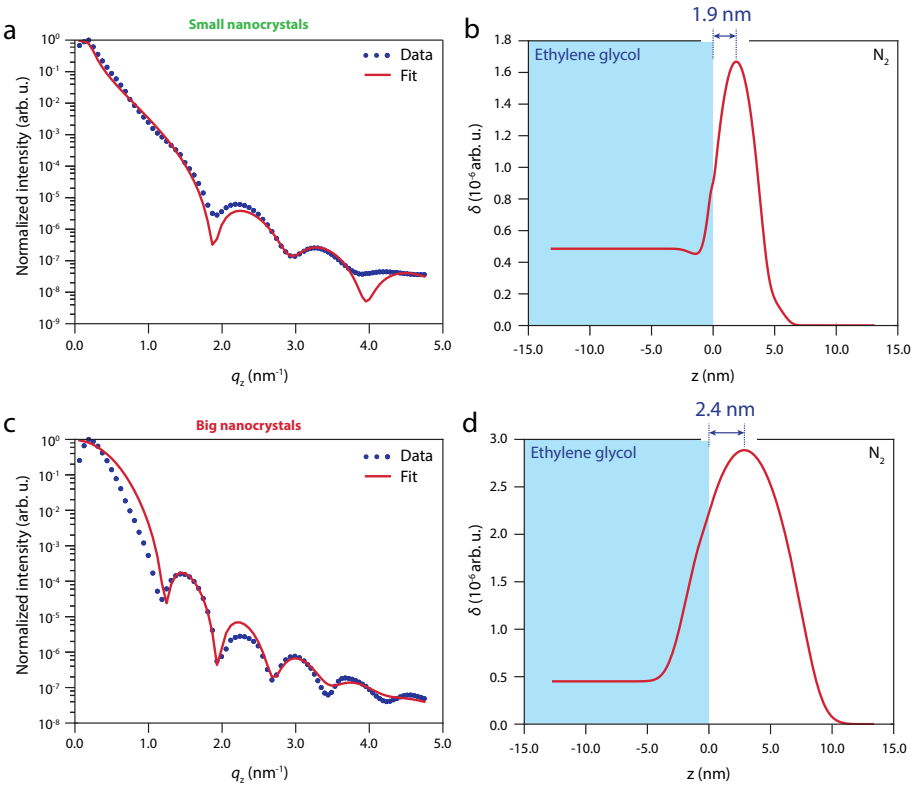

Figure 5.3: Measured XRR patterns (a, c) and scattering length densities (b, d) of the PbSe sNCs (a, b) and bNCs (c, d) at the ethylene glycol/air interface.
The oscillations in the data clearly show one period, meaning that a particle monolayer was observed. The fits to the XRR data correspond to the scattering length densities, which are proportional to the electron density and hence yield a quantitative picture of the NC adsorption geometry. The center of mass of the sNCs is 1.9 nm above the interface, the bNCs are sticking out 2.4 nm.

positions indicate that there is a preference for NC ordering in one dimension, i.e. the formation of linear structures. The center-to-center distance is 7.3±0.7 nm, indicating that the mNCs (almost) touch each other.

The GISAXS pattern of the bNCs, shown in Figure 5.2c, shows Bragg rods at 0.75 nm^{-1}, 1.52 nm^{-1} and 2.18 nm^{-1} in the qy direction with a FWHM of 0.05 nm-1. The 1:2:3 relative peak positions indicate that there is a preference for NC ordering in one dimension, alike to the mNCs. The center-to-center distance is 8.4±0.5 nm, indicating that the bNCs (almost) touch each other, also alike to the mNCs.

Specular reflection XRR results: nanocrystal adsorption geometry

The adsorption geometry of the NCs was obtained by measuring the XRR patterns

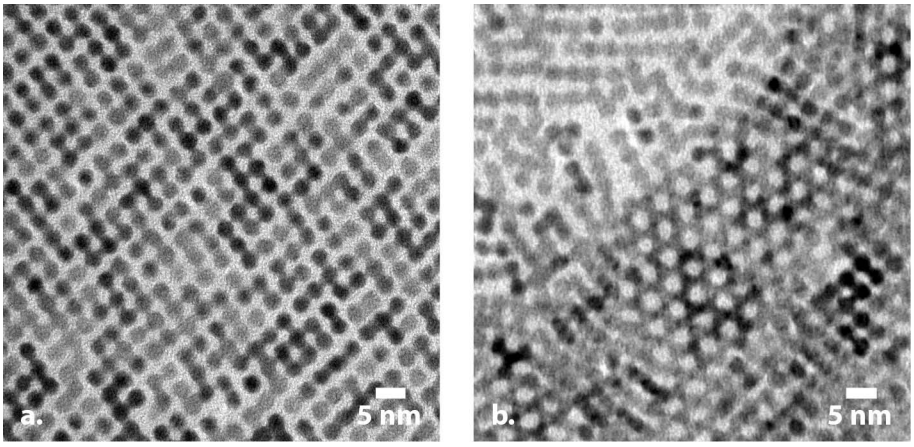

Figure 5.4: TEM images of 2D superstructures made by oriented attachment of wNCs.
(a) highly pure samples of square nanogeometry structures could be obtained with addition of a very small amount of oleic acid or Pb-oleate to the ethylene glycol substrate (b) mixed phases of lines, honeycomb and zigzag structures could be obtained best by drop casting the NCs in more solvent toluene.

from specular reflections of NC's adsorbed at the liquid interface. These results are presented in Figure 5.3. As the adsorption geometry shows little size-dependent behavior and the mNCs and bNCs behaved very similar in GIWAXS and GISAXS, only the extremes (sNCs and bNCs) will be further discussed below.

Figure 5.3a and 5.3c show the measured XRR curves from the sNCs and bNCs as blue dots, with the corresponding fits as a red solid line. For both samples, the oscillations of the signal clearly show only one period, further proving that we observed NC monolayers. The fits in Figure 5.3a and 5.3c are based on electron density profiles as shown in Figure 5.3b and 5.3d, respectively. These show that for both sNCs and bNCs the particles lie on top of the ethylene glycol and penetrate only shallowly into the liquid substrate. Their center-of-masses stick 1.9 nm and 2.4 nm out above the interface, respectively. For a more detailed dissection of the interface, see Figure 5S.7.

5.3.2. Oriented attachment results

Large-scale 2D superstructure flakes with square geometry, such as shown in Figure 5.4a, could be made with thoroughly washed 5.3 nm NCs. All samples also contain some multilayered structures or more randomly attached NCs, but the square phases are dominant by far.

The preferential formation of PbSe NC superstructures with honeycomb geometry superstructures could be stimulated in the following ways: gently applying vacuum in the experimental set-up during solvent evaporation, lowering the temperature to 15~20

°C, not treating the substrate with additional oleic acid surfactants or oleate ligands, drop casting less NCs (around three-fourth), using even more thoroughly washed NCs and performing the procedure with a double amount of solvent. Especially the latter two proved very effective. All resulted in samples that mostly contain mixed flakes of honeycomb, zigzag and linear superstructures, as shown in Figure 5.4b. Interestingly, the treatments were also able to cancel each other out, e.g. performing oriented attachment with even more thoroughly washed NCs at elevated temperatures (>30 °C) produces square superstructures again.

5.4. Discussion

According to our scattering data, the interfacial adsorption behavior of PbSe NCs at ethylene glycol/air interface has two distinct size regimes: NC size <7.3 nm and NC size ≥7.3 nm. From now on, NCs in these size regimes will be referred to as truncated NCs and cuboid NCs respectively, because small PbSe NCs are usually shaped like strongly truncated cubes and bigger ones like cuboids with only little truncation (14, 17, 18).

5.4.1. The adsorption geometry of PbSe nanocrystals at liquid interfaces

We think the acquired scattering data allows for a clear-cut interpretation of how PbSe NCs are adsorbed at the ethylene glycol/air interface, depicted in Figure 5.5. All NCs lie on top of the liquid/air interface and penetrate only shallowly into the ethylene glycol substrate. This might explain why NC superlattices can be easily scooped or stamped of polar liquid interfaces as observed in other studies (2, 19, 20). The reason behind this poor wetting behavior is probably that the NCs are covered with apolar ligands, which do not want to interact with a polar substrate.

Nanocrystal orientation

Interestingly, the observed orientation of the adsorbed NCs shows a sharp transition from disorder for truncated NCs to a <100> up orientation for cuboid NCs. The broad peaks in GIWAXS for the cuboid NCs show those have a ~6° spread in orientation. Still, the differences in rotational freedom within the cuboid NC category is negligible compared to the difference in the transition to full disorder for truncated NCs.

We think that all spreads in orientational order should be interpreted as coming from thermal motions, i.e. the NCs respectively fully rotate or wiggle with thermal motion. Another explanation for the spread in orientations could be that the NCs are 'frozen' in a (biased) random orientation. We think this explanation is very unlikely for two reasons: 1) PbSe NCs such as these can perform oriented attachment, which requires freedom of motion to align and attach; 2) calculations predict energy landscapes in which most randomly oriented NCs can directly lower their energy by rotating towards an energy minimum (10).

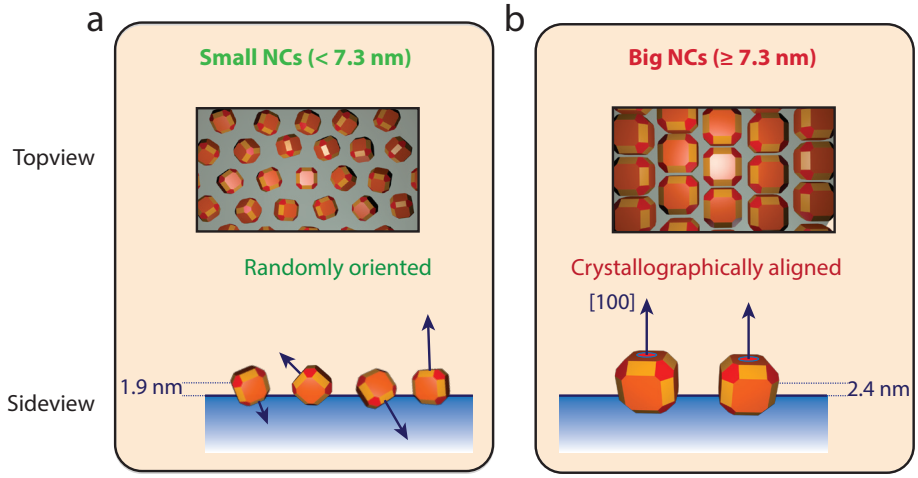

Figure 5.5: Schematic representation of the adsorption geometry of PbSe NCs at the ethylene glycol/air interface.
All NCs shallowly penetrate the liquid substrate. (a) NCs <7.3 nm have no preferred crystallographic orientation and form 2D hexagonal superlattices (b) NCs ≥7.3 nm have a <100> axis perpendicular to the interface and pack in a 2D smectic superlattice.

Notably, Choi et al. observed similarly <100> up oriented particles at the ethylene glycol/toluene interface, but a <111> axis up at the toluene/air interface (11). In that account, cuboid NCs were used. Our previous studies on the formation of square superstructures showed that, initially, truncated NCs at the liquid/air interface have no preferred orientation, but became oriented with the <100> axis up in a later stage of the process. In this later stage, it is not entirely clear if or how much of the toluene phase is still present. (7).

The cuboid NCs have little truncation of their edges and therefore relatively big {100} facets (17, 18). Recently, it was shown that ligandless {100} facets are stable for PbSe NCs (14). PbSe {100} facets are a 'checkboard' of ionically bound Pb and Se species. A qualitative explanation of the observed <100> up wetting orientation is thus that bare {100} facets have a reasonably favorable interaction with the polar ethylene glycol surface. A "flat" orientation in which a complete {100} facet is slightly buried in the ethylene glycol liquid is then constituted as the energetically most favorable orientation.

The fact that the smaller truncated NCs show no preferred orientation on the ethylene glycol surface might be caused by their smaller {100} facets, or by the presence of more dominant {111} facets which are still covered with lead oleate ligands. Possibly, due to the weaker adsorption energy, thermal motion prevents order in orientation. Therefore, the smaller particles continuously rotate by diffusion through thermal motion like a buoy on a rough sea. This might be checked with molecular simulations and temperature dependent measurements.

Nanocrystal packing

The difference in shape and orientational freedom of the NCs might explain why the superlattice ordering of the NCs is also size-dependent. The strong truncation of the smaller NCs causes them to have relatively more ligands, which are also bigger compared to the crystal core. This makes truncated NCs somewhat spherical and makes them pack in hexagonal structures with relatively big center-to-center distances. The cuboid NCs can logically approach each other much closer because as the {111} facets, covered with ligands, are relatively smaller (21). Their cuboid shape then causes them to form a superlattice that can be interpreted as a 2D analogue of a smectic phase, or 1D ordered structures, or simply: lines.

PbSe NCs forming linear structures have been reported previously (22–24). This behavior is usually attributed to an electric dipole moment of the crystal core. An electric dipole in a NC with a centro-symmetric rock salt crystal structure is not obvious. A recent XANES study has shown that the rock salt crystal structure of PbSe NCs is slightly distorted by the Pb-oleate ligands (25); it was calculated that this should give rise to an electric dipole moment along a <111> axis. Instead, we observed that the cuboid NCs pack along their <100> axes. We believe, therefore, that electric dipoles are not the cause for a preference for linear structures along the <100> direction as observed in the present study.

Another explanation for the formation of 1D structures is based on the enhanced action of the ligands of adjacent NCs when the NCs are in contact with a polar liquid surface: apolar ligands show enhanced interactions with each other, when the NCs are present on a polar liquid substrate, such as water or ethylene glycol. A molecular dynamics study of NCs capped with fatty ligand chains on a water surface showed that the particles shallowly penetrate the water surface and preferably form lines (26). Ethylene glycol is not water, as it is less polar. However, the latter study may give a hint on the origin of linear superstructures. Several other studies also explained NC self-assembly on apolar liquid surfaces by considering ligand interactions (16, 27–29).

For our study this means that cuboid NCs should align in such a way that as much of the ligand-dense {111} facets as possible come close to those of neighboring NCs in a superlattice. This is indeed the case when NCs align their {100} facets towards each other.

Finally, from the available data it is not possible to unambiguously determine whether the NC's bare crystal facets are touching, i.e. whether they have performed oriented attachment, because not one single in-situ method can determine both the superlattice spacing and the NC size.

However, we think the NCs are not attached in our present study. First, we performed our experiments by adding oleic acid to the ethylene glycol substrate, known to prevent oriented attachment (3). Second, we observed that the coherent crystalline domain size

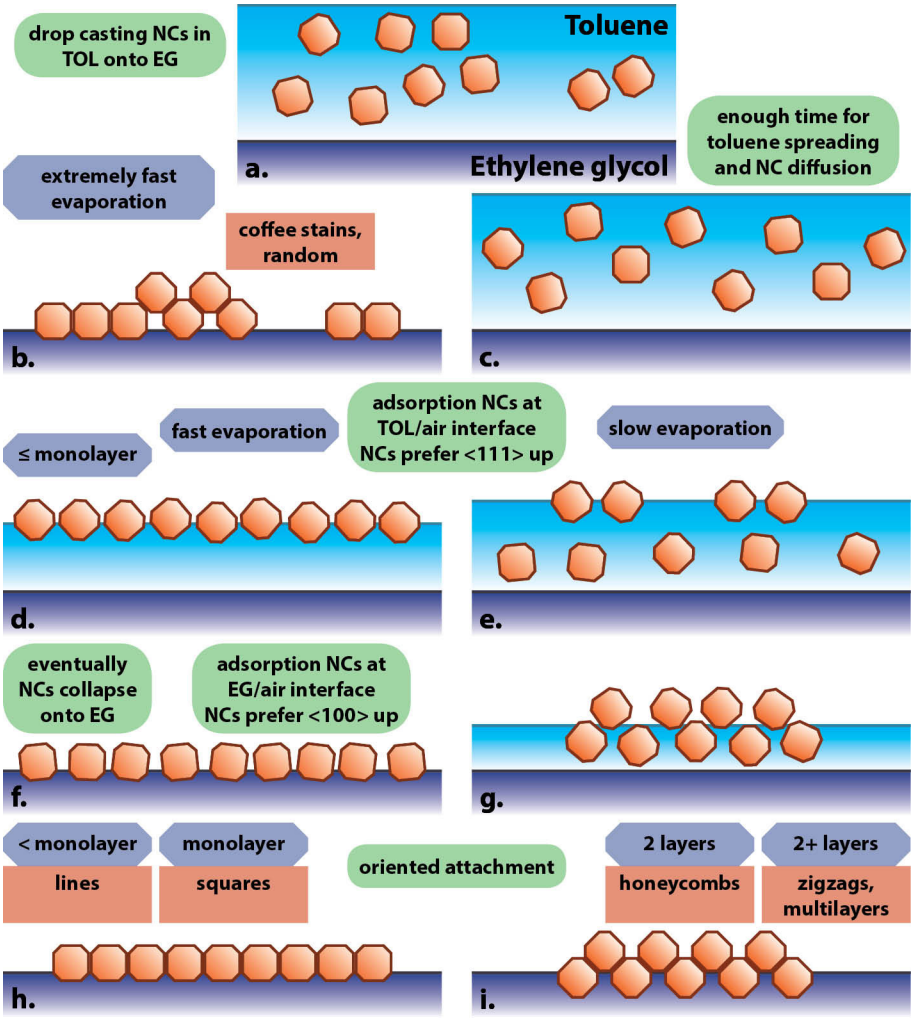

Figure 5.6: Illustration of how PbSe NCs self-assembly at liquid/air interfaces towards different superstructure geometries.
(a) NCs in a polar solvent are drop casted onto an apolar liquid substrate. (b) immediate evaporation of the solvent after drop casting leads to formation of random superstructures and agglomerates such as coffee stains. (c) NCs evenly spread across the interface. (d) fast evaporation leads to all NCs quickly adsorbing to the solvent/air interface in a monolayer. (e) slow evaporation makes part of the NCs adsorb to the solvent/air interface. (f) NC monolayers collapse onto the substrate interface after complete solvent evaporation (g) NCs can form multilayers upon further slow evaporation. (h) monolayers form linear and square superstructures after oriented attachment (i) multilayers form honeycombs, zigzags or denser superstructures after oriented attachment.

5.4

determined by GIWAXS increases only a few percent going from NCs in solution to NCs in a superlattice, whereas this parameter more than doubled in our in-situ studies of square superstructure formation by oriented attachment (7).

5.4.2. Forks in the path of interfacial self-assembly for PbSe nanocrystals

Our scattering and additional oriented attachment data does not allow for the presentation of a definite picture of how and why PbSe NCs form the linear, square, honeycomb and zigzag superstructures that have been observed in the experiments described throughout this thesis. However, I believe that our present data in combination with other recent scientific reports can at least point to some plausible forks in the interfacial self-assembly path, sketched in Figure 5.6. These will hopefully guide future research to more successful synthesis methods of these interesting structures.

NC adsorption orientation

From the first report of 2D PbSe NC superstructures onwards, the interfacial adsorption geometry of the NCs has been identified as a determining factor (3, 10). We can simplify interfacial adsorption geometry to NC orientation (at the liquid interface) in most further considerations.

Calculations that take NC truncation and relative surface energies between the liquid, air and different NC facets (with ligands) into account predict stable <100>, <111> and sometimes <110> up orientations. These are indeed all observed orientations in the superstructures. This makes NC surface adsorption energies a good candidate for explaining observed different structures.

Our present attachment results showed that honeycombs are more likely to form at lower temperature and when more toluene was used in the attachment procedure. Both slow down the evaporation of the toluene. This gives the NCs more time to self-assemble at the toluene/air interface instead of the ethylene glycol/air interface. At these interfaces PbSe NCs respectively have a preferred <111> and <100> up equilibrium orientation as shown by our present data and data from literature (11). Very recent calculations in our research group predict similar behavior depending on the degree of NC ligand coverage. These orientations correspond to the honeycomb and square superstructure geometries, respectively.

For the 2D superstructure formation, truncated NCs are the most interesting, because we have so far not been able to perform oriented attachment with cuboid NCs (at room temperature) nor has this been reported in literature. Although the truncated NCs at liquid interfaces have full rotational freedom, we think our additional attachment experiments corroborate calculations predicting that NCs at the toluene/air interface have at least some <111> up preference. This first self-assembly fork is depicted in Figure 5.6f-g.

Evaporation rate

Although above we showed that slowing down the evaporation of the toluene liquid promotes the formation of honeycomb structures, extremely speeding up the evaporation had the same effect in our experiments. We could speed up the evaporation rate by letting the NCs self-assemble under reduced atmospheric pressure. This might seem a paradox at first, but can be explained by considering that during extremely fast evaporation there is no time for evenly spreading of the toluene over the substrate nor for the NCs to evenly spread by diffusion. The result is the formation of random 2D superstructures or even 3D structures, such as 'coffee stains'. See SI for an example.

During slower evaporation, the NCs have more time to form their equilibrium superstructures at the toluene/air interfaces, which should in theory be honeycombs or other multilayered <111> up structures. In our experiments, we probably didn't manage to slow down evaporation enough to completely access this reaction-limited regime for obtaining pure honeycomb phases. Preliminary experiments on slowing down the evaporation further support this notion, see Figure 5S.8a for an example.

The middle ground is much more peculiar. Making the toluene evaporate fast, but not extremely fast, apparently yields square superstructures with an excellent long-range periodicity. This kinetic formation mechanism can be explained by the work of Bigioni et al. (30). They showed that fast evaporation of solvent can result in the formation of a perfect NC monolayer at the liquid/air interface, similar to our square formation results.

The evaporation rate is then the second fork we can identify, depicted in Figure 5.6a-e. This figure also shows that the underlying parameter of the different superstructures formed by varying the evaporation rate is mostly the local NC density.

NC surface density

When we considered the formation of superstructures with NCs in equilibrium at a toluene/air interface, i.e. a hexagonal-packed monolayer with a <111> up orientation, we left the NC density out of consideration. Silicene-type honeycomb superstructures (the ones we observe) and more multilayered structures are much more NC dense than a monolayer.

I think the NC density is a variable on its own when forming the different superstructures. NC density then constitutes the last fork in the assembly path. As illustrated in Figure 5.6d-g, the local NC density dictates the number of monolayers in a superlattice and thereby the geometry of the resulting superstructure.

Instead of using NC surface density as a variable for determining the geometry of a superstructure, it could also be argued that densification through lattice contraction is the final mechanism. The observed formation mechanism for squares works analogous to such a contraction notion.

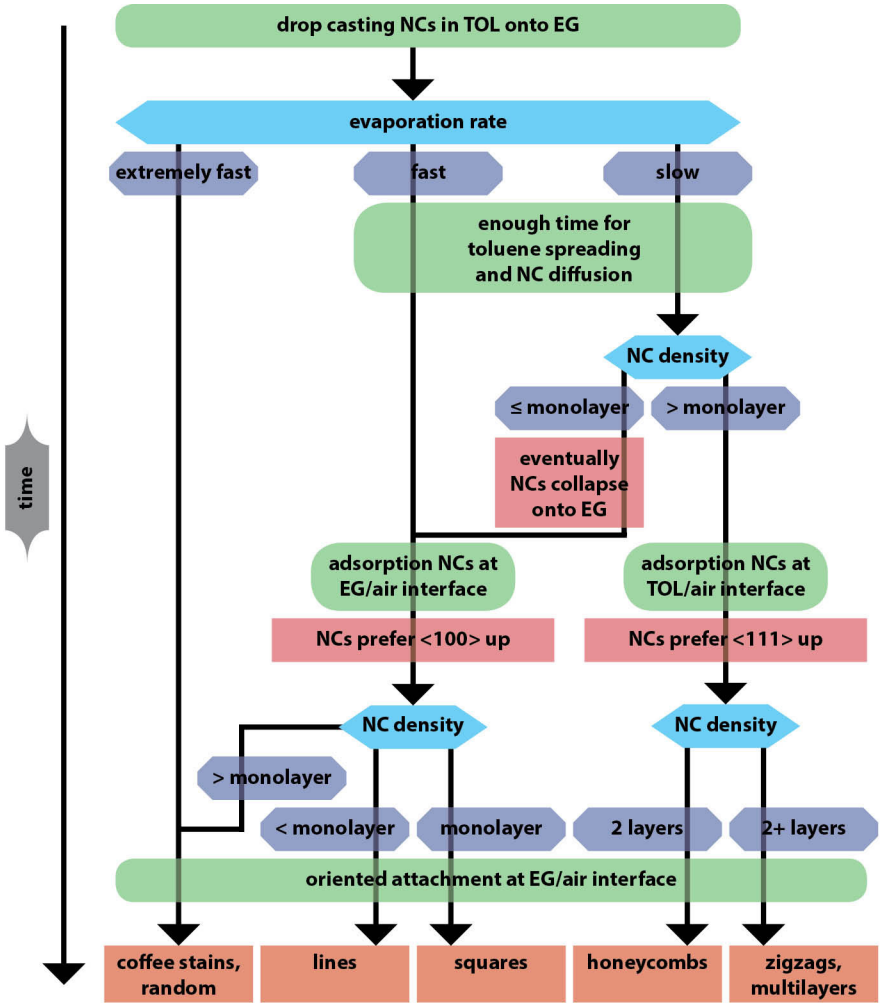

Figure 5.7: A complete phenomenological picture of how truncated NCs form different superstructures at liquid interfaces.
Note how fast evaporation can lead to well-defined monolayer structures and slow evaporation promotes the formation of multilayered structures.

• • • •

5.4

I think it is unlikely that this mechanism is also at work when forming denser superstructures than squares for two reasons. First, we have observed multilayered structures with attached NCs; I believe that these are much more likely formed from multilayers instead of by densification of monolayers. See Figure 5S.8b-c for example images of multilayered superstructures. Second, contraction of a hexagonal monolayer

of particles towards a honeycomb or zigzag superlattice would require a very intricate choreography of the NCs. It seems to me highly unlikely that NCs will spontaneously rearrange in such a way, while they can densify much more easily by forming a square superstructure.

The forks in perspective: towards a full description of PbSe NC behavior at liquid interfaces

Putting all the forks in place, we come to an overall 2D superstructure assembly path. This path might be hard to deduce from Figure 5.6 at first glance, for additional clarity see Figure 5.7.

Before, we considered evaporation rate as the cause for different superstructures, but the real variable is of course time. How much time do the NCs have to reach their thermodynamically favored structure instead of having to settle with a kinetic product?

A 3D close-packed superstructure is of course the thermodynamic minimum for NCs dried from solution. Other lower-dimensional superstructures, like lines, squares, honeycombs, zigzags, etc., are kinetic phases. These can only form, because 2D confinement and oriented attachment stop a reversible self-assembly process at some point in time.

We stress that this picture is mainly phenomenological and only holds for oleate capped ≤7.3 nm PbSe wNCs. Even with these restrictions, the model's applicability might be limited by parameters such as the chosen solvent and oleic acid concentration. A complete formation mechanism should take into account the true driving forces: NC-NC affinity, NC-liquid interface(s) affinity and NC propensity towards oriented attachment; and experimental settings: NC concentration, temperature and solvent vapor pressure. Very recent calculations in our group show that during the assembly process NCs lose part of their capping ligands from the {100} facets. This increases their adsorption energy and affects the NC orientation at the interface. Depending on the interplay of such parameters, superstructures with a different amount of constituent NC layers or even phase-separation might be favorable, as shown in literature (31, 32).

This is also the reason why we left some experimental data out of the discussions until now. For example, it is not trivial that denser honeycomb structures form more often when less NCs are drop casted. We think this is caused by the additional ligands introduced to the system when more NCs are used. Drop casting more surfactant (oleic acid) or Pb-oleate ligands, promotes square over honeycomb superstructure formation. This is probably caused by changes in surface energies and wetting angles of NCs and liquids in the system. More research should be done to combine such mechanistic aspects with the phenomenological model presented above, or to falsify it.

5.5. Conclusions

In the present study, we showed that PbSe NCs adsorb in two distinct ways to the ethylene glycol/air interface depending on their size. All NCs penetrate the liquid substrate shallowly and form a monolayer, but only NCs ≥7.3 nm have a <100> axis up and pack in a 2D smectic phase, whereas NCs <7.3 nm have no orientational preference and pack hexagonally. Furthermore, we deduced several forks in the self-assembly and sequential oriented attachment path of PbSe NCs towards 2D superstructures. The start of the self-assembly process is dictated by the evaporation rate of the solvent, whereas the end is governed by an interplay of liquid/air adsorption energies and local density of the NCs.

5.6. Outlook

Future research should be directed to finding out whether dense NC superstructures, like honeycombs, indeed form through multilayers or lattice contraction of monolayers. This might be possible with in-situ GISAXS and GIWAXS as we did for the square superstructures. The Bragg peaks in GISAXS should shift from a pre-phase signal to the final superstructure signal in a contraction pathway, whereas the peaks of a pre-phase should slowly fade out and a superstructure peak fade in for a multilayer pathway.

A new set-up (33) should probably be built to this end, because our present cell has little opportunity to tune the toluene evaporation rate, which should apparently be as slow as possible for honeycomb formation. When such a cell has been built, the adsorption geometry of PbSe NCs at toluene/air interfaces can also be monitored as precisely as for ethylene glycol/air interfaces in the present study. We can then verify whether NCs can perform oriented attachment at these interfaces as well and at what concentration and/or ligands density multilayers start to nucleate at the toluene/air interface.

5.S. Supporting information

Namocrystal synthesis

5.6

The PbSe nanocrystals used for the oriented attachment experiments in this study were prepared using an adapted method of the synthesis described by Steckel et al. (12). The synthesis was performed in a glovebox with a water and oxygen free environment. (a) 4.77 g of lead acetate trihydrate (99.999% Aldrich), 10.35 g of oleic acid (OA, 90% Aldrich) and 39.75g octadecene (ODE, 90% Aldrich) were heated to 130 °C under low pressure (10^{-3} bar) for approximately 4 hours. (b) A second mixture containing 3.52g Se (99.999% Alfa Aesar), 46.59 mL trioctylphosphine (TOP, 90% Fluka) and 0.41 mL diphenylphosphine (DPP, 98% Aldrich) was prepared by dissolving the Se. Subsequently solution (a) was heated in a three-necked round-bottom flaks to 180 °C after which 15 mL of solution (b) was rapidly injected. The particles were grown for approximately 60 seconds, after which the reaction was quenched with 20 mL butanol. After the solution was cooled down to approximately 50 °C, 10 mL methanol was added to induce precipitation of the nanocrystals. The resulting suspension was centrifuged at 2500 rpm for 10 minutes, the supernatant

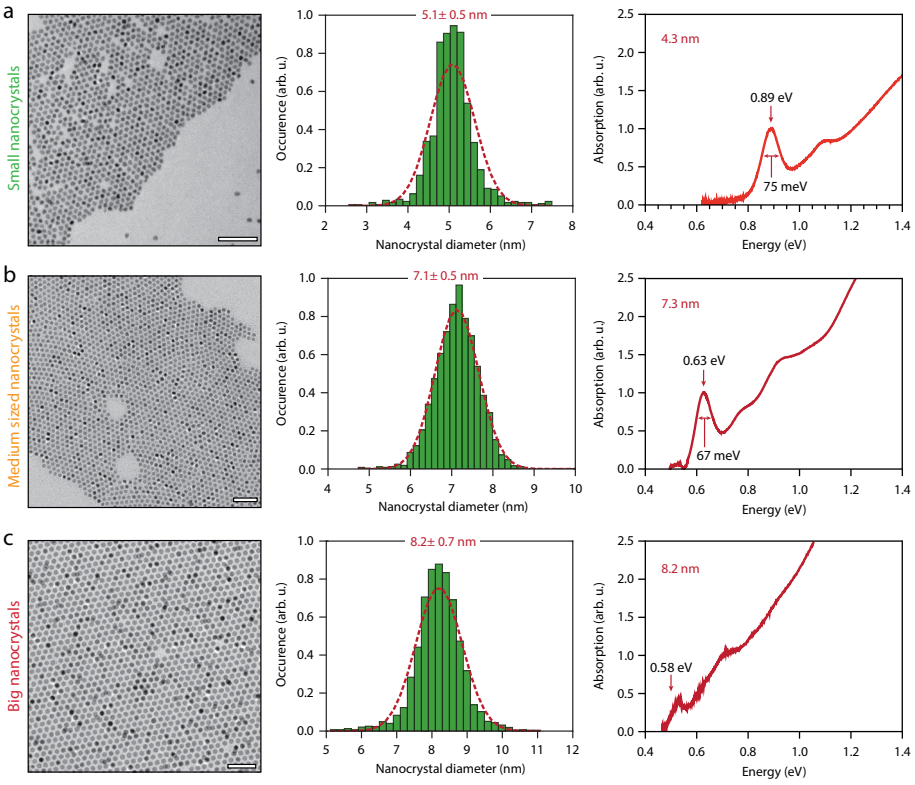

Figure 5S.1: Characterization of PbSe nanocrystals of different size, the used abbreviations refer to the main text.

(a) sNCs, (b) mNCs and (c) bNCs for the scattering experiments. The left, middle and right column show a characteristic TEM image, size distribution of the NCs and optical absorption spectrum, respectively. The size distribution by TEM was obtained with a standard ImageJ application. For each NC size, over 1000 NCs were detected to acquire the distribution. Scale bars in the TEM images denote 50 nm. The absorption spectrum for these large NCs below 0.6 eV is very noisy, due to the contribution of ligand (and possibly residual solvent) absorption.

was removed and the washed sNCs were redispersed in toluene. This washing procedure was repeated two times. For the mNCs, an additional 300 µL of oleic acid was added to the Pb-oleate precursor before injection, and the NCs were grown for 180 seconds. For the bNCs, an additional 1000 µL of oleic acid was added to the Pb-oleate precursor before injection, and the NCs were grown for 20 minutes. Additional oleic acid is known to reduce the activity of the Pb-oleate precursor during the NC formation and hence leads to larger NCs (18).

The wNCs were obtained by growing the particles approximately 90 seconds. After normal washing, the NCs were dispersed in a 50 : 50 mixture of methanol : toluene for 1 hour, centrifuged, supernatant removal and redispersion in toluene.

The NC sizes and concentration as mentioned in the main text were determined by IR-spectroscopy (13). See Figure 5S.1 and 5S.2 below for the NC analysis.

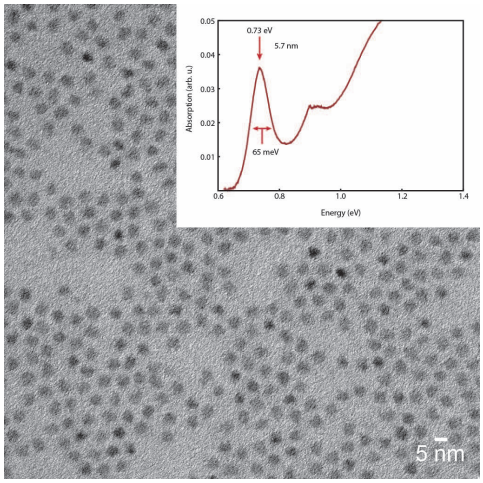

Figure 5S.2: TEM image and IR-adsorption spectrum inset of the PbSe wNCs for the oriented attachment experiments.

Table 4S.1: Values of the real (δ) and imaginary (β) part of the refractive-index decrement at 22 keV for the materials used in these experiments, δ and β define refraction and absorption in a material accordingly.

	δ	β
PbSe	$2.799x10^{-6}$	$2.092x10^{-7}$
Toluene	$4.051x10^{-7}$	$1.224x10^{-10}$
Ethylene glycol	$5.218x10^{-7}$	$2.282x10^{-10}$

In-situ scattering experiments

The in-situ X-ray scattering experiments under grazing incidence were performed at beamline ID10 of the European Synchrotron Radiation Facility (ESRF), Grenoble. See Figure 5S.3 for the full experimental set-up. The scattering was recorded by two Pilatus detectors. The GIWAXS patterns were recorded on a Pilatus 300K detector with 619x487 pixels, each 172x172 µm in size, positioned approximately 36 cm from the sample. The GISAXS patterns were recorded on a Pilatus 300K-W detector with 1475x195 pixels, each 172x172 µm in size, positioned 0.988 m from the sample. The specular XRR experiments were recorded on a 1D Vantec detector, which has a pixel size of 68 µm. The angle of incidence of the X-ray beam was bend down by a dual crystal deflector setup equipped on the ID10 beamline.

The energy of the incident X-ray beam was set at 22.0 keV, since we noticed that there was a lot less beam-induced sample damage at higher photon energies. We optimized the grazing angle to 0.14° for the best signal-to-noise ratio on both GISAXS and GIWAXS detectors. See Table 5S.1 and Figure 5S.4 for the physical parameters behind and the penetration of this optimization.

Before drop casting the dispersion of NCs on top of the EG substrate, the X-ray beam was aligned to the surface. The self-assembly was performed in a home-built liquid cell, which can be flushed with argon (or nitrogen) repeatedly to lower the oxygen and water levels. A Teflon petri dish (Ø 64 mm) was filled to the brim with 28 mL of ethylene glycol. To the ethylene glycol we added 100 µL of an OA solution (1% (v/v) OA in ethylene glycol) for all experiments. The cell was then flushed five times with vacuum/N_2 cycles, and was filled with N_2 gas. Next, the PbSe NC solution (1.0 mL; ~$3.0x10^{-6}$ mol/L for all experiments) was deposited on top of the liquid substrate. Each frame was recorded with a 10 s integration time.

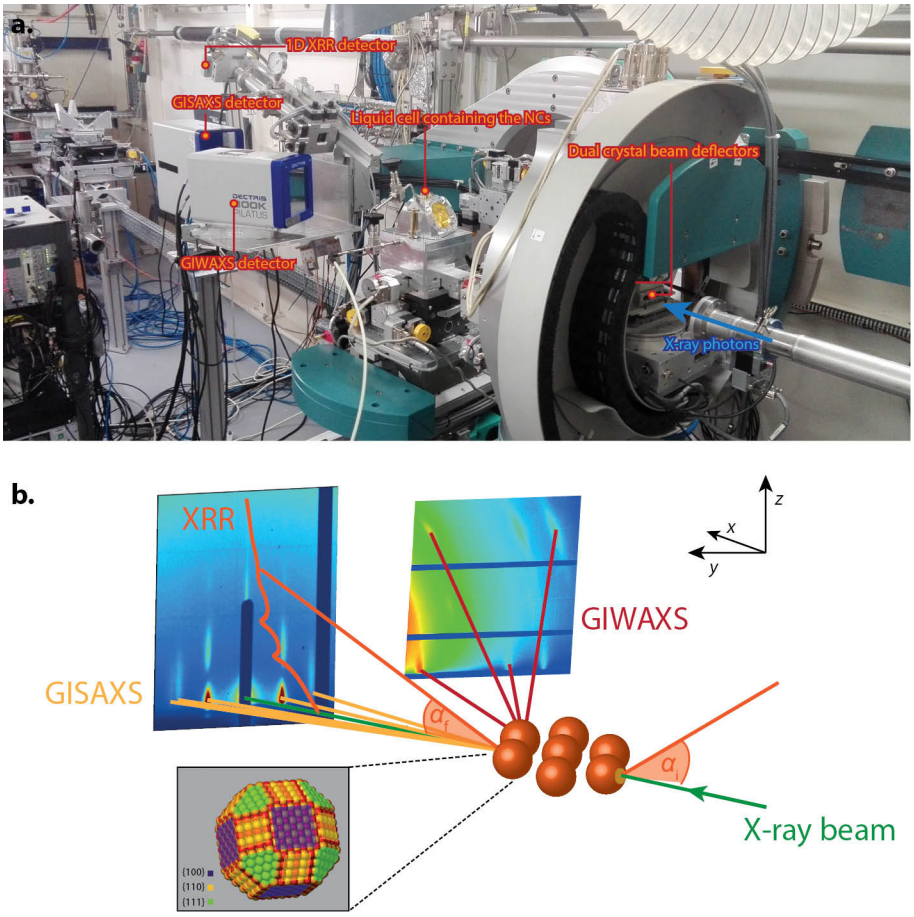

Figure 5S.3: A photograph (a) and a schematic (b) of the experimental geometry at ID10 beamline, ESRF.

The GISAXS signal is collected in the forward scattering direction at a sample-to-detector distance of 988 mm angle to capture the superlattice diffraction. The GIWAXS detector is placed closer to the liquid cell and at a higher angle to capture the atomic diffraction. After complete solvent evaporation, the arm of the diffractometer is lowered to perform XRR experiments. To vary the angle of incidence, we use the new diffractometer of ID10 with a dual crystal deflector to bend the beam down. The intensity of the specular reflection is collected on the 1D XRR detector. The inset of the schematic shows a PbSe truncated nanocube. To enhance clarity in the schematic, the position of the GIWAXS detector was mirrored.

XRR data fitting

The XRR data was fitted using a least-square fitting procedure employing a Parratt formalism (34, 35). Here, we simulate a NC at the ethylene glycol-air interface, and stratify the density profile into *N* layers (by definition, the N'th layer is the bottom ethylene glycol layer). Each layer has a refractive index of the j'th layer, $n_j = 1 - \delta_j + i\beta_j$, and thickness Δ_j. The wavevector in each layer q_j is then calculated as

Eq.5S.1
$$q_j = \sqrt{q^2 - 8k^2\delta_j + i8k^2\beta_j}$$

where k equals $2\pi/\lambda$. The reflectivity of the j'th layer can be calculated using the Fresnel relation

Eq.5S.2
$$r_{j,j+1} = \frac{q_j - q_{j+1}}{q_j + q_{j+1}}$$

The first step is to calculate the reflectivity from the bottom N'th interface. As the substrate is infinitely thick, there are no multiple reflections to consider. From there, it can be iterated upwards through the layers until the top is reached, where the reflectivity amplitude of each layer is calculated as

Eq.5S.3
$$r_{j,j-1} = \frac{r_{j-2,j-1} + r_{j-1,j}p_{j-1}^2}{1 + r_{j-2,j-1} + r_{j-1,j}p_{j-1}^2}$$

Here, $p_j^2 = Exp(i\Delta_j q_j)$ is the phase factor, accounting for the difference in phase between photons scattered between the j'th and j+1'th layer. From the bottom, the reflectivity amplitude is iterated recursively until the total reflectivity amplitude, $r_{0,1}$, at the interface between vacuum and the first layer is obtained.

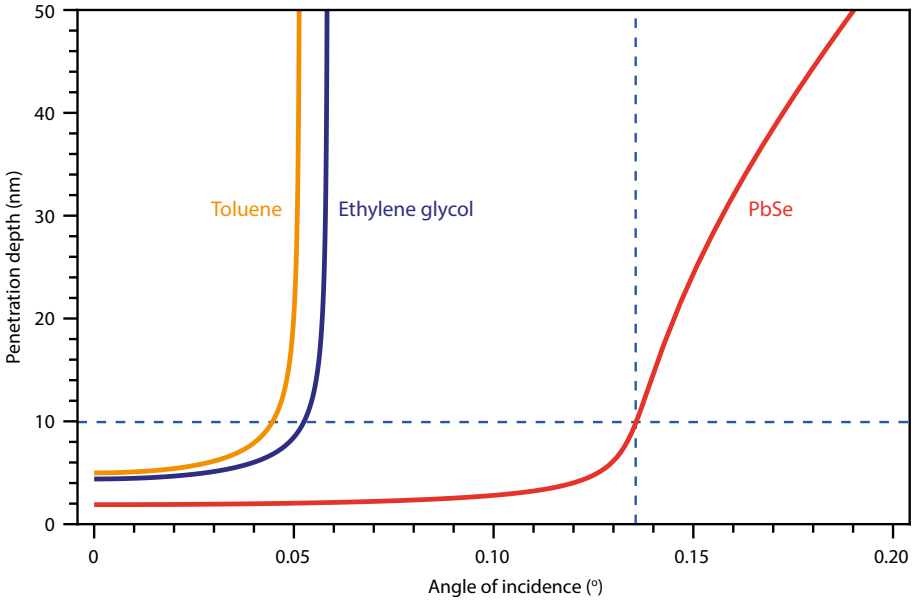

Figure 5S.4: X-ray penetration depth as a function of incident angle.
The red, blue and yellow lines depict the penetration depths as function of incident angle for PbSe, ethylene glycol and toluene, respectively. The blue dashed lines show the incident angle of the experiments (0.14°) and the corresponding penetration depth for PbSe (10 nm). Working at the critical angle of either toluene or ethylene glycol would result in a minute penetration of the X-ray photons into the PbSe superstructure. The above graph is calculated similarly as described in ref. 7, but with different values of the real and imaginary part of the refractive index, since a different photon energy (22 keV instead of 10 keV) was used here.

• • • •

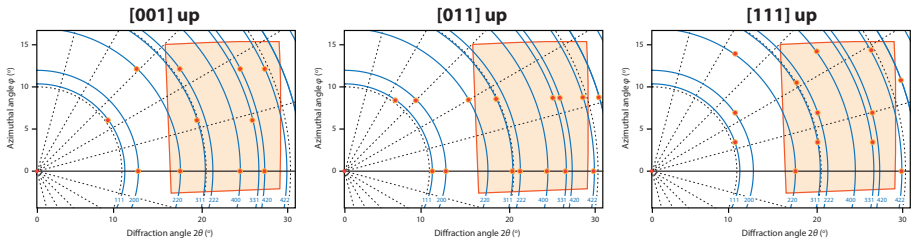

5.5

Figure 5S.5: Theoretical GIWAXS patterns for different crystallographic orientation of the PbSe NCs.
There are three main observed orientations of the PbSe NCs in literature: [001] perpendicular to the plane of the NC monolayer, [011] perpendicular to the plane of the NC monolayer and [111] perpendicular to the plane of the NC monolayer. The acquired GIWAXS patterns match the first orientation, i.e. NCs with a [001] axis pointing upwards, the best.

• • • •

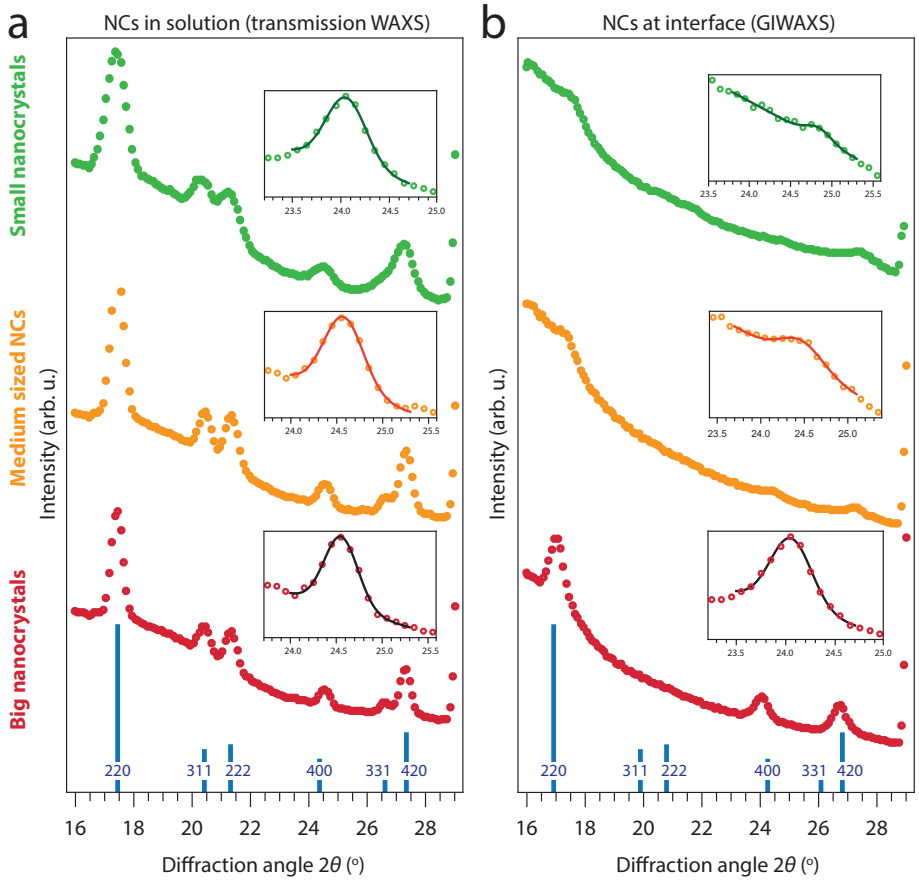

Figure 5S.6: Intensity traces in along the 2θ direction of the GIWAXS signal.
The traces were obtained by integrating the signal in the direction of the azimuthal angle from 1-3° to increase the signal-to-noise ratio. (a) Transmission GIWAXS signal of the small (green), medium-sized (yellow) and large (red) NC solutions. The insets show the GIWAXS signal around the reflection originating from the {400} lattice planes and a Gaussian fit to obtain the FWHM. (b) GIWAXS signal of the NC monolayer, obtained by integrating the signal displayed in Figure 5.1 in the azimuthal angle direction from 1-3°. Note how for the mNCs and bNCs only reflections originating from {hk0} lattice planes are visible, which indicates that the NCs have a {100} facet pointing upwards.

	Solution FWHM (deg)	*Solution diameter (nm)*	*Interface FWHM (deg)*	*Interface diameter (nm)*
Small NCs	*0.57*	*5.8*	*0.59*	*5.6*
Medium-sized NCs	*0.47*	*7.0*	*0.45*	*7.4*
Big NCs	*0.40*	*8.3*	*0.38*	*8.8*

Table 5S.2: FWHM's of the {400} reflections acquired from Figure 5S.6 and the corresponding coherent crystalline NC.

The acquired crystalline sizes of the NCs match the NC diameters obtained with TEM quite well. No significant increase of crystalline size is observed compared to the NC diameter, indicating that the NCs did not perform oriented attachment in the performed experiments.

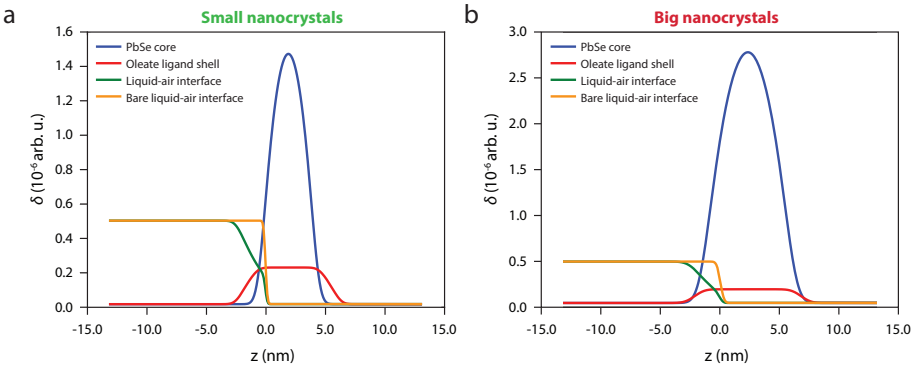

Figure 5S.7: Scattering length density plots of the contributing components for (a) sNCs and (b) bNCs.

The scattering is separated in four contributing parts: NC core (blue), oleate ligand shell (red), the liquid-air interface with applied Gaussian broadening (green) and bare liquid-air interface without Gaussian broadening (yellow).

Table 5S.3: Parameters used to model the XRR data presented in Figure 5.3 and Figure 5S.7. The parameters were optimized with a least-squares fit to the experimental XRR data.

	Small NCs	*Large NCs*
δ N_2 (density = 0.1251×10^{-2} g/cm³)	5.36×10^{-10}	5.36×10^{-10}
β N_2 (density = 0.1251×10^{-2} g/cm³)	2.34×10^{-13}	2.34×10^{-13}
δ Ethylene glycol (density = 1.1132 g/cm³)	5.86×10^{-7}	4.54×10^{-7}
β Ethylene glycol (density = 1.1132 g/cm³)	1.61×10^{-7}	1.05×10^{-7}
δ PbSe core (density = 8.1 g/cm³)	5.49×10^{-6}	4.15×10^{-6}
β PbSe core (density = 8.1 g/cm³)	4.99×10^{-7}	6.04×10^{-7}
PbSe core diameter (Å)	50	80
δ Oleate ligand shell (density = 0.895 g/cm³)	3.79×10^{-7}	4.41×10^{-7}
β Oleate ligand shell (density = 0.895 g/cm³)	1.39×10^{-10}	1.39×10^{-10}
Oleate ligand shell thickness (Å)	18.8	9.0
Area per nanocrystal (Å²)	7272	7406
Particle wetting angle (degrees)	138	126
Roughness between two liquids (Å)	1.3	2.4
Distribution of particle centers (Å)	4.2	6.1

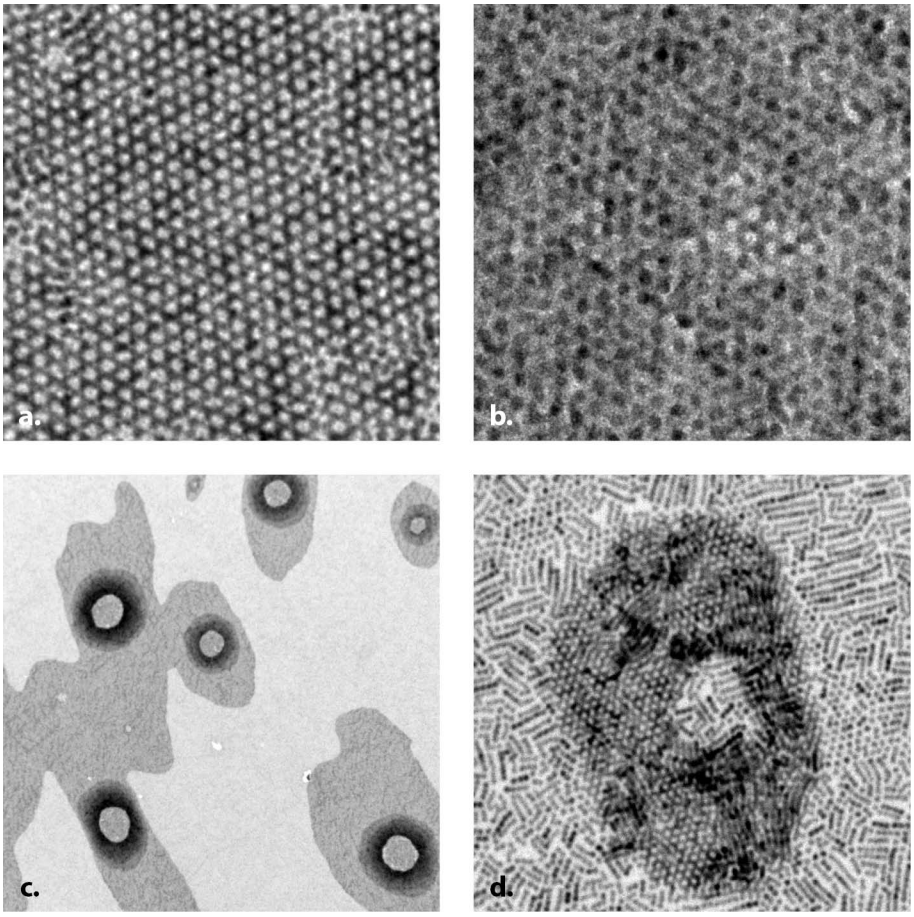

Figure 5S.8: Additional superstructures observed by TEM after self-assembly and sequential oriented attachment of wNCs at the liquid/air interface.
(a) slowing down the solvent evaporation to the time span of several hours instead of just one hour tremendously increased the fraction of honeycomb superstructures; image courtesy Joep Peters. (b) multilayers NCs in the honeycomb superstructure. Note the small regular honeycomb area, where the NC density was supposedly too low to form a homogeneous structure. (c) 'coffee stains' superstructures resulting from inhomogeneous NC spreading over the liquid interface. (d) closer inspection of such structures with inhomogeneous NC densities often show multiple superstructures following the trend in local NC density.

• • • •

References

1. Murray, C. B., Kagan, C. R. & Bawendi, M. G. Self-Organization of CdSe Nanocrystallites into Three-Dimensional Quantum Dot Superlattices. Science (80-.). 270, 1335–1338 (1995).

2. Dong, A., Chen, J., Vora, P. M., Kikkawa, J. M. & Murray, C. B. Binary nanocrystal superlattice membranes self-assembled at the liquid-air interface. Nature 466, 474–7 (2010).

3. Evers, W. H. et al. Low-Dimensional Semiconductor Superlattices Formed by Geometric Control over Nanocrystal Attachment. Nano Lett. 13, 2317–2323 (2013).

4. Boneschanscher, M. P. et al. Long-range orientation and atomic attachment of nanocrystals in 2D honeycomb superlattices. Science (80-.). 344, 1377–1380 (2014).

5. Savitzky, B. H. et al. Propagation of Structural Disorder in Epitaxially Connected Quantum Dot Solids from Atomic to Micron Scale. Nano Lett. 16, 5714–8 (2016).

6. Kalesaki, E. et al. Dirac Cones, Topological Edge States, and Nontrivial Flat Bands in Two-Dimensional Semiconductors with a Honeycomb Nanogeometry. Phys. Rev. X 4, 11010 (2014).

7. Geuchies, J. J. et al. In situ study of the formation mechanism of two-dimensional superlattices from PbSe nanocrystals. Nat. Mater. 15, 1248–1254 (2016).

8. Baumgardner, W. J., Whitham, K. & Hanrath, T. Confined-but-Connected Quantum Solids via Controlled Ligand Displacement. Nano Lett. 13, 3225–3231 (2013).

9. Walravens, W. et al. Chemically Triggered Formation of Two-Dimensional Epitaxial Quantum Dot Superlattices. ACS Nano 10, 6861–6870 (2016).

10. Soligno, G., Dijkstra, M. & van Roij, R. Self-Assembly of Cubes into 2D Hexagonal and Honeycomb Lattices by Hexapolar Capillary Interactions. Phys. Rev. Lett. 116, 258001 (2016).

11. Choi, J. J., Bian, K., Baumgardner, W. J., Smilgies, D.-M. & Hanrath, T. Interface-Induced Nucleation, Orientational Alignment and Symmetry Transformations in Nanocube Superlattices. Nano Lett. 12, 4791–4798 (2012).

12. Steckel, J. S., Yen, B. K. H., Oertel, D. C. & Bawendi, M. G. On the mechanism of lead chalcogenide nanocrystal formation. J. Am. Chem. Soc. 128, 13032–3 (2006).

13. Moreels, I. et al. Composition and Size-Dependent Extinction Coefficient of Colloidal PbSe Quantum Dots. Chem. Mater. 19, 6101–6106 (2007).

14. Peters, J. L. et al. Ligand-Induced Shape Transformation of PbSe Nanocrystals. Chem. Mater. 29, 4122–4128 (2017).

15. Boneschanscher, M. P. et al. Long-range orientation and atomic attachment of nanocrystals in 2D honeycomb superlattices. Science (80-.). 344, 1377–1380 (2014).

16. Novák, J. et al. Site-Specific Ligand Interactions Favor the Tetragonal Distortion of PbS Nanocrystal Superlattices. ACS Appl. Mater. Interfaces 8, 22526–33 (2016).

17. Murphy, J. E. et al. PbTe colloidal nanocrystals: Synthesis, characterization, and multiple exciton generation. J. Am. Chem. Soc. 128, 3241–3247 (2006).

18. Li, H. et al. Size- and shape-controlled synthesis of PbSe and PbS nanocrystalsvia a facile method. CrystEngComm 12, 1127–1133 (2010).

19. Whitham, K. et al. Charge transport and localization in atomically coherent quantum dot solids. Nat. Mater. 15, 557–563 (2016).

20. Alimoradi Jazi, M. et al. Transport Properties of a Two-Dimensional PbSe Square Superstructure in an Electrolyte-Gated Transistor. Nano Lett. acs.nanolett.7b01348 (2017). doi:10.1021/acs.nanolett.7b01348

21. Treml, B. E., Lukose, B., Clancy, P., Smilgies, D.-M. & Hanrath, T. Connecting the Particles in the Box - Controlled Fusion of Hexamer Nanocrystal Clusters within an AB6 Binary Nanocrystal Superlattice. Sci. Rep. 4, 6731 (2015).

22. Cho, K.-S., Talapin, D. V, Gaschler, W. & Murray, C. B. Designing PbSe nanowires and nanorings through oriented attachment of nanoparticles. J. Am. Chem. Soc. 127, 7140–7 (2005).

23. Klokkenburg, M. et al. Dipolar Structures in Colloidal Dispersions of PbSe and CdSe Quantum Dots. Nano Lett. 7, 2931–2936 (2007).

24. Kortschot, R. J., van Rijssel, J., van Dijk-Moes, R. J. A. & Erné, B. H. Equilibrium Structures of PbSe and CdSe Colloidal Quantum Dots Detected by Dielectric Spectroscopy. J. Phys. Chem. C 118, 7185–7194 (2014).

25. Bertolotti, F. et al. Crystal symmetry breaking and vacancies in colloidal lead chalcogenide quantum dots. Nat. Mater. 15, 987–994 (2016).

26. Lane, J. M. D. & Grest, G. S. Assembly of responsive-shape coated nanoparticles at water surfaces. Nanoscale 6, 5132 (2014).

27. Landman, U. & Luedtke, W. D. Small is different: energetic, structural, thermal, and mechanical properties of passivated nanocluster assemblies. Faraday Discuss. 125, 1 (2004).

28. Choi, J. J. et al. Controlling Nanocrystal Superlattice Symmetry and Shape-Anisotropic Interactions through Variable Ligand Surface Coverage. J. Am. Chem. Soc. 133, 3131–3138 (2011).

29. van der Stam, W. et al. Oleic Acid-Induced Atomic Alignment of ZnS Polyhedral Nanocrystals. Nano Lett. 16, 2608–14 (2016).

30. Bigioni, T. P. et al. Kinetically driven self assembly of highly ordered nanoparticle monolayers. Nat. Mater. 5, 265–70 (2006).

31. Rabani, E., Reichman, D. R., Geissler, P. L. & Brus, L. E. Drying-mediated self-assembly of nanoparticles. Nature 426, 271–274 (2003).

32. Born, P., Blum, S., Gerstner, D., Huber, P. & Kraus, T. Self-Assembly of Gold Nanoparticles at the Oil – Vapor Interface: From Mono- to Multilayers. (2014).

33. Calzolari, D. C. E., Pontoni, D., Daillant, J. & Reichert, H. An X-ray chamber for in situ structural studies of solvent-mediated nanoparticle self-assembly. J. Synchrotron Radiat. 20, 306–15 (2013).

34. Als-Nielsen, J. & McMorrow, D. Elements of Modern X-ray Physics. (John Wiley & Sons, Inc., 2011). doi:10.1002/9781119998365

35. Parratt, L. G. Surface Studies of Solids by Total Reflection of X-Rays. Phys. Rev. 95, 359–369 (1954).

Appendices

List of publications	**145**
Summary / Samenvatting	**146 / 150**
Dankwoord - Acknowledgements	**154**
About the author	**160**

List of publications

The contents of this thesis are largely based on the following publications:

- **Carlo van Overbeek**, Joren E. Vos, Joep L. Peters, Marijn A. van Huis, Daniel Vanmaekelbergh;
  Synthesis of 2D superstructures with square or honeycomb nanoperiodicity by interfacial self-assembly and oriented attachment of PbSe nanocrystals, in preparation.
- Jaco J. Geuchies, Ellenor Geraffy, Giuseppe Soligno, **Carlo van Overbeek**, Federico Montanarella, Marlou R. Slot, Oleg Konovalov, Andrei V. Petukhov and Daniel Vanmaekelbergh;
  The adsorption geometry of PbSe nanocrystals at liquid/air interfaces, in preparation.
- **Carlo van Overbeek**, Joep L. Peters, Susan A. P. van Rossum, Marc Smits, Marijn A. van Huis and Daniel Vanmaekelbergh;
  Interfacial self-assembly and oriented attachment in the family of PbX (X = S, Se, Te) nanocrystals, submitted.
- Jaco J. Geuchies*, **Carlo van Overbeek*** (*equal contributions), Wiel H. Evers, Bart Goris, Annick de Backer, Anjan P. Gantapara, Freddy T. Rabouw, Jan Hilhorst, Joep L. Peters, Oleg Konovalov, Andrei V. Petukhov, Marjolein Dijkstra, Laurens D.A. Siebbeles, Sandra van Aert, Sara Bals & Daniel Vanmaekelbergh;
  In-situ study of the formation mechanism of two-dimensional superlattices from PbSe nanocrystals, Nature Materials, **15**, 1248 – 1254 (**2016**).

Other scholarly publications with the author of this thesis:

- Wiel H. Evers, Juleon M. Schins, Michiel Aerts, Aditya Kulkarni, Pierre Capiod, Maxime Berthe, Bruno Grandidier, Christophe Delerue, Herre S. J. van der Zant, **Carlo van Overbeek**, Joep L. Peters, Daniel Vanmaekelbergh & Laurens D. A. Siebbeles;
  High charge mobility in two-dimensional percolative networks of PbSe quantum dots connected by atomic bonds, Nature Communications, **6**, 8195 (**2015**).

Summary

Incomprehensible. That may be a one-word summary of the work in this thesis from one layman to another. Recently, multiple initiatives are undertaken towards closing a growing rift between science and the public. This rift is a threat to publicly subsidized science and thereby the progression of technology in general.

People who are not expert in a respective field of research cannot discern true from pseudo-scientific statements by people claiming the authority of science for their own purposes. Examples of this phenomenon are ample in commercials, new age philosophies and even in politics. When such abusers of science inevitably come to fall, the public will start to distrust real scientists as well. Of course, the public knows real science is trustworthy, but their inability to discern makes it useless to them anyway. This might provide a suggestion to politicians to stop financing scientific research.

This will not be the end of science nor technological progression, because companies will keep investing in research and development. However, it will hamper the more curiosity driven research, as company research is directed towards a very specific final goal, to be reached in a limited time span. Also, the results are owned by the company and not made available for other researchers; this slows down the general expansion of scientific knowledge. It is hard to believe that principal technologies, such as antibiotics, computers and satnavs, would be as far developed as they are today without open and fundamental research in science.

One of the initiatives towards closing the rift mentioned above is by science communication to lay audiences. The goal of this communication is to inform and educate laymen in discerning scientific truth from scientific speculation and pseudo-science. Therefore, with this summary I hope to set an example that shows exact scientific research can be presented in a comprehensive way to a broad audience. Exact scientists missing depth in the following text can read the abstracts of the previous chapters for a more detailed account of what was discovered with the research described in this thesis.

What was the purpose of the research in this thesis?

Making faster computers and more efficient solar cells.

The most essential materials necessary to construct both computers and solar cells are materials that do not conduct electricity unless they are triggered; such materials are called semiconductors. Computer chips are basically a vast network of such semiconductor triggers, called transistors. Solar cells are constructed so that electricity is generated when the semiconductors in the cells are triggered by light. Logically, both

applications will perform better when semiconductor materials are used in which this trigger mechanism is faster or the electrical conductivity is higher.

Recently, a new family of synthetic semiconductor materials made up from microscopic crystallites, 'nanocrystals', was discovered. The synthesis involves connecting the crystallites present at a liquid/air interface, creating an ultrathin, 'two-dimensional', crystalline sheet with microscopic holes in it. The holes can be ordered in a square or hexagonal geometry, the latter can be visualized as a honeycomb. Theoretical calculations showed that particularly the 'honeycombs' should possess the aforementioned electrical properties to a very high degree. Furthermore, this material formed via an also very recently discovered way of crystal growth: 'oriented attachment'.

The combination of these two factors made the research on the formation of honeycomb structures by nanocrystal assembly of high interest. First, although it was clear that oriented attachment was involved in the formation of these materials, the exact mechanism of formation remained unknown. Second, it was (and still is) an outstanding question whether the predicted spectacular electronic properties match experimental reality. Provided that these materials could present a genuine breakthrough in electronics, other conditions such as reliable quality and scalable production are required for industrial application. Therefore, the research in this thesis was dedicated to finding out the formation mechanism of these materials.

Did the research succeed?

Partly.

It turned out that reproducibly making these new materials was harder than anticipated. Naturally, this steered research into the direction of finding out what disrupted the synthesis. In chapter 3 of this thesis, it is shown that trace amounts of specific compounds in the atmosphere of the reaction vessel have a profound effect on the synthesis. The most important and paradoxical example is oxygen. Exposing the nanocrystals to oxygen before the synthesis inhibits oriented attachment, while exposure during the reaction speeds it up to an uncontrollable rate. When this became clear, multiple new set-ups were bought or custom-built to keep all steps of the synthesis as air-tight and oxygen-free as possible.

The synthesis of the new materials was discovered for crystallites made up from the chemical lead selenide. In chapter 4, it is shown that the synthesis also works for the related compounds lead sulfide and lead telluride. This gives insight in the prerequisites of the formation mechanism of the new material. Also, a broader choice of materials allows for tailoring the final product to specific needs in applications. This research was conducted when the disruptive effects of oxygen and other chemicals on oriented attachment were still poorly understood. Hence, the comparative study in this chemical

family may have to be redone, now that we have found out a reproducible synthesis route free of disruptions.

The new materials with a square geometry were the first to be synthesized reproducibly. Therefore, investigating their mechanism of formation was performed first. In chapter 5, well-established and experimental microscopic techniques are described and used to observe their mechanism of formation. The two experimental techniques were atom counting: exactly pinpointing atomic positions in microscopic crystallites; and in-situ GISAXS: observing the live formation of two-dimensional structures with X-ray scattering. The particular use of these two methods was completely new for the field of nanocrystal science, and resulted in unprecedented results. With a lot of effort, and a little luck, it turned out to be possible to capture the whole square material formation in a single experiment. These observations showed multiple stages in the formation mechanism before final oriented attachment of the crystallites. The formation process was finally rationalized with computer models.

The main part of the synthesis of the new materials takes place at the interface of a liquid and air. Therefore, part of the experiments from chapter 5 are repeated in chapter 6 on crystallites when oriented attachment is inhibited to observe the behavior of individual nanocrystals at an interface. In this way, it was found that the crystallites used in this research could be divided in two subsets: big and small crystallites. The big ones showed preferred orientations with respect to the interface, whereas the small ones showed random orientations. These findings were combined with recent advances in reproducible and large-scale honeycomb synthesis, in order to present a tentative mechanism for their formation.

What will be the next steps?

More research.

Scientists always seem to demand more research. It is easy, and not wholly untrue, to say that this is a simple way of providing themselves job security. Still, history shows that further research often results in a broad scientific understanding, and often, robust production of many products used in daily life. In chapter 2, it was shown that it took scientists hundreds of years to prove that crystals are regular arrays of atoms. This knowledge is now simply taken for granted but it is still pivotal to many industrial processes. Another example closer to home are computers. Decades of dedicated large-scale (industrial) research has bridged the gap between the invention of the electronic semiconductor transistor and the affordable personal computers that shape our present society. Moreover, there were decades of curiosity driven research on semiconductors even before that. The public rightfully demands reliability and comfort from science and technology, but that can only be guaranteed after extremely thorough investigation.

Also, a research time span is not as endless as it may seem to the public. Other materials that might enhance computer or solar cell performance are being investigated by other scientists while the research in this thesis was being conducted. If those are at some point proven to work vastly better than the ones presented in this thesis, this line of research will lose major part of its purpose and will eventually be terminated.

But this is not the case, so how can this line of research be successfully continued?

Elucidating the formation mechanism of the honeycomb material with the microscopy techniques from chapters 5 and 6 is an obvious first thing to do. The recent advances in more reproducibly synthesizing honeycombs should greatly enhance further research in this direction. The same holds for measuring whether this material and the squares indeed have the predicted interesting semiconductor properties. If all these experiments are successful and their outcome is positive, then research should continue in finding out how these materials can be integrated in existing technologies to enhance their performance.

However, in the plausible scenario that along this path unforeseen problems arise, those will have to be resolved first with… more research!

Samenvatting

Onbegrijpelijk. Dat zou in één woord de samenvatting kunnen zijn van een leek die het werk in deze thesis aan een andere leek wil uitleggen. Er zijn momenteel meerdere initiatieven gaande die een groeiende kloof tussen wetenschap en publiek proberen te dichten. Zo een kloof is namelijk een bedreiging voor publiekelijk gesubsidieerde wetenschap en daardoor ook een bedreiging voor de vooruitgang van technologie.

Mensen die geen expert zijn in wetenschappelijk onderwerp kunnen geen onderscheid maken tussen ware en pseudowetenschappelijke uitspraken van individuen die zich de autoriteit van wetenschap toe-eigenen voor hun eigen doelen. Voorbeelden van dit fenomeen te over in reclames, 'new age'-levensbeschouwingen en zelfs in de politiek. Wanneer misbruikers van de wetenschap onvermijdelijk ten val komen, zal het publiek echte wetenschappers ook minder gaan vertrouwen. Natuurlijk weet men wel dat wetenschap zelf te vertrouwen is, maar het onvermogen om onderscheid te maken maakt het alsnog waardeloos voor hen. Dit zou politici er uiteindelijk toe kunnen bewegen om te stoppen met het financieren van wetenschappelijk onderzoek.

Dit zou nog niet het eind betekenen van de progressie van wetenschap en technologie, want bedrijven zullen wel daarin blijven investeren. Het zou echter wel onderzoek gedreven door nieuwsgierigheid belemmeren. Onderzoek dat gefinancierd wordt door bedrijven is namelijk altijd gericht op een specifiek doel dat binnen een beperkte tijdsspanne gerealiseerd moet worden. Daarnaast zijn wetenschappelijke vindingen binnen bedrijven niet openbaar. Dit vertraagt het verder verspreiden en gebruiken van nieuwe kennis. Het is onwaarschijnlijk dat belangrijke moderne stukjes techniek, zoals antibiotica, computers en satellietnavigatie, net zo goed ontwikkeld zouden zijn als nu zonder open en fundamentele wetenschap.

Eén van de initiatieven die worden ondernomen om de kloof tussen wetenschap en publiek te dichten is wetenschapscommunicatie naar leken. Daarbij is het doel om hen te informeren en te leren hoe onderscheid te maken tussen wetenschap, pseudowetenschap en wetenschappelijke speculatie. Met deze samenvatting van mijn thesis wil ik graag in deze trend meegaan en laten zien dat het mogelijk is om wetenschappelijk onderzoek begrijpelijk te maken voor een breed en wetenschappelijk niet-onderlegd publiek. Bètawetenschappers die diepte missen in de volgende samenvatting verwijs ik door naar de abstracts van de hoofdstukken hiervoor.

Wat was het doel van het onderzoek in deze thesis?

Snellere computers en efficiëntere zonnecellen maken

De materialen die essentieel zijn voor de constructie van computers en zonnecellen zijn materialen die alleen elektriciteit kunnen geleiden wanneer ze zijn geactiveerd; zulke materialen heten halfgeleiders. Computerchips zijn niets meer dan stukjes halfgeleider die schakelingen, transistoren, vormen in een enorm complex netwerk. Zonnecellen zijn zo gebouwd dat er elektriciteit wordt opgewekt wanneer de halfgeleiders door licht worden geactiveerd. Logischerwijs zullen beide hiervoor genoemde voorbeelden beter worden wanneer ze worden gemaakt met halfgeleiders die sneller kunnen activeren of die sneller elektriciteit kunnen geleiden.

Onlangs is er een nieuw soort halfgeleidermateriaal ontdekt. Dit materiaal wordt gemaakt door microscopisch kleine kristallen aan elkaar te laten binden op een grensvlak tussen een vloeistof en lucht. Hierdoor ontstaat er een ultradun kristallijn laagje waarin microscopisch kleine gaatjes zitten. De gaatjes kunnen worden geordend in een vierkant of honingraadachtig patroon. Theoretische berekeningen tonen aan dat vooral de 'honingraden' beter zouden kunnen presteren dan de halfgeleiders die nu worden toegepast in de praktijk. Daarnaast vormen de nieuw ontdekte materialen op een recentelijk ontdekte manier van kristalgroei: 'gerichte aanhechting'.

De combinatie van deze twee factoren maakten onderzoek naar de vorming van deze materialen zeer interessant. Ten eerste omdat het vormingsmechanisme van de materialen lastig te verklaren was, al was het duidelijk dat ergens in het proces gerichte aanhechting moest plaatsvinden. Ten tweede was (en is) het een openstaande vraag of deze materialen echt de halfgeleidereigenschappen bezitten die voorspeld zijn. Deze materialen zouden een doorbraak kunnen betekenen binnen de elektronica, maar dan moet er eerst ook aan voorwaarden als betrouwbare kwaliteit en schaalbare productie voldaan worden. Daarom is het onderzoek in deze thesis gericht op het ontcijferen van het vormingsmechanisme van deze materialen.

Is het onderzoek geslaagd?

Gedeeltelijk

Het bleek moeilijker dan verwacht om deze materialen reproduceerbaar te maken. Dit stuurde het onderzoek uiteraard in de richting naar het vinden van wat de synthese belemmerde. In hoofdstuk 3 van deze thesis wordt getoond dat zelfs minuscule hoeveelheden van sommige chemicaliën de synthese enorm kunnen beïnvloeden. Het belangrijkste en meest paradoxale voorbeeld is zuurstof. Wanneer de kristalletjes voor de synthese in aanraking komen met zuurstof wordt reactie - die nodig is om de materialen te vormen - geremd. Maar blootstelling tijdens de reactie zorgt ervoor dat de reactie op een oncontroleerbaar snel gaat verlopen. Toen dit duidelijk werd, is er nieuwe

apparatuur gekocht of gebouwd om alle stappen in de reactie zo zuurstofvrij mogelijk te laten verlopen.

Bij de ontdekking van de nieuwe materialen werden loodselenide kristalletjes gebruikt bij de vorming via gerichte aanhechting. In hoofdstuk vier wordt getoond dat de synthese ook werkt met de vergelijkbare stoffen loodsulfide en loodtelluride. Dit geeft inzicht in wat de vereisten zijn voor het vormingsproces van de nieuwe materialen. Daarnaast kan het nieuwe materiaal beter toegespitst worden op beoogde toepassingen met een bredere keus aan grondstoffen. De storende effecten van onder andere zuurstof waren nog niet bekend toen dit onderzoek werd gedaan. Het vergelijkende onderzoek tussen deze materialen zal dus wellicht opnieuw gedaan moeten worden.

Het nieuwe materiaal met een vierkant patroon van gaten was het eerste wat redelijk reproduceerbaar gemaakt kon worden. Daarom is het vormingsmechanisme van dit soort materialen als eerste onderzocht. In hoofdstuk 5 worden gevestigde en experimentele microscopische technieken beschreven en gebruikt om het vormingsmechanisme te observeren. De twee experimentele technieken waren: 'atomen tellen', waarmee onder een microscoop de exacte plaats en hoeveelheid van atomen in microscopische kristallen wordt bepaald; en 'in-situ GISAXS', waarmee microscopische patronen aan een vloeistofoppervlak tijdens een reactie kunnen worden gemonitord. Het was voor het eerst dat deze technieken binnen de wetenschap van nanokristallen werden gebruikt en het leverde ongekende resultaten op. Met veel moeite en een beetje geluk was het mogelijk een volledig vormingsproces vast te leggen met één experiment. Deze waarnemingen lieten zien dat er verschillende tussenstappen in het vormingsproces zitten. Het vormingsproces is later gerationaliseerd met een computermodel.

De synthese van de nieuwe materialen vindt voor het grootste gedeelte plaats aan een vloeistofoppervlak. De experimenten uit hoofdstuk 5 werden daarom in hoofdstuk 6 herhaald op microscopische kristallen waarbij gerichte aanhechting wordt onderdrukt, zodat het gedrag van losse kristalletjes op het oppervlak kon worden bestudeerd. Het bleek dat de onderzochte kristalletjes in twee categorieën konden worden opgedeeld: groot en klein. De grote kristalletjes hebben een voorkeursoriëntatie aan het oppervlak, terwijl de kleintjes een lukrake oriëntatie hebben. Deze bevindingen zijn gecombineerd met recente ontwikkelingen in het reproduceerbaar synthetiseren van de honingraadachtige materialen om zo tot een voorlopig vormingsmechanisme van deze materialen te komen.

Wat worden de vervolgstappen?

Meer onderzoek

Wetenschappers lijken altijd te vragen om meer onderzoek. Het is makkelijk, en niet eens geheel onwaar, om te stellen dat dit een eenvoudige manier is om voor henzelf baangarantie te creëren. Toch laat de geschiedenis zien dat dieper onderzoek vaak

leidt tot breder begrip en robuuste productie van veel producten die dagelijks worden gebruikt. In hoofdstuk 2 is aangetoond dat het wetenschappers honderden jaren heeft gekost om te bewijzen dat kristallen periodieke reeksen van atomen zijn. Hoewel deze kennis nu als zelfsprekend wordt gezien, is het wel nog steeds essentiële kennis voor vele industriële processen. Een ander tastbaarder voorbeeld is de computer. Het heeft tientallen jaren grootschalig (industrieel) onderzoek gekost om het gat te overbruggen tussen de uitvinding van de elektrische halfgeleider en de betaalbare pc die niet meer weg te denken is uit onze samenleving. Bovendien gingen er nog eens tientallen jaren vooraf aan onderzoek dat werd gedreven door nieuwgierigheid naar de werking van halfgeleiders. De maatschappij eist terecht betrouwbaarheid en comfort van wetenschap en technologie, maar dit kan alleen worden gegarandeerd na het voltooien van extreem grondig onderzoek.

Daarnaast is de tijdsspanne van wetenschappelijk onderzoek ook niet zo eindeloos als het voor het publiek misschien lijkt. Andere materialen die de prestaties van computers en zonnecellen kunnen verbeteren werden ook onderzocht door andere wetenschappers, terwijl dit onderzoek liep. Mocht ineens bewezen worden dat deze materialen een stuk beter zullen presteren, dan zal het onderzoek naar het materiaal uit deze thesis een belangrijk doel verliezen en zal de onderzoekslijn uiteindelijk stoppen.

Dit is echter niet het geval, dus hoe kan dit onderzoek het beste worden voortgezet?

Het vormingsmechanisme ophelderen van de honingraadachtige materialen met de technieken uit hoofdstuk 5 en 6 is een vanzelfsprekende optie. Dit zou nu mogelijk moeten zijn, omdat deze materialen met de huidige kennis reproduceerbaarder gemaakt kunnen worden. Hetzelfde geldt voor het meten of deze materialen inderdaad de voorspelde halfgeleidereigenschappen hebben. Als al deze experimenten succesvol verlopen en de uitkomst positief is, dan zou er vervolgonderzoek moeten plaatsvinden hoe deze materialen geïntegreerd kunnen worden in bestaande technologieën om hun prestaties te verbeteren.

Echter, in het mogelijke geval dat er zich op dit uitgestippelde pad onvoorziene problemen voordoen, dan zullen die eerst opgelost moeten worden met… meer onderzoek!

Dankwoord - Acknowledgements

Dat was het dan. Deze thesis luidt het einde in van mijn promotietraject, mijn formele opleiding en misschien ook wel mijn rol in de academische wetenschap. Zoals zoveel eindes is ook dit einde slechts een illusie. De munt waarop aan één kant het woord “einde” staat, heeft aan de andere kant het woord “begin” staan. De munt als geheel zou je een mijlpaal kunnen noemen. Terwijl ik dit schrijf, weet ik nog niet zo goed wat voor nieuw begin de toekomst mij gaat brengen. Het lijkt me in ieder gepast om te beginnen met de mensen te bedanken die mij hebben geholpen bij deze mijlpaal te komen.

Allereerst wil ik daarbij uiteraard Daniel Vanmaekelbergh, mijn promotor, vermelden. Heel erg bedankt voor het richting geven aan mijn onderzoek op de momenten dat ik de ogenschijnlijk ondoorgrondelijke wegen van de wetenschap even kwijt was. Daarnaast wil ik je complimenteren op je schrijfkunsten en je vermogen schrijfwerk te verbeteren. Er is misschien een groot eindredacteur aan je verloren gegaan. Je was geen zachte heelmeester en ik ben zeer dankbaar voor al je goede kritiek. Ik denk dat ik daarvan later ook nog lang zal profiteren. Hopelijk heb je me zo goed afgericht dat ik mijn dankwoord nu ook foutloos schrijf!

Marijn van Huis, mijn copromotor, is natuurlijk de tweede die niet in het rijtje kan ontbreken. Vanaf ongeveer halverwege werd je mijn copromotor om me verder te begeleiden met mijn promotietraject en daar ben ik zeer blij mee. Het was erg fijn om samen te kunnen reflecteren op mijn soms onsamenhangende data. Ook was je erg handig als deskundige over elektronenmicroscopie. Helaas zijn onze gewaagdere projectjes daarmee nooit een succesverhaal geworden, maar ik ben ervan overtuigd dat jij nog vele succesverhalen voor je hebt met alle nieuwe ontwikkelingen binnen de elektrononenmicroscopie in Utrecht.

Ik moet het toch één keer opschrijven in mijn proefschrift: het allerleukste aan mijn promotietraject waren de superleuke collega’s! En waar kan ik dat nou beter vermelden dan bij het bedanken van mijn kamergenoten? OL110 is de leukste kamer van de Uithof en omstreken! Uiteraard maakte dit feit vele anderen jaloers en dit soort slechte verliezers hebben dan ook snel andere titels voor hun kamer verzonnen. Ik zal geen kamernummers noemen, maar slappe aftreksels zoals “de gezelligste kamer van CMI”, “de productiefste kamer” en “de beste kamer ooit” zijn de revue gepasseerd.

Kamergenote Elleke van Harten en ik hebben elkaars promotietraject vrijwel helemaal meegemaakt, maar daar houdt onze parallelle levensloop nog niet op. We hebben dezelfde studieloopbaan gevolgd, (soort van) op dezelfde vakgroep onze masterstage gedaan en zelfs in hetzelfde bestuur van de studievereniging Proton gezeten! We hebben veel overeenkomstige ups en downs gehad en die met elkaar kunnen delen.

Ik kan me geen beter persoon indenken om mee te klagen over slechte werkcolleges, falende syntheses en existentiële onzekerheid, en ook geen beter persoon om opgelucht problemen mee weg te lachen.

Tussendoor waren er de kamergenoten Tim Senden en Robin Geitebeek, die later samen een nieuwe kamer zijn gestart. Ik heb jullie nuchtere observaties en droge humor enorm gewaardeerd. Helaas werd de lol die we hadden niet altijd gewaardeerd door de buren. Tegen het einde van mijn promotietraject kwam Annelies van der Bok erbij op OL110 en nog meer tegen het einde Bas Salzmann. Helaas hebben we niet lang genoeg samengewerkt om echt epische dingen samen mee te maken, maar ik vond het heel erg leuk om het enthousiasme en optimisme van nieuwe promovendi nog één keer van dicht bij te kunnen zien. Uiteraard het beste toegewenst met het verdere verloop van jullie promoties!

En dan de laatste - maar zogezegd - niet de minste kamergenoot, Jaco Geuchies. Er valt zoveel te zeggen dat het moeilijk is om het in abstracte termen te bevatten, dus hier volgt maar een greep uit de dingen die we samen hebben meegemaakt: scattering data overinterpreteren ("bastardo glietches!"), eindeloos le zap de spi0n kijken, same-sex tangodansen, quatorze juillet, en nog zoveel meer! Ik zit hardop te lachen, terwijl ik dit schrijf.

Voor de iets meer ingewijde lezer is dan nu de stap naar de rest van 'team attachment' snel gemaakt. Dan is de eerste die genoemd moet worden natuurlijk Joep Peters; de man die van team attachment een echt team heeft gemaakt, inclusief WhatsApp-groep! Wat ben je als team tegenwoordig nog zonder? Ik kan wel zeggen dat we een passie delen voor wat je netjes zou kunnen formuleren als maatschappijkritische gesprekken, je zou het natuurlijk ook slap lullen vanaf de zijlijn kunnen noemen. Maar wie weet in wat voor politieke functie we ooit terecht komen, misschien komen de pseudogegronde opvattingen van de andere dan toch nog eens van pas.

Then there was also Maryam Alimoradi Jazi in team attachment. I am very sorry I have never been able to provide you the samples you needed for your research. Perhaps more unfortunately you are now finding out that the synthesis is still not so easily reproducible. Nevertheless, you are still going and are even succeeding with your very nice first paper! And on a not so work-related level, it was wonderful to meet someone with such polite and exquisite gestures and mannerisms as you.

Ongeveer hetzelfde geldt voor Marlou Slot. Ook jij hebt helaas last gehad van alle falende syntheses. Gelukkig ben je een overtuigd optimist en dat is ook bij jou beloond met een mooi artikel. Het was altijd leuk om je enthousiaste updates 'uit de kelder' te horen en, later, te babbelen over Duitsland en zingen.

And then there are Sophia Buhbut-Sinai and Guiseppe Soligno, the 'newbies' in team attachment, although actually you both are well-experienced postdocs. It is fascinating to see how fast you both picked up things in our group and started to work very efficiently and productively. Is this normal for all people who finished a PhD? It makes me very hopeful about my own future job performance.

Ik wijd ook graag wat ruimte in mijn dankwoord aan Wiel Evers, de 'God Father' van het hele oriented attachment verhaal in Utrecht. Helaas heeft nog niemand in Utrecht je syntheseskills kunnen evenaren. Toch bleef je altijd behulpzaam en bescheiden als er weer eens verhalen van niet-attachende, veel te snel attachende of gewoon fout attachende deeltjes uit Utrecht kwamen.

Behalve leuke collega's heb ik ook het geluk gehad samen te mogen werken met heel leuke studenten.

Mijn eerste masterstudente was Susan van Rossum. Gek genoeg heb je mij ingewerkt in plaats van andersom, maar wat telt is dat je dat uitstekend hebt gedaan. Ook daarna hebben we denk ik nog veel samen en van elkaar geleerd.

I shared Paolo Accordini as a master student with Jaco. Physicists tend to underestimate the struggles of lab work done by chemists. Still, they usually never attempt any lab work in case they fail at it and would so be proven wrong that it's so easy. More the glory for you for boldly trying and sometimes succeeding!

Mijn enige bachelorstudente was Laura de Kort. Ik heb heel veel bewondering voor je doorzettingsvermogen na alle tegenslagen tijdens je 'high risk - high gain' project.

Marc Smits was mijn masterstudent met wiens data eindelijk een deel van het verhaal van het vergelijkend warenonderzoek binnen de attachment groep gesloten worden. Verder hebben we vaak leuke nerdy gesprekken gehad bij de elektronenmicroscoop.

Joren Vos was mijn laatste masterstudent en aan hem valt de eerste reproduceerbare synthese van de honingraadstructuren in de nieuwe glovebox toe te schrijven, zeker het vermelden waard! Ook met jou was het zeer leuk om nog meer nerdy gesprekken bij de elektronenmicroscoop te hebben.

Naast al deze studenten heb ik ook nog een hoop tweedejaarsstudenten gehad, namelijk Gerrit-Jan de Bruin, Iris ten Have, Ellen Heuven, Maartje Koppelman, Liselotte Olthof, Yoni Nederstigt, David Verbart, Sander Vonk en Kari-Anne van der Zon. Allemaal heel erg bedankt voor jullie frisse interesse en enthousiasme!

Een andere leuke categorie van mensen waarmee ik heb samengewerkt zijn de mensen met wie ik op 'beam trip' ben geweest. Om mijn dankwoord niet te langdradig te laten worden, benoem ik alleen de mensen die nog niet genoemd zijn.

Bij mijn eerste beam trip waren onder andere Jan Hilhorst en Freddy Rabouw aanwezig. Het was erg leuk om samen met jullie met de Olympische Spelen, flauwe filmpjes van het internet, klagen over het eten en nog veel meer invulling te geven aan de ultieme verveling die al snel de kop opsteekt in een synchroton. Verder hoop ik voor jullie dat jullie nooit meer lang op een plek hoeven te verblijven waar geen Nederlandse frituur wordt geserveerd.

De beam trip waar Ward van der Stam bij aanwezig was, is me bijgebleven door de fantatische 'wifi scattering data' en natuurlijk 'kwantumfeest'.

During my last beam trip Ellenor Geraffy, Federico Montanarella and Tim Prins were in the fellowship. I have very fond memories of endless Ed Sheeran loops, discussions about pasta hardness, hiking in the snow, total brain farts in card games and the 'boy talk' on the way back.

Of course, I would also like to thank all the other people with whom I had the pleasure of working towards the science contained within this booklet. Andrei Petukhov and Oleg Konovalov, thank you for helping out in reciprocal space. Sandra van Aert, Sara Bals, Annick de Backer en Bart Goris heel erg bedankt voor de fantastische hoge resolutie afbeeldingen van jullie elektronenmicroscopen. Anjan Gantapera and Marjolijn Dijkstra, thank you for doing the modelling required to better understand the behavior of our nanocrystals.

Degenen die niet direct naar het dankwoord zijn gebladerd en daadwerkelijk eerst de rest van deze thesis hebben doorgenomen, hebben misschien een aantal mooie elektronenmicroscopieafbeeldingen gezien. Dit is mede te danken aan Hans Meeldijk en Chris Schneijdenberg. Heel erg bedankt voor het uitleggen van de machines en het opnieuw uitleggen als ik het bestaan van een essentieel knopje was vergeten.

Dan komen we soort van naadloos aan bij de technici van onze eigen vakgroep. De eerste labtechnica waar ik mee in aanraking kwam was Relinde Moes, heel erg bedankt voor je lessen 'quantum dots maken'. De wat meer 'technische technicus' was Hans Ligthart, heel erg bedankt voor het elke keer maar weer repareren van de attachment glovebox, toch wel één van de zorgenkindjes op het lab. Tegen het einde van mijn promotietraject nam Peter van den Beld het stokje als technische technicus over. In tegenstelling tot alle apocalyptische profetieën die door het lab de ronde gingen als 'de Hans' zou vertrekken, is het allemaal toch best meegevallen en dat is zeer waarschijnlijk jouw verdienste. Ten slotte was er de ICT-technicus Stephan Zevenhuizen. Sorry Stephan, maar ik zal gewoon Photoshop en InDesign blijven gebruiken totdat GIMP en Scribus capabelere programma's worden, ik wil mezelf wel graag Python gaan leren.

Someone who slipped through when I was discussing my room at office was Celso de Mello-Donega. We never shared a room at office, but you were often present in an indirect way. We never heard you talk, but whenever you had discussions, the other people present in your room tended to laugh out loud. Also, if fun got out of hand in our room, you would rightfully complain and we soon learned to mind our levels of noise. Finally, you are such a hard worker and always carry with you the air of being busy with something, but when spoken to you immediately thaw. I really value the couple of nice conversations that we had. You really were a model neighbor.

Harold de Wijn wil ik ook nog een eervolle vermelding geven in zijn verwoede pogingen om het stelletje scheikundigen bij CMI toch nog een beetje natuurkunde bij te brengen. Volgens mij heb ik vrijwel al je colleges gevolgd, heel erg bedankt daarvoor! Ook nog bedankt trouwens voor het uitleggen hoe je het beste van Utrecht naar Lund en terug kunt rijden met de auto.

Wie hier uiteraard ook niet kan ontbreken is Gerhard Blab. Helaas hebben we nooit samen 'echte wetenschap' bedreven, maar het geduldig tweaken van de 3D-printer kwam daarbij toch wel erg dicht in buurt. Ik zal nog met veel plezier aan deze momenten terugdenken, als mijn blik langs de plastic prullaria glijdt die we samen hebben geproduceerd in naam van de voortschrijding der technologie.

I am sorry for stopping here with the personal anecdotes and affections for my colleagues, although I could possibly still write multiple about any of you, but the length of these acknowledgements is really starting to get out of hand! I do hope that you will think back with a smile about the time we worked at the same place when later seeing this thesis on your book shelve, as I will, when I reread your name in these acknowledgements. Anne Berends, Mark Boneschanscher, Annalisa Brodu, Serena Busatto, Saoirsé Freeney, Thomas Gardenier, Onno Gijzeman, Nadine van der Heijden, Jacobine van Hest, Peter Jacobse, Mathijs de Jong, Linda Kumeling, Joost van der Lit, Andries Meijerink, Christa Oversteeg, Christiaan Post, Kelly Sowers, Maaike van der Sluijs, Ingmar Swart, Pedro Villanueva-Delgado, Winston Wang, Chenghui Xia, Allan Xu, Wenjin Xu, Ting Yu; thank you all for giving CMI such a pleasant working atmosphere!

Naast de positieve bijdragen van al mijn collega's zijn natuurlijk ook de bijdragen van de mensen uit mijn persoonlijke sfeer belangrijk geweest om vier jaar lang professionele tunnelvisie mogelijk te maken. Tijdens mijn promotie heb ik met veel plezier 'stoom afgeblazen' met dansen bij de Utrechtse Studentendansvereniging U Dance en met zingen bij het Utrechts Studenten Koor en Orkest. Het gaat te ver om de leden- en contribuantenlijsten daarvan hier volledig neer te zetten, maar heel erg bedankt iedereen die daar eens een pasje met me heeft gedanst of een noot heeft gezongen. Technisch gezien was ik geen lid meer van de Utrechtse Scheikundige Studentenvereniging

"Proton" toen ik ging promoveren, maar ook die vereniging wil ik niet onbenoemd laten aangezien ik daar veel leuke mensen heb leren kennen die ik ook tijdens mijn promotie nog regelmatig heb gezien.

Tijdens ongeveer de eerste helft van mijn promotie heb ik in een studentenhuis gewoond samen met Berend, Elise, Onno, Renee en Rudy. Heel erg bedankt voor de leuke vooral avonden met Grolsch, wodka proeven, speciaal bier proeven, The Pokemon Drinking game, cocktails… er zat in ieder geval een duidelijk thema in wat we graag deelden. Uiteraard een iets uitgebreider bedankje aan Renee. Je hebt in de twee jaar dat we samen op de Cambridgelaan 267 woonden mijn persoonlijkheid op zoveel vlakken verrijkt, heel erg bedankt!

Ook zijn er nog de mensen waarmee ik graag door kerkers heen loop, muntjes verzamen, de Koude Oorlog herleef, Tokyo verwoest, treinrails leg; kortom de mensen met wie ik bord- en videospelletjes speel. Bart, Cha, Jasper, Jordy, Nico, Paul, Stephan, Teun en alle mensen in deze categorie die hiervoor al zijn genoemd; heel erg bedankt voor alle keren lol in fantasiewerelden en in de echte wereld.

Dan zijn we nu eindelijk aangekomen bij de drie-eenheid: Leon, Reza en ik. We hebben zoveel speciale dingen meegemaakt! Een Romereis, vakanties in België, bijna in elkaar geslagen worden aan de Oude Gracht, eindeloze sessies lollige spelletjes, filmavonden, een 21-diner... Daarnaast hebben we al zoveel met elkaar gedeeld. Als ik jullie zie, dan herinner ik me weer hoe groot mijn problemen op de middelbare school leken en hoe klein ik die nu vind. Ik kan dan goed relativeren dat mijn problemen in mijn huidige situatie waarschijnlijk ook veel kleiner zijn, dan ze in de waan van de dag lijken. Ik ben blij dat twee fantastische vrienden als jullie mijn paranimfen willen zijn.

Pa en ma. Jullie hebben in de opvoeding van Yvonne en mij altijd gedaan wat jullie dachten dat goed voor ons was. Beter kun je het als ouder denk ik niet doen. Het gezinsleven van ons vier was door jullie ouderschap bevoorrecht. Eeuwig dank! Ik hoop dat er in de toekomst nog vele gezellige familieavonden volgen met jullie, Yvonne, Mark, Babette, Amélie, oma en verdere familie.

Ameli. We kennen elkaar eigenlijk pas twee jaar, maar we hebben nu al zoveel leuke dingen samen meegemaakt. Daaraan denkend kan ik alleen maar wensen dat we elkaar eerder zouden hebben gevonden. Je vult me op precies de goede plekken aan. Je geduld en medeleven zijn kenmerkend voor je eindeloze liefde en ik voel me bevoorrecht dat ik daarvoor mag genieten. Ik wil niet meer zonder je. Ich liebe dich.

Carlo van Overbeek, 14 januari 2018, Utrecht

About the author

Carlo van Overbeek was born on the 20th of February 1989 in Utrecht (Overvecht to be precise), the Netherlands. After completing a preposterous amount of video games, and high school, in 2007 he started his studies in chemistry at the Utrecht University. He became chairman of the chemistry students association "Proton" in 2009 and, to focus on the accompanying duties, paused his studies for one year. In 2011 his obtained his bachelor's degree in chemistry with a minor in game and media technology. He continued his studies by obtaining a master's degree in the master program 'nanomaterials: chemistry and physics' also at Utrecht University. His master thesis, however, he performed at NIZO food research and Forschungszentrum Jülich under supervision of dr. Hans Tromp and prof.dr. Willem Kegel. There, he investigated the shear behavior - particularly the peculiar shear banding behavior - of water/water emulsions formed by dextran/gelatin solutions.

In 2013 he started with his doctoral studies in chemistry at Utrecht University in the Condensed Matter & Interfaces group under supervision of dr. Marijn van Huis and prof.dr. Daniel Vanmaekelbergh. In his doctoral studies, he researched the interfacial self-assembly and oriented attachment behavior of lead chalcogenide nanocrystals; the main results of which are described in this thesis, have been published in scientific journals and have been presented at scientific conferences. Next to researching, he taught students in courses on nanomaterials, analytical chemistry and quantum chemistry, and supervised numerous graduate and undergraduate students in his own field of research. During his time as a doctoral researcher he developed a fondness of presenting science in ways that non-expert and non-scientific audiences can understand, preferably accompanied by vivid images. Most notably, this led to an invited interview on poster design and winning the university round of the 2016 FameLab science communication competition.

When not professionally performing science, he likes to brew beer. Other favorited pastimes include playing board games, choir singing, ballroom dancing and reading peculiar non-fiction.